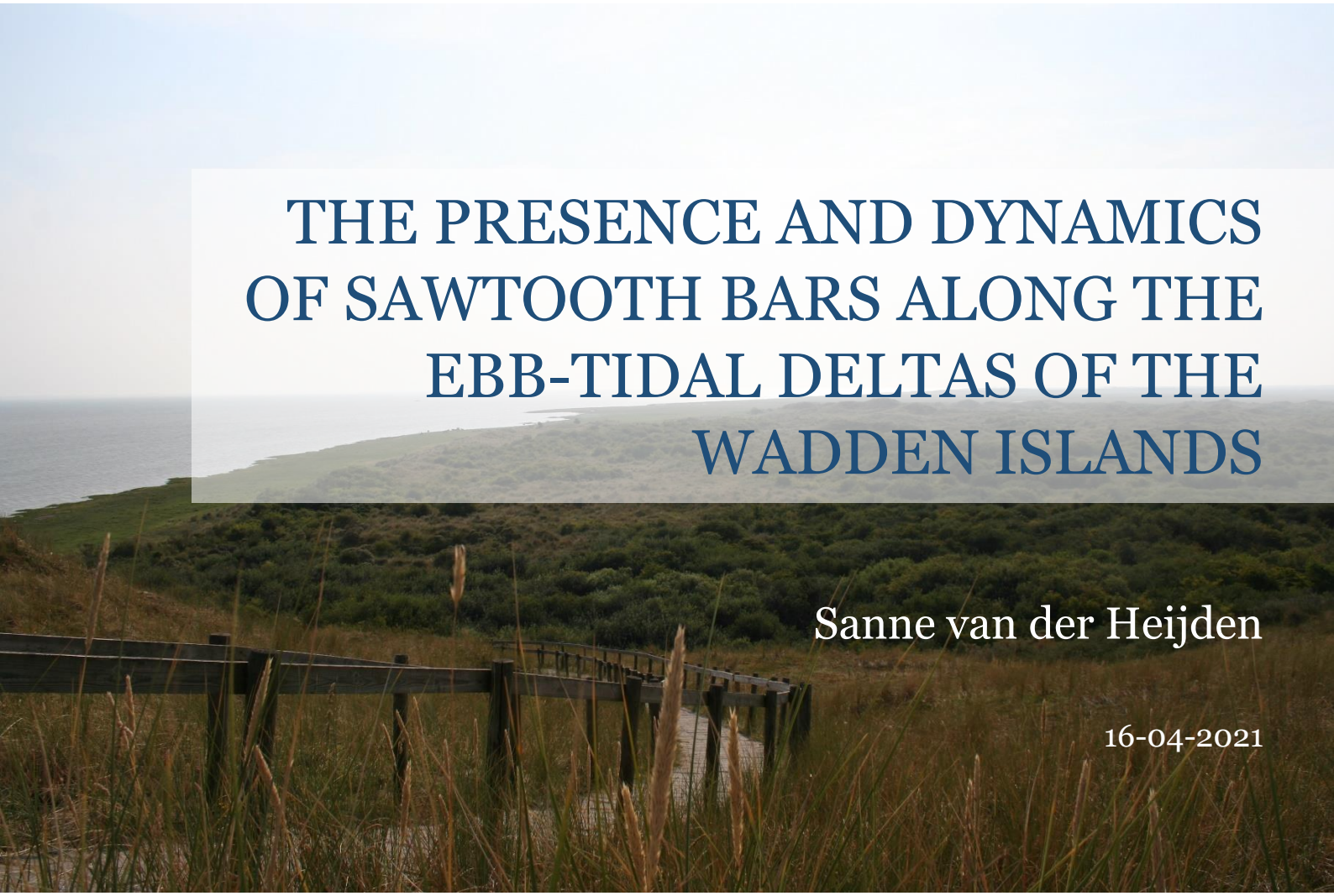

THE PRESENCE AND DYNAMICS OF SAWTOOTH BARS ALONG THE EBB-TIDAL DELTAS OF THE WADDEN ISLANDS

Sanne van der Heijden

16-04-2021

Supervisors:
Dr. M. van der Vegt
Prof. Dr. G. Ruessink

Universiteit Utrecht

Master thesis Earth Surface and Water
Faculty of Geosciences
Utrecht University

Preface

As a child, my parents took me on holidays to the Wadden islands and I think this might be the start of my interest in the region. It is one of Hollands only 'real' nature areas in which nature has free rein. This makes the Wadden a special place in terms of the ecology, morphodynamics, and of course, recreation. Last summer I visited Ameland which led to the beautiful picture on the cover, taken from the highest dune on Ameland.

I accomplished my Bachelor Earth Sciences at the Utrecht University with a thesis on the channel and shoal dynamics in the German Wadden region. This was the first time I looked at the Wadden islands from a research perspective instead of a recreational perspective and made me hungry for more. Therefore, to finish my Master Earth, Surface, and Water, I delved again into the morphodynamics of the Wadden region, now from a model perspective.

Although I started this master thesis during the corona pandemic in April 2020, I had a lot of fun doing research. Learning new things gave me a lot of energy which was very valuable in world with social restrictions. Of course, writing this thesis was not possible with some help. Above all I want to thank my supervisor Maarten van der Vegt for all the weekly meetings. Thank you for answering my questions, all the research suggestions, and feedback, you were a huge help. I want to thank Laura Brakenhoff for the research about sawtooth bar characteristics and for providing me some scripts. This helped me a lot with the model analysis and your research enabled that I could place my results in perspective. Additionally, I also want to thank Klaas Lenstra for providing me some input of the Delft3D model that you used to model the ebb-tidal delta of Ameland. This helped me a lot to get acquainted with the Delft3D model which resulted in a quick start of my thesis. Last but not least, I want to thank both my supervisors Maarten van der Vegt and Gerben Ruessink for assessing my master thesis. You both inspired me during your lectures about tidal and wave processes and the coupling to the morphodynamics, which made me enjoy my research.

Table of contents

Summary 3

Chapter 1. Introduction 4

Chapter 2. Background 6

2.1 The morphodynamics of ebb-tidal deltas 6
2.2 Sawtooth bars: a literature review 7
2.3 Generation hypotheses 8
2.4 Research questions and objectives 11

Chapter 3. Methodology 13

3.1 Model set-up 13
3.2 The forcing in the study area 18
3.3 Overview model simulations 19
3.4 Model analyses 22

Chapter 4. Results 30

4.1 The influence of the sawtooth bars on the hydrodynamics 30
4.2 The influence of the sawtooth bars on the sediment transport 37
4.3 The relative importance of the forcing mechanisms and bar characteristics for the generation and morphological change of the sawtooth bars 40
4.4 The relative influence of the forcing mechanisms and bar characteristics on the migration speed of the sawtooth bars 45
4.5 Natural bar growth by random small amplitude perturbation 48

Chapter 5. Discussion 55

5.1 Discussion on the causes for bar growth and decay 55
5.2 On the hypotheses regarding sawtooth bar formation 56
5.3 Modelled outcomes compared to observations 58
5.3 Future research 59

Chapter 6. Conclusions 60

Appendix A. Wave data (1994-2014) from the station of Schiermonnikoog 61

References 62

Summary

Sawtooth bars are located at the downstream side of the ebb-tidal deltas in the Dutch and German Wadden Sea. According to Brakenhoff et al. (2019), they are bar patterns with a down contour orientation of ±25° and with a typical wavelength of 300 to 900 meters. Their crest length is 800 to 2200 meters and they occur at a depth between 3 and 12 meters. Sawtooth bars are 0.5 to 2 meters high and migrate between 2 and 112 meters per year. However, the generation mechanism and the morphological evolution of sawtooth bars have not been studied. Therefore, the objective of this study is to clarify the generation mechanism and the morphological drivers of sawtooth bars.

A Delft3D model was set-up in which the modules FLOW and WAVE (SWAN) were used to model the hydrodynamics and morphodynamics in the study area with the forcing of tides, waves, and wind. Two types of simulations were accomplished, simulations with prescribed sawtooth bars and simulations with a random small amplitude perturbation between ±0.25m in which bars could naturally develop. The simulations with prescribed sawtooth bars were accomplished to study the sensitivity of the bar characteristics and forcing mechanisms on the bar dynamics. The simulations with a random small amplitude perturbation, were accomplished to research the feedback mechanisms that result in the natural development of sawtooth bars. These runs were forced by wind, waves, and tides of which only the significant wave height was a variable.

The main results show that the alongshore flow, driven by tides, waves and wind, is altered in its direction and magnitude due to the presence of sawtooth bars. As a result of the flow acceleration on the bar crests and the deceleration in the bar troughs, in combination with the down contour orientation of the bars, the resulting tidally averaged flow pattern attempts to follow the depth contours. This flow pattern results in a sediment transport pattern that causes erosion near the updrift side of the bar crest and deposition near the downdrift side of the bar crest. Sediment transport is mainly caused by the forcing of waves in the sawtooth bar area, which is overall suspended load dominated.

Whether sawtooth bars grow or decay depends primarily on the bar characteristics, the location of the bars and the forcing by waves. Therefore, most runs with prescribed bars resulted in bar decay. This could be concluded with the results of the simulations in which bars could freely develop. In two simulations with random small amplitude perturbation, with an initial significant wave height of 5.67m and 3.5m, bars developed that resembled sawtooth bars. These bars developed in a shallower, lower sloping area on the ebb-tidal delta, compared to the prescribed bars and had slightly different characteristics. Additionally, the results show that an initial significant wave height of 2m is not favourable for bar growth. Lastly, the local mean wave direction on the bars seems to have an influence on the bar growth/decay. Waves that entered the local bar area with a large angle (±90°) ('high-angle waves') between the wave crest and the shoreline trend, resulted in bar growth.

The migration speed of the sawtooth bars increases with an increasing significant wave height, wind speed and tidal amplitude, of which the wave height is the most important factor. Without waves, almost no migration is observed. The migration speed, as quantified from the simulations with prescribed bars, ranges between 161 and 227m/year when scaled to a normal wave climate. This depends on the bar height since higher bars tend to migrate faster, which was also observed by Brakenhoff et al. (2019). However, the migration speeds of the freely developed bars were higher with the same forcing, which is possibly related to the location of the bars. Hence, the outcomes of this study overestimate the yearly migration speed compared to observations.

This study shows that sawtooth bars can be generated by stormy weather with high significant wave heights in combination with local high-angle waves, and that bar decay can be a result of fair-weather conditions. More research is necessary on the generation mechanism to find out what the physical key is for bar growth and decay, but this study gives valuable insights to accomplish this.

Chapter 1. Introduction

The Wadden islands are a mixed energy tide dominated barrier island system in the North Sea along the Dutch, German, and Danish coast (Davis and Hayes, 1984). There are around fifty Wadden islands and they tend to become smaller towards the east. The barrier islands are separated by tidal inlets in which waves tend to close the inlet and the tidal currents keep them open (Wang et al., 2012). The strong tidal flows in the inlet create a deep channel. When ebb-tidal currents flow through the tidal inlet, an ebb-tidal delta forms seaward of the inlet. Vice versa for flood tidal currents, which tend to form a flood tidal delta in the Wadden Sea basin (Figure 1.1).

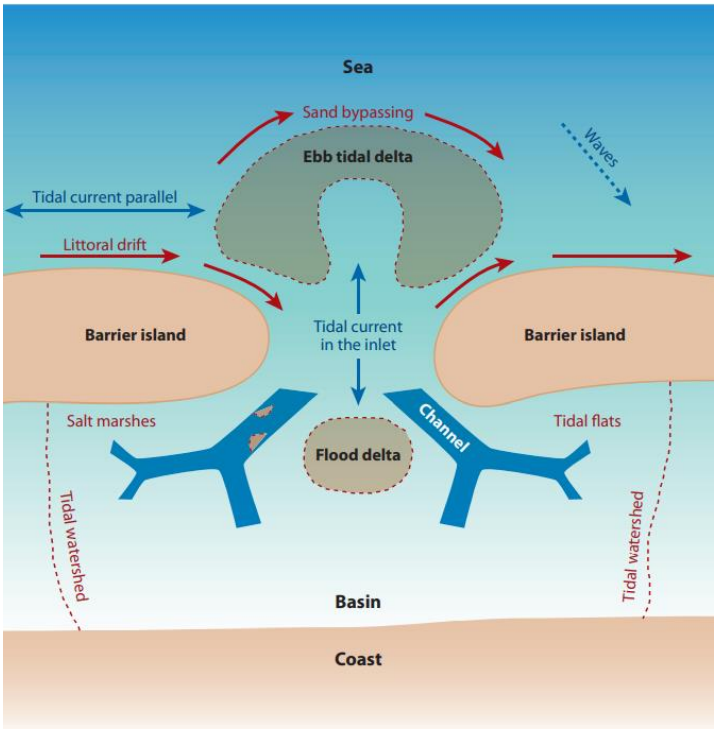

Figure 1.1. *A sketch of the ideal morphology of a tidal inlet system including the main forcing mechanisms of tides and waves (De Swart and Zimmerman, 2009).*

Along the Wadden islands, sediment is transported from west to east by the residual current, generated by wave and tidal forces. This is the littoral drift which results in a general sediment transport pattern on the ebb-tidal deltas from the updrift side, passing the ebb-tidal delta, towards the downdrift side (Figure 1.1.) (De Swart and Zimmerman, 2009; Ridderinkhof et al., 2016).

On the ebb-tidal delta, multiple bar types appear, which are swash bars, ebb-tidal delta shoals and sawtooth bars (Figure 1.2). Swash bars form when waves break on the edges of the ebb-tidal delta. Therefore, their crest orientation is perpendicular to the dominant wave direction. Sometimes these swash bars merge to form large bar complexes, called 'ebb-tidal delta shoals' (FitzGerald, 2000). At the downdrift side of the tidal inlet, sawtooth bars appear at most ebb-tidal deltas in the Wadden Sea (Figure 1.2). Sawtooth bars have a down contour orientation of approximately 25° and a typical wavelength of 300 to 900 meters. Their crest length is 800 to 2200 meters and they occur at a depth between 3 and 12 meters. Sawtooth bars are 0.5 to 2 meters high and migrate between 2 and 112 meters per year. The migration speed differs by location and bars that are higher tend to migrate faster. Additionally, larger ebb-tidal deltas tend to have higher sawtooth bars. However, sawtooth bars are not found at all Wadden inlets. They are absent in the North-West oriented German and Danish inlets (Brakenhoff et al., 2019).

Knowledge about the morphology of sawtooth bars contributes to the understanding of the morphodynamics in the Wadden region which is essential for the management and protection of the system. The impact of environmental changes and human influences, such as sea level rise and sand nourishments, are of great concern since it is a challenge to maintain coastal safety and to protect the morphological and ecological system (Wang et al., 2012).

The characteristics of sawtooth bars in the Wadden Sea were studied by Brakenhoff et al. (2019). However, it has not been researched what drives their morphology and how they are generated since

there are no earlier studies accomplished with this objective. Therefore, the aim of this research is to clarify the generation mechanism and the morphological drivers of sawtooth bars.

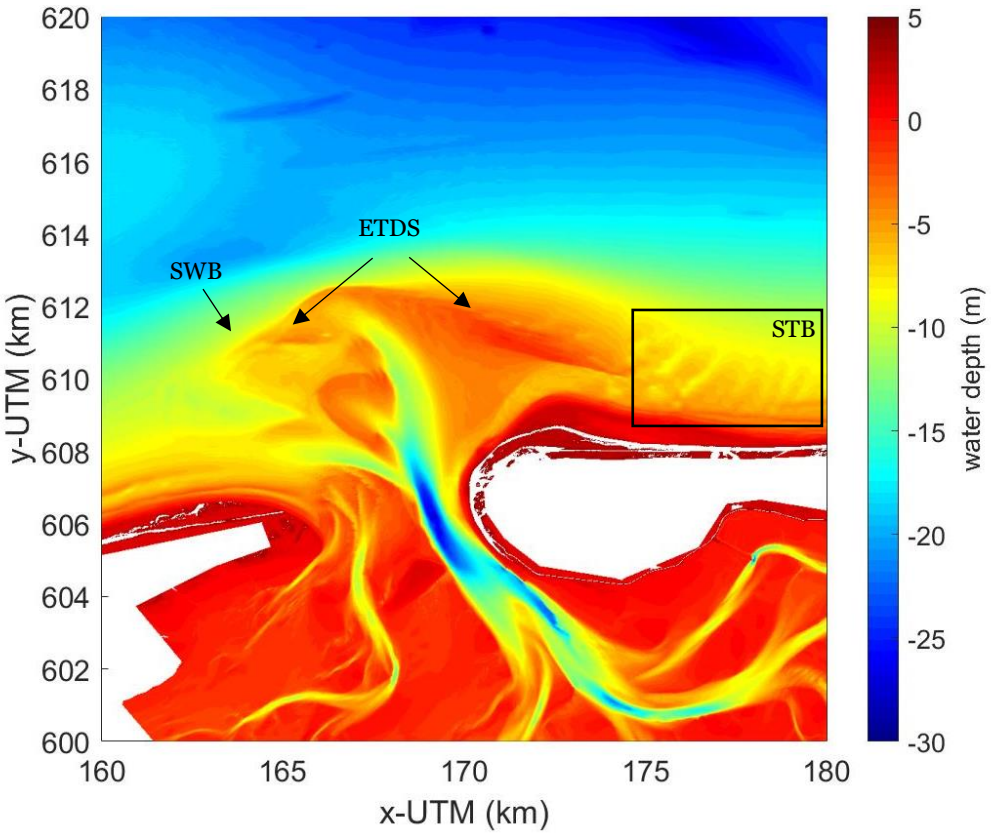

Figure 1.1. *The bathymetry of the Ameland Inlet between Terschelling (west) and Ameland (east) in 2011. The sawtooth bars are visible in the black square (STB). The ebb-tidal delta shoals (ETDS) and the swash bars (SWB) are highlighted by the arrows.*

Chapter 2. Background

2.1 The morphodynamics of ebb-tidal deltas

Ebb-tidal deltas are morphologically highly dynamic due to the forcing of tides and waves. The morphology of each ebb-tidal delta depends on the cooperation between the tidal currents and wave-driven currents (Sha, 1989). Obliquely incident waves break close to the shore and thereby create an alongshore current. This current results in an alongshore sediment transport that tends to make the cross-sectional area of the inlet smaller or even close the system (De Swart and Zimmerman, 2009). The tide, on the other hand, generates a cross-shore tidal current inside the inlet and an along shore tidal current along the inlet. When the cross-sectional area of the inlet is reduced by waves, the cross-shore tidal current becomes larger. This is because the same volume of water must go through the inlet between ebb and flood, known as the tidal prism. This results in a cross-sectional area that tends to reach a stable equilibrium (Escoffier, 1940).

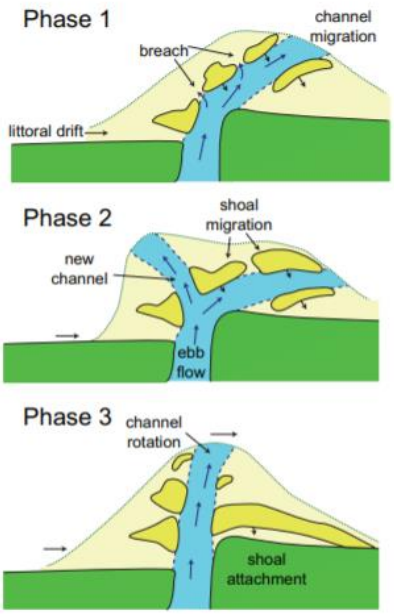

Figure 2.1.1. *The conceptual model 'ebb-tidal delta breaching' of FitzGerald (1988) showing the cyclic behaviour of shoals on ebb-tidal deltas.*

The orientation of the main ebb-tidal channel is determined by the relative magnitude of the wave energy and the phase difference between the alongshore tidal current and the cross-shore tidal current. For the Wadden islands, the tidal wave propagates from west to east. This results in an alongshore flood current towards the east and an alongshore ebb-current towards the west. Tides in the inlets of the Wadden islands have a standing wave character because of their short basin. Therefore, the tidal currents cross-shore and alongshore are in phase. With zero degrees phase difference between the cross- and alongshore tidal currents, the flow at max ebb is directed against the wave direction (west) and so is the orientation of the channel. This is only the case when the western waves are not significant relative to the tidal currents and is seen at most Dutch inlets. When the waves from the west are more significant relative to the tide, the channel is forced to have its orientation towards the east. This is seen at the German inlets where the tidal prisms are smaller and so the cross-shore tidal currents (Sha, 1989; Sha and van den Berg, 1993).

The orientation of the main inlet channel is not completely static but shifts in position due to the formation of shoals on the ebb-tidal delta. For example, the Ameland Inlet channel orientation shifts roughly from west towards the east. However, note that its main orientation stays towards the west. Towards the east, the channel size decreases until the channel disappears and a new channel forms in the west. In this cycle, swash bars and shoals form on the ebb-tidal delta, migrate towards the east and attach to the downdrift island (FitzGerald et al., 1988; Lenstra et al., 2019). FitzGerald et al. (1988) created conceptual models that visualise this cyclic behaviour for different inlet types. The Ameland inlet shows similar behaviour compared to the conceptual model 'ebb-tidal delta breaching' which is visualised in Figure 2.1.1. This cyclic behaviour of sandy shoals that appear and attach to the downdrift island is observed at most ebb-tidal deltas in the Wadden sea. The duration between two successive shoal attachments ranges between 4 and 130 year which varies per tidal inlet. Overall, a larger tidal prism results in a longer duration time between two successive shoal attachments when only one tidal channel is present in the inlet (Ridderinkhof et al., 2016).

2.2 Sawtooth bars: a literature review

Sawtooth bars are symmetric bars at the downdrift side of most Wadden inlet systems of which the characteristics and correlations between the characteristics were studied by Brakenhoff et al. (2019). The time scale of the formation and growth of the sawtooth bars is 2 to 5 years and the bars are present at almost each Dutch and German tidal inlet system with a well-developed ebb-tidal delta. Figure 2.2.1 shows the 9 inlets where sawtooth bars are present. The characteristics of the bars are in depth described below, and an overview is given in Table 2.2.1.

Figure 2.2.1. *The Wadden Sea tidal inlet systems where sawtooth bars are present. 1 Texel Inlet, 2 Vlie Inlet, 3 Ameland Inlet, 4 Frisian Inlet, 5 Osterems, 6 Norderneyer Seegat, 7 Accumer Ee, 8 Otzumer Balje Inlet, 9 Harle Inlet.*

The bar heights between the inlets decrease towards the east and ranges between 0.5 and 2 meters. At each individual inlet, the bar height stays approximately the same over the ebb-tidal delta but can vary in time. For example, the growth and decay cycle of sawtooth bars at the Ameland inlet took approximately 10 years. This cycle was also observed at other inlets, but they did not take place simultaneously. The cycle durations are shorter for bars at the German inlets. It was observed that the bars even disappeared for an amount of time and reappeared within a few years. Additionally, the bar height is negatively correlated to the slope of the area, meaning that the smaller the slope of the area the higher the bars. Lastly, the bar height is positively correlated to the orientation of the area. The orientation of the area is the angle between the depth contour lines and the north. So, a larger angle corresponds to a higher sawtooth bar.

The wavelengths vary between 313 and 909m with an average of 672m. The median wavelengths decrease from the Vlie inlet towards the east. However, the Texel inlet, which is the most western inlet next to the Vlie inlet shows the smallest median wavelength of 400m. At each inlet, the wavelength is varying on the same multiannual time scale as the bar height, but the maximum heights and wavelengths do not occur simultaneously.

The orientation of the sawtooth bars, calculated as the angle between the bar crest and the mean orientation of the area, is ranging between ±20° and ±82°, of which 66° is the average. The bar orientation is not changing in time.

The sawtooth bar crest length ranges between 800 and 2200 m and increases towards the east for the Dutch inlets. However, for the German inlets the bar crest length decreases from the western

towards the eastern inlets. The bar crest tends to be shorter with a steeper bed slope or a more oblique orientation. Additionally, bars with a larger wavelength tend to have longer crest lengths.

Table 2.2.1. *Sawtooth bar characteristics as studied by Brakenhoff et al. (2019).*

Morphology feature	Magnitude
Height	0.5-2 m
Wavelength	300 – 900 m
Orientation (angle between the depth contour lines and the bar crest)	20° - 82°
Crest length	800 – 2200 m
Depth of occurrence	3 – 12 m
Migration speed	2 - 112 m/year

The Bars occur at depths between 3 and 8 meters at the landward side and between 5 and 12 meters at the most seaward side. Bars that emerge deeper also reach deeper at their seaward end. The depth of occurrence is related to the steepness of the transverse slope. When the slope is steeper the bars start at a shallower location and end at a deeper location, compared to a gentler slope. There is also a relation with the wavelength. When bars occur deeper, they tend to have longer wavelengths.

The migration speed varies enormously among the ebb-tidal deltas, between 2 and 112m/year (30m/year on average). For example, the migration speeds are relatively large at the Ameland and Harle inlet and relatively small at the Accumer Ee Inlet and the Norderneyer Seegat. Additionally, bars that are higher, tend to migrate faster. On top of that, the steeper the transverse slope, the larger the migration speed.

2.3 Generation hypotheses

2.3.1 Generation mechanisms of similar bar features

It is valuable to look at generation mechanisms of similar bar features, to formulate the hypothesis about the generation mechanism of sawtooth bars (Section 2.3.2). When looking at the characteristics of sawtooth bars, they are most similar to tidal sand waves and shoreface-connected sand ridges. The generation mechanisms of these bars are explained below, together with the concept of 'high-angle wave instability' which can result in downdrift oriented shoreline shapes.

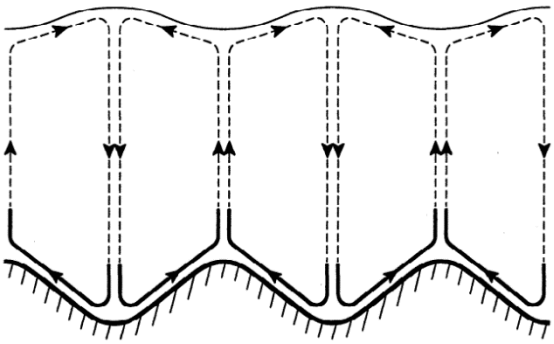

Figure 2.3.1.1. *The recirculation cells which result in the generation of sand waves. The near-bed flows are stronger and result in growth of the sand waves. The backward flow in the upper part of the water column is weaker because it is averaged over a larger amount of water (Hulscher, 1996).*

Tidal sand waves

Tidal sand waves are similar to sawtooth bars in wavelength (±500m) and bar height (±3m), but they occur at depths in the order of 30 meters, migrate only several meters a year, and their crest orientation is perpendicular to the main tidal current (Németh et al., 2002;

Hulscher, 1996). The morphological time scale of tidal sand waves is ±10 years, which is in the same order of magnitude as sawtooth bars (Hulscher, 1996; Knaapen and Hulscher 2002; Besio et al., 2008).

Tidal sand waves form due to the instability between the oscillatory tidal current and the flat bed. The bottom friction and the oscillatory tidal current generate vertical recirculating cells in the water column (Figure 2.31.1). The steady relatively strong velocity component near the bottom drags the sediment from the troughs towards the crest and the gravity causes the sediment to go from the crest towards the trough. The compensating flow in the upper part of the water column results in almost no sediment transport because this flow is averaged over a larger amount of water and is therefore weaker. Secondly, there is hardly any sediment so high up in the water column (Hulscher, 1996). The growth of the sand waves depends on the balance between the gravity and the strength of the near-bed flows. The migration is caused by the residual current (Besio et al, 2006; Blondeaux and Vittori, 2011) and the wavelength is decreasing with increasing tidal velocities and grain sizes (Van Santen et al., 2011).

Shoreface-connected sand ridges

Shoreface-connected sand ridges (SCR) show similarities with sawtooth bars in terms of the depth occurrence (4-20m) and height (1-6m). Only the wavelengths of the SCR are much larger, in the order of 5 kilometres as well as the length of the ridge crests, which are between 10 and 25 km. Additionally, the growth of the ridges takes place on very large time scales, in the order of 10^3 years, which is not similar to sawtooth bars. The migration speed on the other hand, is much smaller compared to sawtooth bars, in the order of 1 to 10m/yr and their orientation is different. Sawtooth bars have a downdrift orientation with respect to the local depth contours while SCR are updrift oriented (20°-25° with respect to the coastline) (Falques et al., 1999; Calvete et al., 2001).

The SCR form due to the transverse sloping bottom that generates a deflection of the alongshore current over the bars which results in a decrease in sediment transport capacity towards deeper water

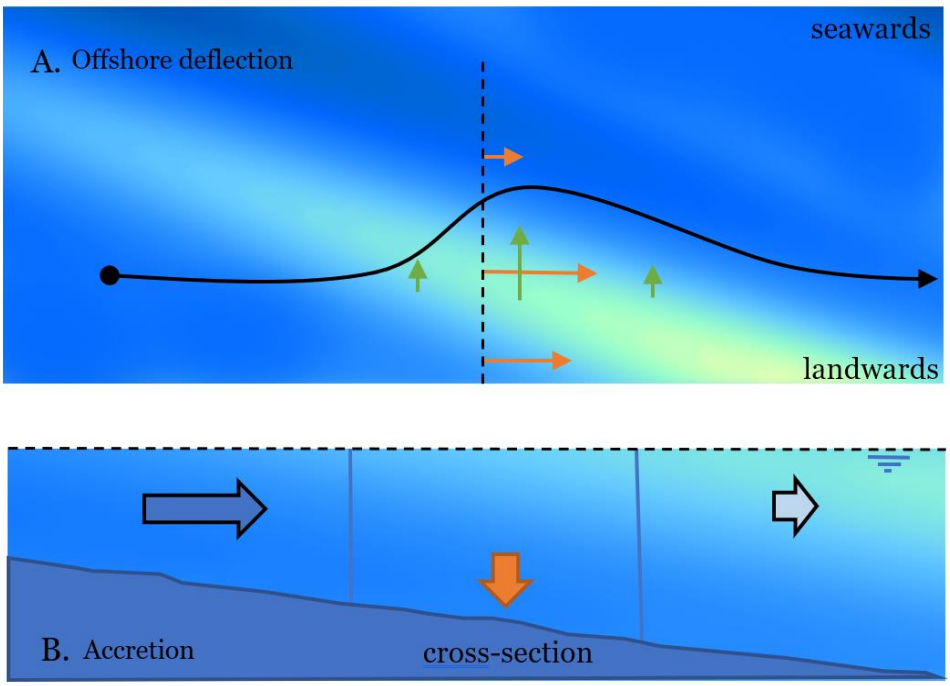

Figure 2.3.1.2. *The generation mechanism of SCR.* ***A)*** *The alongshore current is deflecting offshore over the ridge,* ***B)*** *resulting in a decrease in sediment transport capacity into deeper water. Therefore, sediment is deposited on the ridge (Calvete et al., 2001).*

(Trowbridge, 1995; Falques et al., 1999; Calvete et al., 2001). The deflection of the alongshore current is caused by the increase in flow velocity on the crest of the SCR due to the conservation of mass. The magnitude of the velocity change when crossing the ridge depends on the relative depth change. Therefore, the flow is stronger in the shallow area at the inner flank of the ridge compared to the deep outer flank (Figure 2.3.1.2.a, orange arrows) which results in an offshore deflection of the current (Figure 2.3.1.2.a, green and orange arrows summed). The resulting cross-shore velocity decay over the ridge crest causes a decrease in sediment transport capacity towards deeper water, and therefore accretion takes place on the ridge (Figure 2.3.1.2.b). This theory was first derived by Trowbridge (1995).

SCR grow due to storm driven alongshore currents and their generation is mainly related to suspended sediment, whereas the migration is related to bed load transport (Calvete et al., 2001). The growth rate and the spacing between the ridges is related to the relative contribution of the wind and the longshore pressure gradient which are both factors that determine the magnitude of the alongshore current. With an increasing wind force, the spacing increases but the growth rate decreases (Falques et al., 1999). Lastly, the growth rate, migration speed and spacing are all decreasing with an increasing transverse slope, but the slope must be higher than the critical value of $0.05 \cdot 10^{-4}$ (Calvete & De Swart, 2003).

High-angle wave instability

The mechanism 'High-angle wave instability' can result in downdrift oriented shoreline shapes. Waves that enter the near shore with a large angle (>45°) between their crests and the shoreline are called 'high-angle' waves. When high angle waves enter a straight shoreline with a single bump, the alongshore transport is strongest on the updrift side of the bump and decreases in magnitude towards the downdrift side (Figure 2.3.1.3.b). Due to the decrease in magnitude of the alongshore transport,

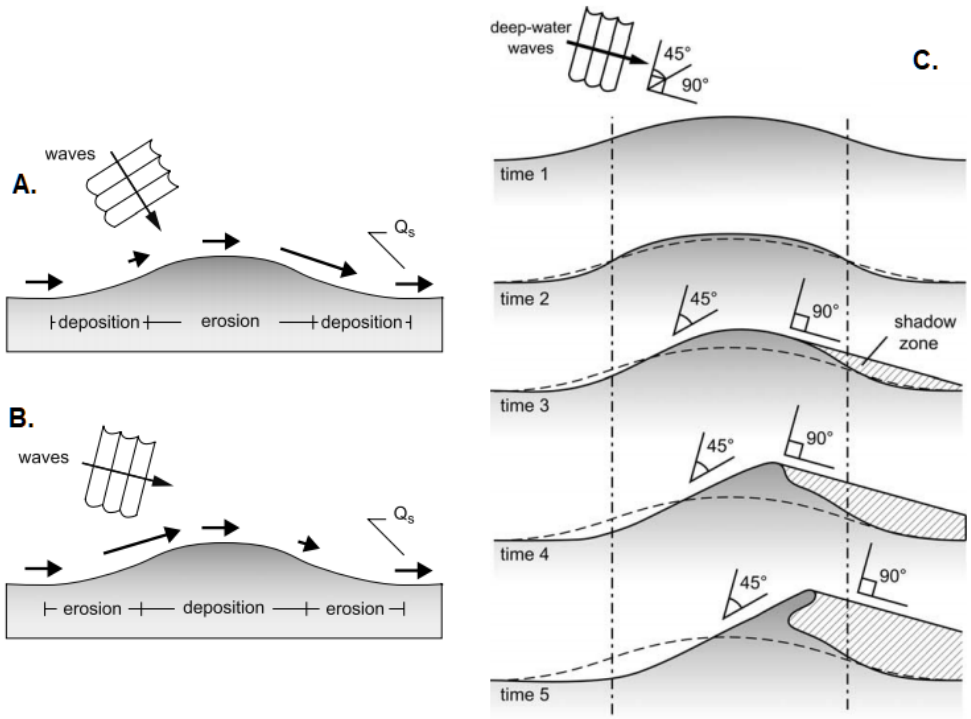

Figure 2.3.1.3*. The high-angle wave instability mechanism as described by Ashton and Murray (2006). The black arrows are the alongshore transport (Q_s). **A)** The response of a straight shoreline with a single bump due to low-angle waves (<45°). **B)** The response of a straight shoreline with a single bump due to high-angle waves (45°>). **C)** The shore-line evolution affected by waves with a constant high angle.*

deposition takes place on the bump which can develop in a so-called spit extension. The zone that is shadowed from direct wave impact is called the shadow zone (Figure 2.3.1.3.c). In contrast, when low angle waves (<45°) approach a straight shoreline with a single bump, erosion takes place on the bump and it will flatten over time (Figure 2.3.1.3.a).

2.3.2 Generation hypotheses for sawtooth bars

It was hypothesised by Brakenhoff et al. (2019) that sawtooth bars are a type of sand waves, forced by tidal and wave-driven currents. Along the Wadden islands a decreasing sawtooth bar wavelength is observed towards the east. This could be related with the tide since the tidal amplitude increases in easterly direction. Therefore, it is hypothesised that sawtooth bars are a type of tidal sand waves, since it is observed that the wavelengths of tidal sand waves are smaller for larger tidal currents. Additionally, since no simultaneous bar growth was observed for sawtooth bars between different inlets during storms, it is even more likely that the generation mechanism is similar to the generation mechanism of sand waves since SCR are generated during storms.

Secondly, it was hypothesised by Brakenhoff et al. (2019) that sawtooth bars are generated by the instability mechanism resulting from 'high-angle waves'. The observations show that the bar height has a linear relation with the orientation of the area. The orientation of the area is dependent on the shoals that form, migrate on the ebb-tidal delta and attach to the downdrift island, which results in a changing orientation of the depth contours over time. This suggest that the shoal cycle is playing an important role in the formation of the sawtooth bars. When a shoal is almost attached to the downdrift island, the orientation angle of this local area is changing, so that north-western waves enter this local area almost parallel to the depth contours. These 'high angle waves' are known to create an instability as explained in Section 2.3.1 which might be suitable for the generation of sawtooth bars. The disappearance of sawtooth bars towards the east along each island might be due to the absence of shoals that result in this instability. This could also be the cause for bar decay when the shoals are completely attached to the downdrift island. On top of this, the bar wavelength and height might be decreasing in easterly direction due to the ebb-tidal deltas that become smaller towards the east. A smaller ebb-tidal delta contains smaller migrating shoals and so a smaller shadow zone in which sawtooth bars can develop. Additionally, the average period between two successive shoal attachments becomes shorter for inlets towards the east (Ridderinkhof et al., 2016). A shorter cycle might result in a shorter time span in which the sawtooth bars can grow.

2.4 Research questions and objectives

The general aim of this research is to clarify the generation mechanism and the morphological drivers of sawtooth bars. No earlier studies were accomplished with this aim and no earlier modelling studies were achieved on sawtooth bars. So, very little is known about the interaction between the bars and the hydrology, the sediment transport patterns on the bars and the cause for bar migration, growth, and decay. These research gaps are subdivided in five research questions, starting with the flow and sediment transport patterns.

(1) *What is the influence of the sawtooth bars on the hydrodynamics and how is this depending on the characteristics of the bars and the forcing mechanisms?*

(2) *What is the influence of the sawtooth bars on the sediment transport and how is this depending on the characteristics of the bars and the forcing mechanisms?*

These questions focus on the different forcing mechanisms that result in the overall flow and sediment transport patterns on the bars, which are wind, waves, and tides. The forcing mechanisms all play a separate role in the spatial change in flow and sediment transport in the sawtooth bar region. The hydrodynamics and sediment transport patterns are studied to gain knowledge about how they

interact with the bars. The individual and cumulative effects of the forcing mechanisms and the effect of different bar characteristics are considered.

Sediment transport patterns can reveal the areas were erosion or deposition might take place, which in time, can result in bar growth or decay. This leads to research question *(3)*.

(3) What is the relative importance of the forcing mechanisms and bar characteristics for the generation and morphological change of the sawtooth bars?

The objective of this question is to look at the location of the erosion and depositional areas and the amount of bar growth/decay over a certain amount of time. If the location of the depositional area is far from the bar crest, bar decay might occur and if it is close to the bar crest, bar growth might occur. To answer this research question, it is analysed how each forcing mechanism and bar characteristic is related to the location of the erosional/depositional area and the amount of bar growth/decay.

When the depositional/erosional area is not exactly on the bar crest/trough, the bars migrate, which leads to research question *(4)*.

(4) *How are the bar characteristics and forcing mechanisms influencing the migration speed of the sawtooth bars?*

The objective of this research question is to find the relationship between different forcing parameters (wind speed, wave height etc.) and the migration speed, and to find the relationship between the bar characteristics and the migration speed.

The above four research questions are focussing on the flow and sediment transport patterns and the morphological change when sawtooth bars are present. In contrast, the next research question aims to research the natural growth of sawtooth bars, with the use of a small random perturbation of the bed.

(5) How and what kind of bars are developing for a system with random small amplitude perturbation, driven by different forcing parameters?

The development of this unstable bed might result in sawtooth bars with the use of the 'correct' combination of forcing mechanisms, which is obtained from the answers on the previous research questions. The objective is to quantify the characteristics and the migration speeds of the freely developed bar patterns and to analyse if they resemble sawtooth bars or not and why. This also includes the feedback mechanisms that result in the establishment of the bars.

Each research question is answered in a separate section in Chapter 4, in the same order. In Chapter 5 the answers to all the research questions are combined to discuss whether the hypotheses on the generation of sawtooth bars formulated by Brakenhoff et al. (2019) were correct. Additionally, the outcomes of this study are compared to the observations as described in Section 2.2.

Chapter 3. Methodology

3.1 Model set-up

The aim of this research is achieved by a model approach. A depth average Delft3D model was set-up in which the modules FLOW and WAVE (SWAN) were used to model the hydrodynamics and morphodynamics of the study area. The Delft3D model is a process-based numerical model that solves the momentum balance, the water mass conservation, wave-action balance for waves (SWAN) and is coupled to a sediment mass balance and a sediment transport predictor to model the morphological evolution.

3.1.1 The hydrodynamics

(1) Currents

The currents were modelled with the FLOW-module, in which the shallow water equations and continuity equation were solved in two dimensions.

$$\frac{\partial u}{\partial t} + u\frac{\partial u}{\partial x} + v\frac{\partial u}{\partial y} - fv = -g\frac{\partial \eta}{\partial x} - \frac{\tau_x}{\rho h} + \frac{F_{w,x}}{\rho h} + \frac{1}{h}\left[\frac{\partial}{\partial x}\left(A\frac{\partial u}{\partial x}\right) + \frac{\partial}{\partial y}\left(A\frac{\partial u}{\partial y}\right)\right] \quad 3.1.1.1a$$

$$\frac{\partial v}{\partial t} + u\frac{\partial v}{\partial x} + v\frac{\partial v}{\partial y} + fu = -g\frac{\partial \eta}{\partial y} - \frac{\tau_y}{\rho h} + \frac{F_{w,y}}{\rho h} + \frac{1}{h}\left[\frac{\partial}{\partial x}\left(A\frac{\partial v}{\partial x}\right) + \frac{\partial}{\partial y}\left(A\frac{\partial v}{\partial y}\right)\right] \quad 3.1.1.1b$$

$$\frac{\partial h}{\partial t} + \frac{\partial (hu)}{\partial x} + \frac{\partial (hv)}{\partial y} = 0 \quad 3.1.1.2$$

Here, the flow velocities in the x- and y-direction are represented by u and v, t is the time, f the Coriolis parameter, g the gravitational acceleration, h the local water depth, ρ the density of water, η the water level with respect to the still water level, $F_{w,x}$ and $F_{w,y}$ are the wave induced forces, τ_x and τ_y are the shear stress components and A represents the horizontal eddy viscosity of 5m²/s. The terms on the left-hand side of Equation 3.1.1.1a and 3.1.1.1b represent inertia, advective acceleration and the Coriolis force. The terms on the right-hand side represent the pressure force, the shear stresses for wind, waves and currents, the wave-induced forces per surface area (computed by the WAVE-module) and turbulence. The continuity equation (Equation 3.1.1.2) is for incompressible fluids and therefore equal to zero.

The shear stress components τ_x and τ_y are a result of the shear stress by waves, currents, and wind. The shear stress formulation for waves and currents was used according to the model of Van Rijn et al. (2004) which was computed with the parameterization of Soulsby et al. (1993). The bottom stress was formulated with a uniform Chézy coefficient of 65m$^{1/2}$ s^{-1}. The shear stress by wind was defined as:

$$|\vec{\tau_s}| = \rho_a C_d U_{10}^2 \quad 3.1.1.3$$

In which ρ_a is the density of air, U_{10} is the wind speed 10 meter above the free surface (time and space depended) and C_d is the wind drag coefficient dependent on U_{10}. The wind drag coefficient was 0.00055 with a wind speed of 0m/s and 0.0018 with a wind speed of 20m/s (Zijlema et al., 2012). The drag coefficient for a specific wind speed in between 0 and 20m/s was calculated with a linear interpolation between these two specified drag coefficients. The wind speeds were spatially uniform and entering the area from the west (-90°) which is one of the dominant wind directions in the

Wadden area (KNW atlas). The wind speeds itself were varied for several model runs, as can be seen in the overview of the model simulations (Section 3.3).

(2) Waves

The wave-induced forces per surface area, used in Equation 3.1.1.1.a and b, are calculated by the WAVE-module with the third-generation SWAN wave model (acronym for Simulating WAves Nearshore) (Rooij et al., 1999). The SWAN model computes the evolution of waves in all water depths and with present currents by solving the wave action balance equation in the spectral and directional domain using the action density spectrum $N(\sigma,\theta)$.

$$\frac{\partial}{\partial t}N + \frac{\partial}{\partial x}c_x N + \frac{\partial}{\partial y}c_y N + \frac{\partial}{\partial \sigma}c_\sigma N + \frac{\partial}{\partial \theta}c_\theta N = \frac{S}{\sigma} \qquad 3.1.1.4$$

Here, c_x and c_y are the wave group velocity components, σ is the relative frequency (as observed in a frame of reference moving with the current velocity, with propagation velocity c_σ in σ-space), θ is the wave direction and S represents the generation, dissipation, and redistribution of wave energy. Note that the $N = E/\sigma$, where E is the energy density spectrum. The terms on the left-hand side of Equation 3.1.1.4 represent the local rate of change of N in time, the propagation of wave energy in the x- and y-direction, the change in relative frequency due to currents and depth variation and the refraction due to spatial gradients in currents or water depth. The right-hand side of the formula represents the sources & sinks, which for this study includes the breaking of waves (according to Battjes and Janssen (1978) with α =1 and γ = 0.73), whitecapping (according to Van der Westhuysen et al. (2007)), bottom friction (according to the JONSWAP model with coefficient 0.067 m^2s^{-3} (Hasselmann et al., 1973)) and wind growth. The transfer of wind energy to the waves is formulated as a resonance mechanism (according to Phillips (1957)) in combination with a feed-back mechanism (according to Miles (1957)).

The depth averaged wave-induced forces per surface area are computed following Dingemans et al. (1987) with the dissipation rate.

$$F_{w,x} = D\frac{k_x}{\omega} \qquad 3.1.1.5.a$$

$$F_{w,y} = D\frac{k_y}{\omega} \qquad 3.1.1.5.b$$

Here, D is the dissipation rate due to bed friction, whitecapping and wave breaking, calculated with the use of the wave-action balance. k_x and k_y are the wave numbers in the x- and y-direction and ω is the wave frequency. The dissipation rate is computed by SWAN and communicated every hour towards the FLOW-module. This is necessary to consider the wave-current interaction.

3.1.2 Sediment transport and bed level evolution

Sediment can be transported as bed load or suspended load. Below a certain reference height sediment is modelled as bed load transport and above as suspended load transport. Both types are divided into transport due to currents and transport due to waves. For this study, the bed load transport was calculated using the equation of Van Rijn et al. (2007a) and the suspended load transport was calculated using Van Rijn et al. (2007b). The bed load transport was altered to include also gravitational bed-slope effects.

The sediment concentration required to compute the suspended sediment transport by currents is calculated by solving a depth average advection-diffusion equation.

$$\frac{\partial(hc)}{\partial t} + \frac{\partial(huc)}{\partial x} + \frac{\partial(hvc)}{\partial y} - D_H\left[\frac{\partial}{\partial x}\left(h\frac{\partial c}{\partial x}\right) + \frac{\partial}{\partial y}\left(h\frac{\partial c}{\partial y}\right)\right] = w_s(c_{eq} - c) \qquad 3.1.1.6$$

Here, c is the depth integrated sediment concentration, c_{eq} is the equilibrium concentration (depends on the skin friction due to the currents and waves), D_H is the horizontal eddy diffusivity of 1m²/s and w_s is the hindered settling velocity (depending on the median grain size (D_{50})). The term 'hindered' means that it incorporates the effect that particles can hinder each other when attempting to settle. The terms on the left-hand side of Equation 3.1.1.6 represent the change in depth-integrated sediment concentration over time, advective transport in both directions and diffusive transport in both directions. The terms on the right-hand side represent the sediment exchange between the bed and the water column. For this study no suspended sediment was transported by waves, since this would give the best results according to Deltares (2014).

The sediment transport is calculated with the use of the bed shear stress components (τ_x and τ_y), the depth average flow velocities and the sediment characteristics. For this study, a uniform sediment layer with a median sediment diameter (D_{50}) of 250µm, a specific density of 2650kg/m³ and a dry density of 1600kg/m³ was used. A D_{50} of 250µm was chosen for simplicity but is somewhat coarse for the Wadden system (Herling and Winter, 2018; Son et al., 2011). However, for a model study, this median grain size is a good representation of the morphology around Ameland inlet and is therefore used (Lenstra et al., 2019).

The change in bed elevation ($\frac{\partial Z_b}{\partial t}$) is calculated with a sediment mass balance and is updated at each computational time-step, which was for this study 0.2 minutes.

$$\frac{\partial Z_b}{\partial t} = -\frac{M}{1-p}\left(\frac{\partial q_{b,x}}{\partial x} + \frac{\partial q_{b,y}}{\partial y} + w_s(c_{eq} - c)\right) \qquad 3.1.1.7$$

Here, $q_{b,x}$ and $q_{b,y}$ are the bed load transport components by waves and currents in the x- and y-direction, $w_s(c_{eq} - c)$ is the suspended load transport, P is the porosity and M is the morphological acceleration factor that determines the speed of the morphological changes. For this study, the morphology started to change after 48 hours of spin-up time in which other calculations are proceeded as normal.

3.1.3 Grids and boundary conditions

The equations for the hydrodynamics and morphology are solved numerically on staggered grids. The wave-related equations are solved on a grid used in the WAVE-module, and the current and morphology related equations are solved on a grid used in the FLOW-module. Both grids have their own boundary conditions.

❖ FLOW-grid and boundary conditions

The grid used in the FLOW-module was based on cartesian coordinates and split into two domains, the outside 'coarse' domain with a grid cell size of 210m and the inside 'fine' domain with a grid cell size of 70m. The outer domain contained three boundaries: North, West and East (Figure 3.1.3.1). East and West were defined as Neumann boundaries (alongshore water level gradients) and North was defined as a water level boundary. All boundaries were astronomically forced by the tide, using only the S_2 tidal constituent for simplification. Although, the M_2 tide is the dominant tidal constituent in the North Sea (Kvale, 2006), the S2 tide was used to make the postprocessing easier due to its exact period of 12 hours.

The tide was prescribed by setting the phase, amplitude, and water level gradient at the boundary corners. For the northern water level boundary, western corner, the phase of the tidal wave was set to 0°. The phase at eastern side was determined by calculating the wavelength of the tidal wave with $\lambda_t = C_t T$. Where λ_t is the wavelength, C_t is the propagation speed and T is the tidal period. Since a tidal wave can be seen as a shallow water wave near the coast, the propagation is given by $\sqrt{gh}$. Here, h is the water depth along the northern boundary. Knowing the distance between the eastern and western boundaries and the wavelength of the tidal wave, the phase could be calculated by dividing them and multiplying by 360°. The phase of the Neumann boundaries is +90° the phase of the water level

boundaries. So, the northern and southern corner of the western Neuman boundary is 90°. The alongshore water level gradient set at each of the corners was calculated with $\frac{2\pi}{\lambda_t} a_t$, in which a_t is the tidal amplitude. At the land boundaries, no normal flow is allowed.

❖ WAVE-grid and boundary conditions

For the Delft3D WAVE module, a nested grid was used to be able to model the sawtooth bars in detail. The coarse outside grid had a grid cell size of 210m by 210m and the fine inner grid had a grid cell size of 70m by 70m. The created grids were rectangular and based on cartesian coordinates (Figure 3.1.3.2).

Three boundaries were defined containing the same conditions (north, east, and west) (Figure 3.1.3.2). The conditions along the boundaries were uniform and consisted of the significant wave height, the mean wave period (T_{m01}), the wave direction, and the directional spreading. The latter is the

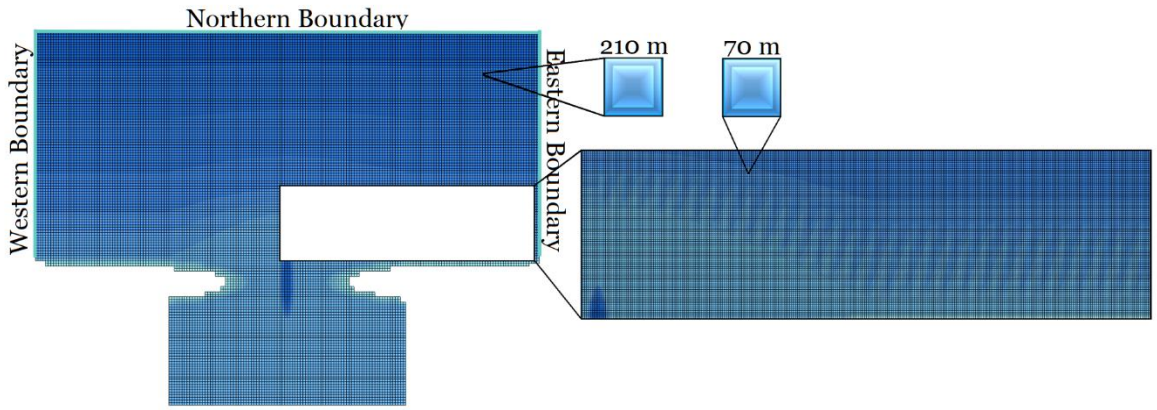

Figure 3.1.3.1. *Outer (left) and inner (right) domain grid of the Delft3D-FLOW module. The outer domain has a grid cell size of 210m by 210m and the inner domain has a grid cell size of 70m by 70m. The boundaries of the outer domain are also presented (the northern, eastern, and western boundary).*

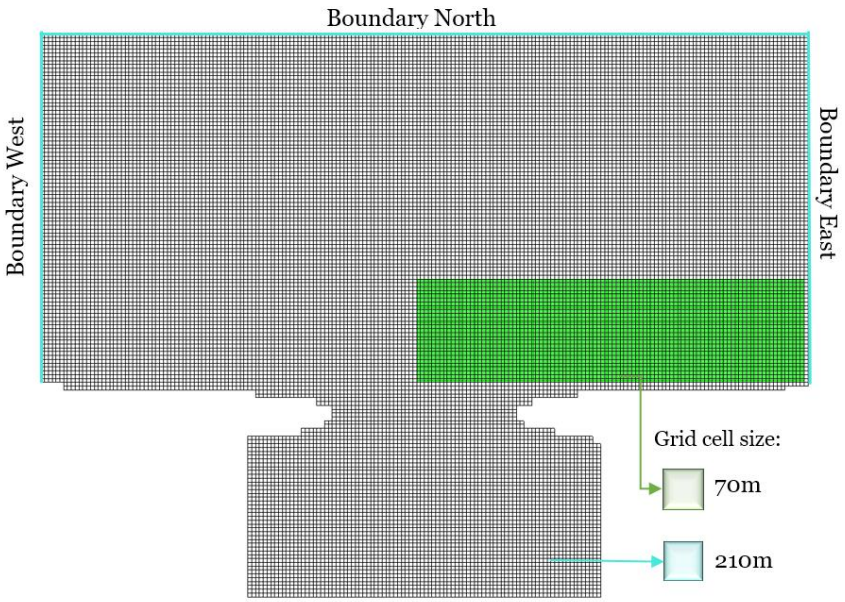

Figure 3.1.3.2. *The nested computational grids of the Delft3D-WAVE module. The coarse grid has a grid cell size of 210m by 210m, and the nested fine grid has a grid cell size of 70m by 70m. The boundaries are also presented (north, east, and west).*

directional standard deviation expressed in a cosine power, which is 4 for all the runs. The wave height, mean period and wave direction vary for several model simulations as can be seen in the simulation overview (Section 3.3). The shape of the wave spectrum is defined as a JONSWAP type of spectrum with a peak enhancement parameter of 3.3. The spectral wave direction covers a full circle with 24 directions and the incoming waves have a frequency between 0.05Hz and 1Hz divided in 18 bins.

3.1.4 The bathymetry input

All the bathymetries used as input were based on an ideal ebb-tidal delta inlet system with an inlet of 3.5km wide, a straight tidal channel and a basin depth of 3 meters (Figure 3.1.4.1). The basin depth was chosen to be uniform for the sake of simplicity.

Sawtooth bars were added in the bathymetry to answer research question 1 to 4, which are focussing on the processes that take place due to the presence of sawtooth bars. They were added between the -5m and -9m depth contours at the downdrift side of the tidal inlet. The bar height, wavelength and orientation were varied per model run which is specified in the overview of the model simulations (Section 3.3). In Figure 3.1.4.1 an example is given of an input bathymetry with sawtooth bars that are 3 meter high, have a wavelength of 700m and an orientation of 14° with respect to the north. Additionally, a bathymetry without bars was made to be able to isolate the effects of the bars on hydrodynamics, sediment transport and morphological change.

To answer research question 5, focussing on the natural growth of sawtooth bars, random small amplitude perturbation between ±0.25m was added to the bathymetry between the -5m and -9m depth contours on the downdrift side of the ebb-tidal delta.

The bathymetries were made in Matlab (.mat files) and were then converted to sample files (.xyz). The depth files were created in the pre-processing program QUICKIN by combining the sample files and computational grids. These files could be used as depth input for the Delft3D FLOW- and WAVE-module.

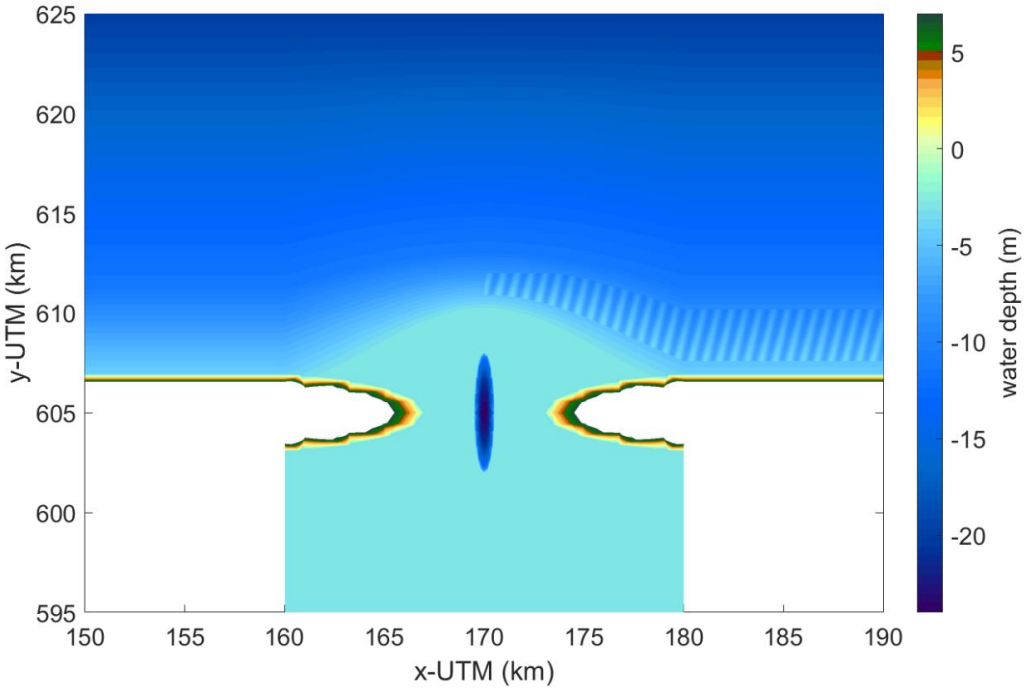

Figure 3.1.4.1. *The bathymetry of the ebb-tidal delta including sawtooth bars with a wavelength of 700m a hight of 3m and an orientation of 14° with respect to the north.*

3.2 The forcing in the study area

In the Wadden region the tidal, wave and wind forcing varies spatially and temporally. The model parameters of the tidal amplitude, wave height, wave direction, wave period, wind speed and wind direction were selected based on these variations.

The M2 tidal constituent is most dominant tidal constituent in the North Sea which results in roughly two tidal cycles a day (Kvale, 2006). The mean tidal range increases from 1.4m near the Texel inlet to 2.5m near Osterems and is 3m near the Harle inlet (Elias et al., 2012; Balke et al., 2016). The increase in tidal range towards the east in the Wadden region is caused by the tidal Kelvin wave that travels in an anti-clockwise direction around the two amphidromic points in the North Sea. At the amphidromic points the tidal range is zero, which is roughly between England and Denmark and between England and The Netherlands. The tidal range increases with increasing distance from the amphidromic points as is seen in the Wadden region. This results in alongshore tidal velocities between 0.5 and 1 m/s (Elias et al., 2012).

The wave height in the North Sea varies over the year, with a mean significant wave height of 1.3m and with a wave height of approximately 6 meters during storms (Elias et al., 2012). Only 3.11% of the incoming waves is higher than a H_s of 3m (Lenstra et al., 2019). The significant wave heigh (H_s) is related to the mean wave period (T_{m01}). Wave data collected by Rijkswaterstaat between 1994 and 2014 from the station of Schiermonnikoog was used to find this relation for waves in the study area (Lenstra et al., 2019) (Appendix A). The data shows a positive linear relation between H_s and T_{m01} (Figure 3.2.1). The trendline ($H_s = 1.0824T_{m01} - 3.6289$) with an R^2 value of 0.951 was used for the selection of the model parameters, to identify the correct mean wave period to the chosen significant wave height. Additionally, the data in Table 3.2.1 shows that most waves enter the Wadden area between -90° and 0° with respect to the north, which is also the direction of the highest incoming waves.

The wind speeds are varying over the year with the highest velocities in the winter and the lowest in the summer (Coelingh et al., 1996). The winds are typically coming from the west-southwest, which is also the direction of the winds with the highest velocities. The wind speeds are generally below 16 m/s but during storms this can become ±25 m/s (KNW atlas).

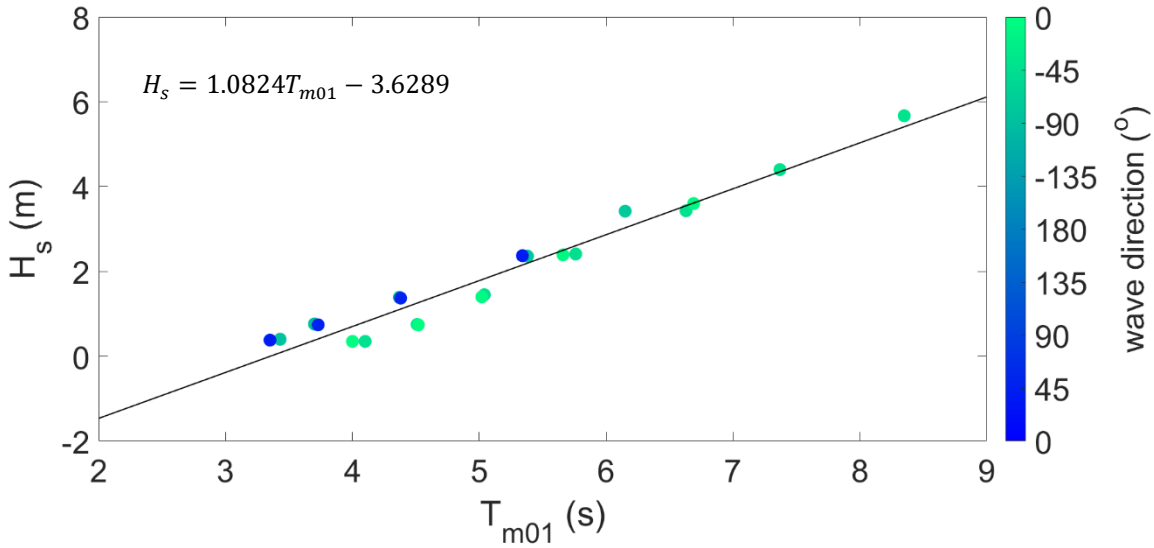

Figure 3.2.1. *The significant wave height (H_s) with respect to the mean period (T_{m01}) extracted from the wave data collected by Rijkswaterstaat between 1994 and 2014 from the station of Schiermonnikoog (Lenstra et al., 2019). The wave direction is indicated by the colours.*

3.3 Overview model simulations

Two types of model simulations were accomplished:

(1) Simulations to research the sensitivity of the bar characteristics and forcing mechanisms on the bar dynamics (to answer research question 1 to 4).
(2) Simulations to research the feedback mechanisms that result in the natural development of sawtooth bars (to answer research question 5).

The tables in this section give an overview of the forcing mechanisms and input bathymetries used in each run. The forcing mechanisms are represented by 7 forcing parameters: the tidal period, tidal amplitude, H_s, T_{m01}, wave direction, wind direction and wind speed. The tidal period and the wind direction remain 12 hours (S2) and -90° (west) for all model runs. The other forcing parameters were varied. The T_{m01} is not shown in the tables but is related to H_s with the relation $H_s = 1.0824T_{m01} - 3.6289$, as seen in Figure 3.2.1.

3.3.1 Simulations to research the sensitivity of the bar characteristics and forcing mechanisms on the bar dynamics

The simulations to research the sensitivity of the bar characteristics and forcing mechanisms on the bar dynamics were split into 8 run series. Run series 1 to 5 were used to research the sensitivity of the external forcing on the bar dynamics (Table 3.3.1.2) and run series 6 to 8 were used to research the sensitivity of the bar characteristics on the bar dynamics (Table 3.3.1.3). All these simulations were accomplished with a morphological acceleration factor of 1 and had a duration of 6.2 days.

Certain forcing parameters and bar characteristics were set as default for convenience (Table 3.3.1.1). The runs with default forcing parameters are underlined with blue in Table 3.3.1.2 and the runs with default bar characteristics are underlined with orange in Table 3.3.1.3.

Table 3.3.1.1. *Input parameters of the default run with the default forcing parameters and default bar characteristics.*

Default forcing parameters		Default bar characteristics	
Tidal amplitude (m)	1	Bar height (m)	3
H_s (m)	5.67	Bar wavelength (m)	700
Wave direction (°)	-38	Bar orientation with respect to the north (°)	14
Wind speed (m/s)	15		

Run series 1 was used to research the influence of each individual forcing mechanism on the bar dynamics, by doing a run with only tide, only wind and only wave forcing. Also, a run with all three forcing mechanisms was accomplished, using the default parameters, to research the combined influence. The runs were completed with the default bar characteristics and without bars, to isolate the effects of the bars on hydrodynamics, sediment transport and morphological change.

Run series 2 to 5 were used to study the effect of the tidal amplitude, wave height, wave direction and wind speed on the bar dynamics. The default forcing parameters were used as a base, from which 1 parameter was changed per run series. The runs were completed with the default bar characteristics and without bars, to isolate the effects of the bars on hydrodynamics, sediment transport and morphological change. Additionally, the simulations in run series nr. 3 were also completed with bars of 0.5m high, with a wavelength of 700m and an orientation of 14°. This was done to see the difference in bar dynamics between two bar heights for different wave heights.

Run series 6 to 8 were used to study the effect of the bar wavelength, height, and orientation on the bar dynamics. The default bar characteristics were used as a base, from which 1 parameter was changed per run series. All the runs were forced by the default forcing parameters and a run without bars was performed to isolate the effects of the bars on hydrodynamics, sediment transport and morphological change.

Table 3.3.1.2. *Overview of the model simulations that aim to research the sensitivity of the external forcing on the bar dynamics. Each row corresponds to a model simulation with these forcing parameters. All the runs were done with the default bar characteristics and without bars. The runs in series nr. 3 were also completed with bars of 0.5m high, with a wavelength of 700m and an orientation of 14°. The runs with default forcing parameters are underlined with blue.*

Number run series	Tidal amplitude (m)	H_s (m)	Wave direction (°)	Wind speed (m/s)
Nr. 1	1	5.67	-38	15
	0	5.67	-38	0
	0	0	-	15
	1	0	-	0
Nr. 2	0.5	5.67	-38	15
	1	5.67	-38	15
	1.5	5.67	-38	15
	2	5.67	-38	15
Nr. 3	1	0	-	15
	1	1	-38	15
	1	2	-38	15
	1	3.5	-38	15
	1	4.5	-38	15
	1	5.67	-38	15
Nr. 4	1	5.67	-90	15
	1	5.67	-67.5	15
	1	5.67	-38	15
	1	5.67	-20	15
	1	5.67	0	15
	1	5.67	25	15
	1	5.67	45	15
Nr. 5	1	5.67	-38	0
	1	5.67	-38	5
	1	5.67	-38	10
	1	5.67	-38	15
	1	5.67	-38	20

Table 3.3.1.3. *Overview of the model simulations that aim to research the sensitivity of the bar characteristics on the bar dynamics. Each row corresponds to a model simulation with these bar characteristics. All the runs were done with the default forcing parameters. The runs with default bar characteristics are underlined with orange.*

Number run series	Bar wavelength (m)	Bar height (m)	Bar orientation (degrees from north)
Nr. 6	700	3	14
	1050	3	14
	1400	3	14
	2100	3	14
Nr. 7	700	0.5	14
	700	1.5	14
	700	2	14
	700	3	14
Nr. 8	700	3	0
	700	3	14
	700	3	25
	700	3	35
	700	3	45

3.3.2 Simulations to research the mechanisms that result in the natural development of sawtooth bars

Three long-term runs with a random small amplitude perturbation (±0.25m) were accomplished to research under which forcing parameters sawtooth bars might develop. The simulations were forced by the default forcing parameters, from which only the significant wave height was varied, as specified in Table 3.3.2.1. Since the development of bars takes a relatively long time, the morphological acceleration factor was set to 5, 8 or 20, depending on the wave height. For a run with a morphology factor of 5 this means that the morphology is changing 5 times as fast. For example, when a run duration is 1 month, the morphological change at the end of the run is equal to 5 hydrodynamic months. Therefore, the duration is expressed in hydrodynamic days.

Table 3.3.2.1. *Overview of the model simulations with a small amplitude perturbation. Each row is corresponding to a model run forced by the default forcing parameters, of which only the significant wave height was changed for run nr. 2 and 3.*

Run nr.	H_s (m)	Morphology factor (-)	Duration (hydrodynamic days)
1	5.67	5	744
2	3.5	8	1239
3	2	20	1618

A bathymetry from long-term run nr. 1, in which bars developed that resembled sawtooth bars, was used in two additional runs to analyse their generation mechanism (Table 3.3.2.2). The bathymetry after 50 hydrodynamic days with morphological change was chosen for these additional runs. The two simulations were forced by different wave heights, a H_s of 2m and a H_s of 5.67m, the other parameters were kept as default. Additionally, two simulations with an initial H_s of 2m and a H_s of 5.67m (B and D) contained the bathymetry of the spatial running mean, which resembles the bathymetry of the bed excluding the bars. This was done to isolate the effects of the bars on hydrodynamics, sediment transport and morphological change. These simulations were accomplished with a morphological acceleration factor of 1 and had a duration of 6.2 days.

The running mean was calculated by using a square moving window over the area. The mean of the grid cells in the window was calculated and assigned to the central grid cell in the window. Then, the window moved with one grid cell and the calculation was repeated until the whole area was completed. The window size was the approximated wavelength of the bars.

Table 3.3.2.2. *Overview of the model simulations that aim to research the feedback mechanisms that resulted in the development of the bars as seen in long-term run nr. 1. The simulations were forced by the default forcing parameters, of which only the significant wave height was changed for run C and D.*

Run	H_s (m)	Used bathymetry
A	5.67	Natural developed bars
B	5.67	Running mean
C	2	Natural developed bars
D	2	Running mean

3.4 Model analyses

3.4.1 Harmonic analysis

A harmonic analysis was used to calculate the tidally mean flow velocity and the tidally mean sediment transport. The analysis contains a fitting routine of one or more tidal constituents on a measured record by minimizing the root-mean-square-error. Because the tide in the model was only forced by the S_2 tide the fit was only based on this one tidal constituent. The harmonic analysis was applied to the following Delft3D output: the depth average flow velocity, the suspended sediment transport, and the bedload transport. The tidally mean suspend transport was combined with the tidally mean bed load transport to calculate the total tidally mean sediment transport.

3.4.2 Spatial-correlation technique

A spatial correlation technique was used to calculate (1) the phase difference between the bar pattern and the erosion/deposition pattern and (2) the migration speed of the natural developed bars. This method is based on the technique described by Duffy and Hughes-Clarke (2005) which determines the distance between two spatial data sets where they are most similar. For example, when a bar migrates in time, the distance between the initial bar position and the bar position after an amount of time can be found with this spatial cross-correlation technique. Finding the location where the two datasets are most alike is done with the help of moving windows *f(x,y)* and *g(x,y)* (Figure 3.4.2.1) which is step by step described below.

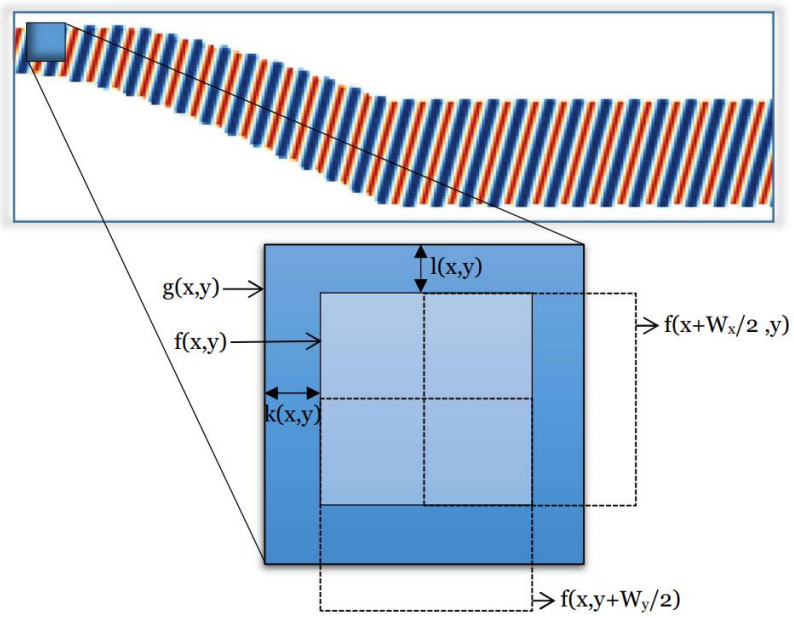

Figure 3.4.2.1. *Calculation of the spatial correlation between two datasets with the windows g(x,y) and f(x,y) including the displacements k and l.*

The first step in the spatial-correlation technique is to identify a square search area in dataset A in which one sawtooth bar could be defined *(g(x,y))*. Secondly, a smaller square fitting window *f(x,y)* is created in the middle of *g(x,y)* containing the data of dataset B. Then, the search window *g(x,y)* is moved around *f(x,y)* with the displacement *(k, l)* and the correlation r is calculated for every *(k, l)* value by multiplying the two matrices and taking the sum (Figure 3.4.2.1 & Equation 3.4.2.1).

$$r_{k,l}(x,y) = \sum_{k=0}^{kmax} \sum_{l=0}^{lmax} f(x,y)g(x+\Delta x_k, y+\Delta y_l) \qquad 3.4.2.1$$

The maximum value of r, with the corresponding (k_{max}, l_{max}) values, reveals the distance between the windows *f(x, y)* and *g(x, y)* where the correlation is highest. Because the value r is depended on the window size, r is normalized to *R* so that *R* becomes a value between -1 and 1. This is done by subtracting the mean from each dataset and dividing this by the standard deviation:

$$R_{k,l=} \frac{\sum_{k=0}^{kmax} \sum_{l=0}^{lmax} \left[f(x,y) - \bar{f}\right] \left[g(x+\Delta x_k, y+\Delta y_l) - \bar{g}_{k,l}\right]}{\sqrt{\sum_{k=0}^{kmax} \sum_{l=0}^{lmax} \left[f(x,y) - \bar{f}\right]^2 \sum_{k=0}^{kmax} \sum_{l=0}^{lmax} \left[g(x+\Delta x_k, y+\Delta y_l) - \bar{g}_{k,l}\right]^2}} \qquad 3.4.2.2$$

Finally the search area *g(x, y)* is moved with half the length of the window *f(x, y)* and the above steps are repeated until the whole dataset is searched (Figure 3.4.2.1). For every search window the displacement is then known between the two datasets. The mean is taken to calculate the average displacement.

The size of the search matrix is dependent on the bar wavelength. It must be less than two times the wavelength of the bars to avoid that the maximum cross-correlation *R* is found at 2 locations. In Table 3.4.2.1 an overview is given of the used window sizes corresponding to the bar wavelengths. The window sizes are a multiple of 70 due to the grid size in the inner domain.

Table 3.4.2.1 *Bar wavelength and the corresponding window sizes for g(x,y).*

Bar wavelength	Window size g(x,y)
700m ±175m	700m x 700m
1050m ±175m	980m x 980m
1400m±175m	1400m x 1400m
1750m±175m	1680m x 1680m
2100m±175m	2100m x 2100m

(1) Computation of the phase difference between the bar pattern and the erosion/ deposition pattern

The phase difference between the bar pattern and the erosion deposition pattern, was calculated to determine if the bars would grow (< 90°) or decay (> 90°) and what their relative migration speed would be. With a phase difference of 90°, the migration speed is optimal and with a phase difference of 0° or 180° degrees the bars do not migrate, only growth or decay will occur.

The sawtooth bar pattern $H'(x,y,t)$ was calculated by taking the difference between the bottom depth of a run with sawtooth bars and the bottom depth of a run without sawtooth bars in time.

$$H'(\mathrm{x},\mathrm{y},t) = H(x,y,t) - H_{Bars}(x,y,t) \qquad 3.4.2.3$$

Here, $H(x,y,t)$ is the output bathymetry of a run without sawtooth bars and $H_{Bars}(x,y,t)$ is the output bathymetry of a run with sawtooth bars. The locations where $H'(\mathrm{x},\mathrm{y},\mathrm{t}) > 0$ are the bar crests and where $H'(\mathrm{x},\mathrm{y},\mathrm{t}) < 0$ are the bar troughs (Figure 3.4.2.2 (left)). Note that both runs must be forced by the same forcing parameters to obtain $H'(\mathrm{x},\mathrm{y},\mathrm{t})$.

The erosion deposition pattern ΔH (x, y) was calculated by taking the difference between $H'(x, y, t)$ at the start and end of the first tidal cycle in which morphological change is allowed.

$$\Delta H(\mathrm{x,y}) = H'_{start}(\mathrm{x,y}) - H'_{end}(\mathrm{x,y}) \qquad 3.4.2.4$$

Here, $H'_{start}(\mathrm{x,y})$ and $H'_{end}(\mathrm{x,y})$ are the bar patterns at the start and end of the first tidal cycle and the locations where $\Delta H(\mathrm{x,y}) > 0$ is a depositional area and $\Delta H(\mathrm{x,y}) < 0$ is an erosional area (Figure 3.4.2.2 (right)).

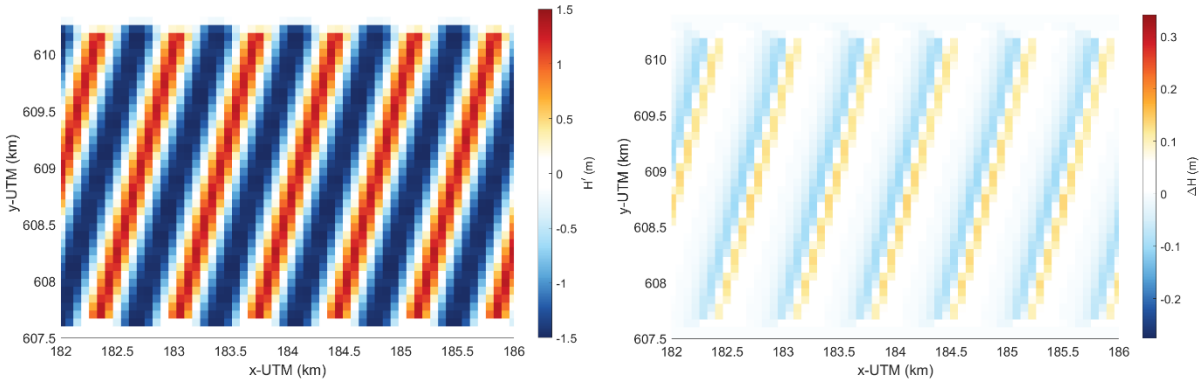

Figure 3.4.2.2. *Example of $H'_{start}(x, y)$ (left) and ΔH (x, y) (right), for the default simulation.*

The phase difference between the bar pattern $H'_{start}(x, y)$ and the erosion/deposition pattern $\Delta H(x, y)$ was calculated by taking H'_{start} for the *g(x, y)* matrices and ΔH for the *f(g, y)* matrices. The mean displacement of a certain area was divided by the wavelength of the initiated sawtooth bars and multiplied by 360 to calculate the phase difference in degrees, denoted as ε.

The mean displacement was calculated for the whole sawtooth bar area, the downdrift area and the updrift area to be able to study the phase difference (between H' and ΔH) among the areas. The downstream area is defined as the area where the ebb-tidal delta ends and the coastline of the downdrift Wadden island becomes straight. The upstream area is defined as the area where the sawtooth bars are located on the ebb-tidal delta (Figure 3.4.2.3).

(2) Computation of the bar migration speed

The natural developed bars from the long-term runs migrated more than a few grid cells (210m>) in the time span of the run. Therefore, this spatial correlation technique is suitable to calculate their migration speed.

The bar pattern $H'(\mathrm{x,y},t)$ from the natural developed bars, was calculated by subtracting the spatial running mean from the bottom depth at each time step. The migration speed was calculated by taking H' at two time steps in which the bars migrated at least a few grid cells (210m >). The search window g(x,y) was assigned to the dataset at the first time step and the fitting window f(x,y) was assigned to the dataset at the second time step. The mean displacement of the area was then divided by the time in between the two datasets to calculate the migration speed.

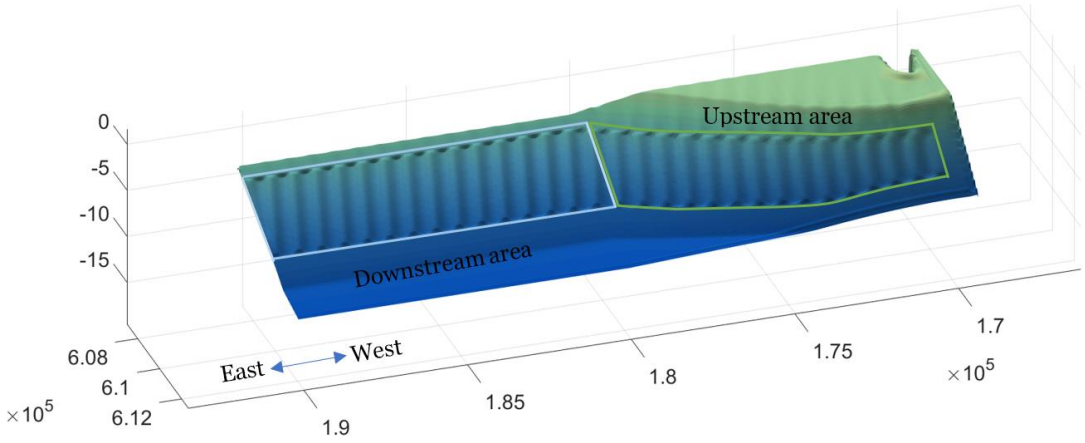

Figure 3.4.2.3. *Visualisation of the downstream and upstream part of to the sawtooth bar area. The downstream area is defined as the area where the ebb-tidal delta ends and the coastline of the downdrift Wadden island becomes straight. The upstream area is defined as the area where the sawtooth bars are located on the ebb-tidal delta.*

3.4.3 Mathematical analysis to calculate small migration speeds and the bar growth/decay rate

This mathematical analysis resembles partly the approach of a linear stability analysis, which is valid for small migration speeds and bar growth/decay rates. Since the migration speeds of the prescribed bars were smaller than one grid cell (70m) in the time span of the runs, the spatial-correlation technique was not a suitable approach. Additionally, the bar growth/decay rate could be determined with this analysis.

Mathematical computation of the migration speed

The evolution of sinusoidal bars on a reference plane can be approached by the following formula (Dodd et al., 2003).

$$H_{tot}(x,y,t) = H_{ref}(x,y,t) + h \cdot e^{i(k_y y + k_x x - \omega t)} \qquad 3.4.3.1$$

In which,

- $H_{tot}(x,y,t)$ is the total bathymetry in time *t,*
- $H_{ref}(x,y,t)$ is the reference bathymetry excluding the bars in time *t,*
- $h(x,y,t) \cdot e^{-i(k_y y + k_x x - \omega)t}$ describes the bar evolution in time *t,*
- h is the amplitude of the bars (m),
- x and y determine the extent of the bar area,
- k_x is the wavenumber in the x-direction (alongshore) (1/m),
- k_y is the wavenumber in the y-direction (cross-shore) (1/m),
- ω is the frequency (1/s).

The frequency ω can be expressed as a complex number.

$$\omega = \omega_{re} + i\omega_{im} \qquad 3.4.3.2$$

Here, ω_{im} is the imaginary part of ω which represents the bar growth and ω_{re} is the real part of ω. When ω_{re} is divided by the wavenumber it represents the migration speed of the bars. It is assumed that the bars only migrate alongshore (x-direction). So ω_{re} can be rewritten as:

$$\omega_{re} = c_x \cdot k_x \qquad 3.4.3.3$$

Rewriting Equation 3.4.3.1 given Equation 3.4.3.2 and 3.4.3.3, and taking only the real parts gives:

$$H_{tot}(x,y,t) = H_{ref}(x,y,t) + h \cdot \cos\left(k_y y + k_x x - c_y k_y t\right) \cdot e^{\omega_{im} t} \qquad 3.4.3.4$$

This equation is differentiated over time to be able to calculate the evolution of the bars within a certain amount of time ∂t, which results in the following equation:

$$\frac{\partial H_{tot}}{\partial t}(x,y,t) = \frac{\partial H_{ref}}{\partial t}(x,y,t) + h \cdot e^{\omega_{im} t} \cdot (\omega_{im} \cdot \cos\left(k_y y + k_x x - c_y k_y t\right) + c_y k_y \cdot \sin\left(k_y y + k_x x - c_y k_y t\right)) \qquad 3.4.3.5$$

$\frac{\partial H_{tot}}{\partial t}(x,y,t) - \frac{\partial H_{ref}}{\partial t}(x,y,t)$ is defined as ΔH(x, y) when ∂t is equal to the duration of the first tidal cycle in which morphological change is allowed (Equation 3.4.2.4). Additionally, the relation between $c_y k_y$ and ω_{im} can be expressed as:

$$\tan(\varepsilon') = \frac{c_y k_y}{\omega_{im}} \qquad 3.4.3.6$$

When Equation 3.4.3.5 is combined with Equation 3.4.3.6, Equation 3.4.3.7 is obtained in which T is the duration of one tidal cycle.

$$\Delta H(x,y) = T \cdot h \cdot e^{\omega_{im} t} \sqrt{{\omega_{im}}^2 + {c_y}^2 \cdot {k_y}^2} \cdot \sin\left(k_y y + k_x x - c_y k_y t - \varepsilon'\right) \qquad 3.4.3.7$$

The phase difference ε between the bar pattern H' and the erosion deposition patten ΔH as calculated with the spatial-correlation technique (Subsection 3.4.2), is equal to $-c_y k_y t - \varepsilon'$ in Equation 3.4.3.7. It is assumed that $c_y k_y t \approx 0$ which states that the equation is only suitable for small migration speeds. Then $\varepsilon' = \varepsilon$ and the relation between $c_y k_y$ and ω_{im} can be expressed as:

$$\tan(\varepsilon) = \frac{c_y k_y}{\omega_{im}} \qquad 3.4.3.8$$

$T \cdot h \cdot e^{\omega_{im} t} \sqrt{\omega_{re} + c_y k_y}$ is the amplitude of the sinusoid ΔH(x, y) (Equation 3.4.3.7). The amplitude can be determined by taking the standard deviation of ΔH(x, y) and multiplying this by $\sqrt{2}$ (Smith, 2013). Then, Equation 3.4.3.9 is obtained:

$$\sqrt{2} \cdot \mathrm{std}(\Delta H(x,y)) = T \cdot h \cdot e^{\omega_{im} t} \sqrt{{\omega_{im}}^2 + {c_y}^2 {k_y}^2} \qquad 3.4.3.9$$

It is assumed that $\omega_{im} t \approx 0$, which states that the bar growth/decay over time is small. Therefore, Equation 3.4.3.9 is rewritten into:

$$\sqrt{2} \cdot \mathrm{std}(\Delta H(x,y)) = T \cdot h \cdot \sqrt{\frac{{c_y}^2 {k_y}^2}{tan(\varepsilon)^2} (1 + tan(\varepsilon)^2)} \qquad 3.4.3.10$$

The final equation that was used to calculate the migration speed for all the prescribed bars is:

$$c_y = \sqrt{\frac{\left(\sqrt{2} \cdot \frac{\text{std}(\Delta H(x,y))}{T \cdot h}\right)^2}{k_y{}^2 \cdot (1 + \frac{1}{tan(\varepsilon)^2})}} \qquad 3.4.3.11$$

The migration speed was calculated for the whole area, and the upstream and downstream area separately to distinguish between both areas. For this, the standard deviation of $\Delta H(x,y)$ and ε were also calculated for these specific areas. The areas are specified in Figure 3.4.2.3.

Mathematical computation of the bar growth/decay rate

The growth/decay rate φ is determined by:

$$\varphi(x,y) = H'(x,y) \cdot \Delta H(x,y) \qquad 3.4.3.12$$

When φ is positive, bar growth is observed at a location, and when φ is negative decay is observed at a location. Growth or decay is determined by H' and ΔH , which can both be negative or positive at a location. Consequently, there are four possible scenarios:

- Bar growth (φ>0) when $H' > 0$ and $\Delta H > 0$
  Growth is seen at a location when H' and ΔH are positive. When H' is positive, this area is a sawtooth bar crest and when ΔH is positive there is net deposition. So, the bar crest becomes higher which is determined as bar growth.
- Bar growth (φ>0) when $H' < 0$ and $\Delta H < 0$
  Growth is seen at a location when H' and ΔH are negative. When H' is negative, this area is a sawtooth bar trough and when ΔH is negative there is net erosion. So, the bar trough becomes even deeper which is determined as bar growth.
- Bar decay (φ<0) when $H' < 0$ and $\Delta H < 0$
  Decay is seen at a location when H' is negative and ΔH is positive. When H' is negative, this area is a sawtooth bar trough and when ΔH is positive there is net deposition. So, the trough becomes less deep which results in bar decay.
- Bar decay (φ<0) when $H' > 0$ and $\Delta H < 0$
  Decay is seen at a location when H' is positive and ΔH is negative. When H' is positive, this area is a sawtooth bar crest and when ΔH is negative there is net erosion. So, the crest of the bar is eroding which results in bar decay.

The mean growth/decay rate $\bar{\varphi}$ was calculated mathematically using the assumptions: $\omega_{im} t \approx 0$ and $c_y k_y t \approx 0$. Then $H'(x,y)$ and $\Delta H(x,y)$ are given by Equation 3.4.3.13 and 3.4.3.14 and $\varphi(x,y)$ is given by Equation 3.4.3.15 which can be rewritten into Equation 3.4.3.16.

$$H'(x,y) = h \cdot \sin(k_y y + k_x x) \qquad 3.4.3.13$$

$$\Delta H(x,y) = T \cdot h \sqrt{\omega_{im}{}^2 + c_y{}^2 \cdot k_y{}^2} \cdot \sin(k_y y + k_x x - \varepsilon) \qquad 3.4.3.14$$

$$\varphi(x,y) = h^2 \cdot T \cdot \sqrt{\omega_{im}{}^2 + c_y{}^2 \cdot k_y{}^2} \sin(k_y y + k_x x) \cdot \sin(k_y y + k_x x - \varepsilon) \qquad 3.4.3.15$$

$$\varphi(x,y) = h^2 \cdot T \cdot \sqrt{\frac{c_y{}^2 \cdot k_y{}^2}{\tan(\varepsilon)} + c_y{}^2 \cdot k_y{}^2} \cdot \frac{1}{2}\cos(\varepsilon) - \frac{1}{2}\cos(2k_y y + 2k_x x - \varepsilon) \qquad 3.4.3.16$$

When $\varphi(x,y)$ is averaged over a large area of bars $\cos(2k_y y + 2k_x x - \varepsilon) \approx 0$. Therefore, Equation 3.4.3.16 can be rewritten into Equation 3.4.3.17 in which as $\overline{\varphi}$ is $\varphi(x,y)$ averaged over an area. Equation 3.4.3.11 was used to calculate c_y.

$$\overline{\varphi} = h^2 \cdot T \cdot \sqrt{\frac{{c_y}^2 \cdot {k_y}^2}{\tan(\varepsilon)} + {c_y}^2 \cdot {k_y}^2} \cdot \frac{1}{2}\cos(\varepsilon) \qquad 3.4.3.17$$

$\overline{\varphi}$ was calculated for the whole area, and the upstream and downstream area separately to distinguish between both areas. For this, the standard deviation of $\Delta H(x,y)$ and ε were also calculated for these specific areas. The areas are specified in Figure 3.4.2.3.

3.4.4 Bar property calculations

This Subsection contains the analyses to quantify the bar properties of the bars that developed in the simulations with random small amplitude perturbation. The bar height, wavelength and orientation were calculated mathematically, and the crest length was calculated manually and is therefore not further explained.

To calculate the bar height, the bar pattern $H'(x,y,t)$ was first extracted by subtracting the spatial running mean from the bottom depth at each time step, as explained in Subsection 3.4.2. Then, the bar height was calculated from $H'(x,y,t)$ by taking the standard deviation over the area where the bars occurred and multiplying by $2\sqrt{2}$. This is following Smith (2013) with the assumption that the bars are sinusoidal shaped which was also used in the study of Brakenhoff et al., (2019).

The bar wavelength (λ_b) and the bar orientation with respect to the north (θ) were calculated with a 2D Fast Fourier Transform (FFT). The analysis was applied on $H'(x,y)$, whereafter the absolute value was taken to visualise the amplitudes of the frequency domain. This was then squared to ease the

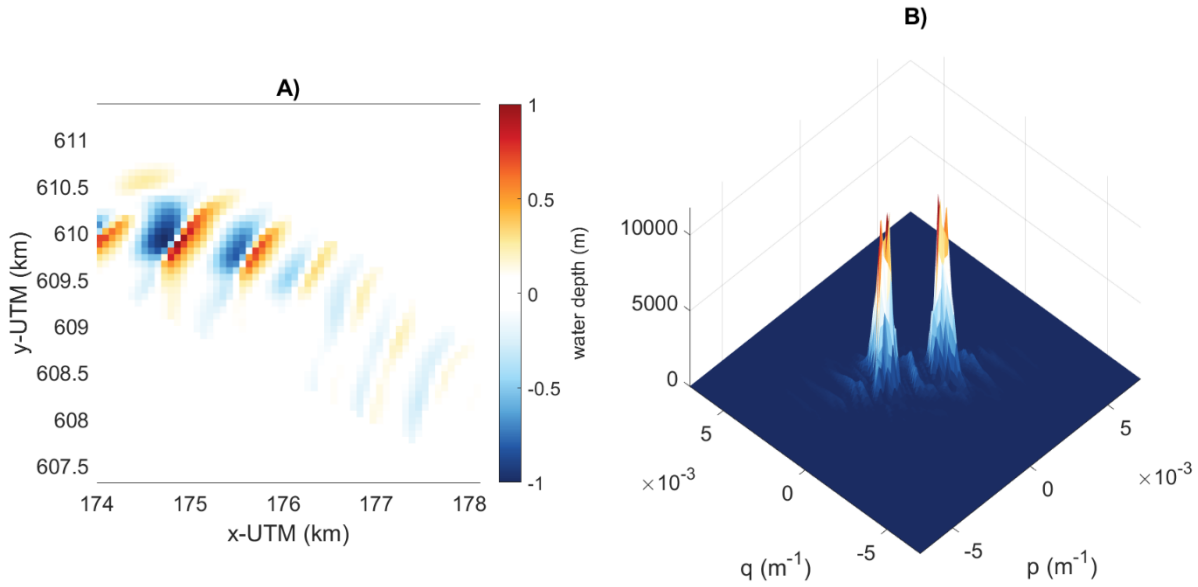

Figure 3.4.4.1. ***A)*** *H' with the corresponding* ***B)*** *output of the FFT visualised as the amplitudes of the frequency domain. The domain was squared to ease the quantification of the locations of the peaks. The peak locations in figure* ***B)*** *were used to calculate the wavelength and orientation of the bars as shown in figure* ***A).***

quantification of the peak frequencies, which represent the most prevailed bar wavelength of the sawtooth bars (Figure 3.4.4.1). The wavelength was calculated with the use of Pythagoras's theorem and the locations of the peak frequencies.

$$\lambda_b = \frac{1}{\sqrt{{P_{max}}^2 + {q_{max}}^2}} \qquad 3.4.4.1$$

Here, P_{max} and q_{max} are the x- and y-locations of the peak frequencies that represent the inverse wavelength. Note that the locations of both peaks result in the same bar wavelength. Subsequently, the bar orientation with respect to the north (θ) was calculated with the inverse tanged.

$$\theta = -1 * tan^{-1}(\frac{q_{max}}{p_{max}}) \qquad 3.4.4.2$$

The bar crest orientation with respect to the orientation of the area (γ) was calculated to be able to compare the orientations of the developed bars with the orientations as found by Brakenhoff et al. (2019). To accomplish this, the angle between the orientation of the area and the north (α) was calculated with the use of the spatial running mean. First, the sawtooth bar area was manually defined by drawing a polygon (Figure 3.4.4.2.a). Then, by using the spatially running mean map, the mean depth within the polygon, was calculated (Figure 3.4.4.2.b). Consequently, a trendline was fitted through the grid cells that were closest to this chosen depth in the polygon (Figure 3.4.4.2.c). The angle between the trendline and the north (α) was calculated by taking the inverse tangent of the slope. Finally, γ was calculated by subtracting θ from α (Figure 3.4.4.2.d).

$$\gamma = \alpha - \theta \qquad 3.4.4.3$$

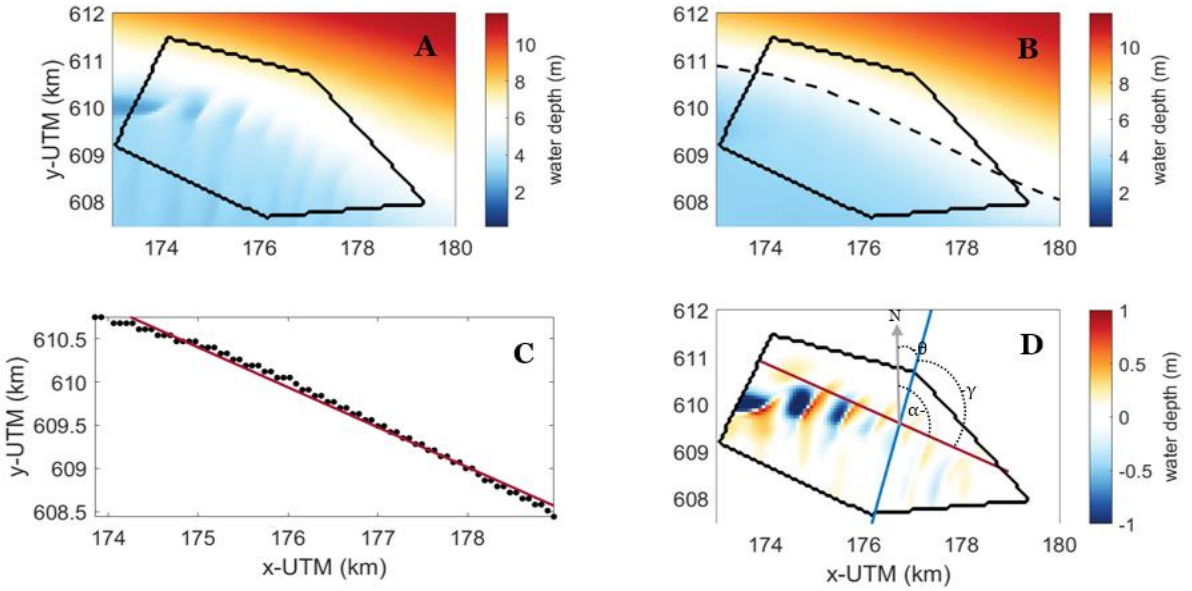

Figure 3.4.4.2. *The calculation of γ.* ***A)*** *The bottom depth with a manually drawn polygon around the sawtooth bar area.* ***B)*** *The running mean map with the depth contour (dotted line) of the average depth in the contoured area.* ***C)*** *A trendline (red line) through the grid cells (black dots) that are closest to the average depth in the contoured area.* ***D)*** *The orientation of the area (red line as in C), the orientation of the bar crests (blue line) and the angles α, γ and θ calculated from these orientations. The grey arrow is pointing north.*

Chapter 4. Results

4.1 The influence of the sawtooth bars on the hydrodynamics

This section describes the influence of the sawtooth bars on the hydrodynamics, taking the forcing mechanisms and bar characteristics into account. The flow velocity patterns shown in this section are the tidally mean depth average velocities only due to the presence of sawtooth bars. This was achieved by subtracting the tidally mean depth average velocity of a run without bars from the tidally mean depth average velocity of a run with bars, both with the same initial forcing.

4.1.1 The flow velocity patterns due to the presence of sawtooth bars

With only tidal forcing (1m amplitude) a downdrift directed alongshore current is generated. The velocity only due to the presence of sawtooth bars, results in a different flow path in the upstream compared to the downstream area (Figure 4.1.1.1.a left and right). In the downstream area, a sinusoidal bending flow path over the bar crests and troughs is visible. The flow velocities due to the perturbation are highest on updrift side of the crest and in the trough the flow velocities are lowest. In the upstream bar area the tidally mean flow due to the presence of the bars shows a converging and relatively strong flow towards the downdrift side of each bar crest and a diverging flow in the troughs.

With only wave forcing (H_s = 5.67m and with wave direction -38°), a strong alongshore downdrift directed flow is generated. The flow only due to the presence of sawtooth bars shows a converging flow on the downdrift side of the bar crest and a diverging flow at the updrift side of the bar crest (Figure 4.1.1.1.b). Additionally, the magnitude of the flow on the bar crests becomes less strong towards the shore. This is further explained in Subsection 4.1.2.

When using only wind forcing (15m/s and -90 degrees), an alongshore downdrift flow is generated. The flow pattern only due to the presence of sawtooth bars shows convergence at the downdrift side of each bar crest and divergence on the updrift side of the bar crests (Figure 4.1.1.1.c). What is striking is that the flow pattern remains almost equal in magnitude over the bars. Only a slight increase in flow magnitude is seen in the shallower areas.

Forced by tides, waves, and wind (default forcing parameters), the generated tidally averaged flow pattern only due to the presence of sawtooth bars shows an overall converging flow on the downstream side of the crests and a diverging flow on the upstream side of the crests. This pattern is dominated by the wave forces since the flow magnitudes are largest at the most offshore area (Figure 4.1.1.2.a).

For different sawtooth bar characteristics, the pattern remains roughly the same, only the magnitude differs. When lowering the bar height, the magnitude of the flow due to the presence of the bars becomes smaller, but the pattern remains the same (Figure 4.1.1.2.a compared to Figure 4.1.1.2.c). With a larger wavelength the bending flow path becomes broader, and the magnitude of the flow becomes larger (Figure 4.1.1.2.a compared to Figure 4.1.1.2.b). When the orientation of the bars is changing, the flow pattern remains the same with respect to the bars, only the location of the pattern is changing in the same way the location of the bars in changing (Figure 4.1.1.2.d).

The flow pattern is most altered by the wave direction. For a run forced by tides, waves and wind in which waves enter the sawtooth bars on the east (default forcing parameters), the resulting pattern shows a clockwise flow pattern over the bar crests (Figure 4.1.1.2.a). When only the wave direction changes to waves that enter the sawtooth bars from the west, an anti-clockwise flow pattern is seen around the most downdrift bar crests (Figure 4.1.1.3). This results in a diverging flow is on the downdrift side of the bar crest and a converging flow on the upstream side of the bar crest. This is not seen for the more upstream sawtooth bars due to the alongshore downdrift flow generated by wind and tides that oppose this.

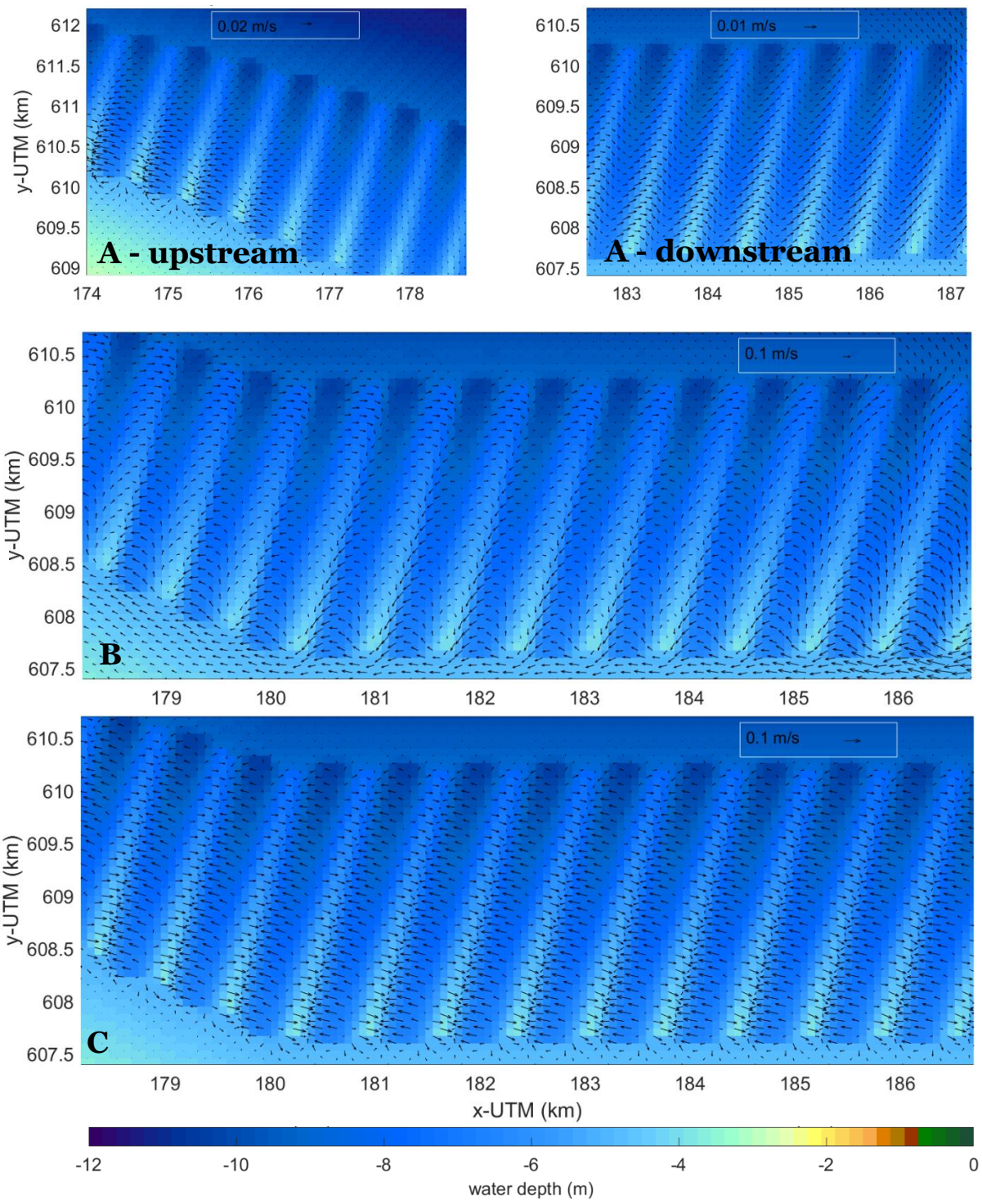

Figure 4.1.1.1. *Difference between the tidally mean depth average velocity of a model run with sawtooth bars and a model run without sawtooth bars containing* ***A)*** *only the forcing of tides of 1m amplitude (S2) (left: upstream area and right: downstream area)* ***B)*** *only the forcing of waves with a significant wave height of 5.67m coming from the northwest (-38°) and* ***C)*** *only the forcing of wind of 15m/s coming from the west (-90°). The sawtooth bars had the default bar characteristics.*

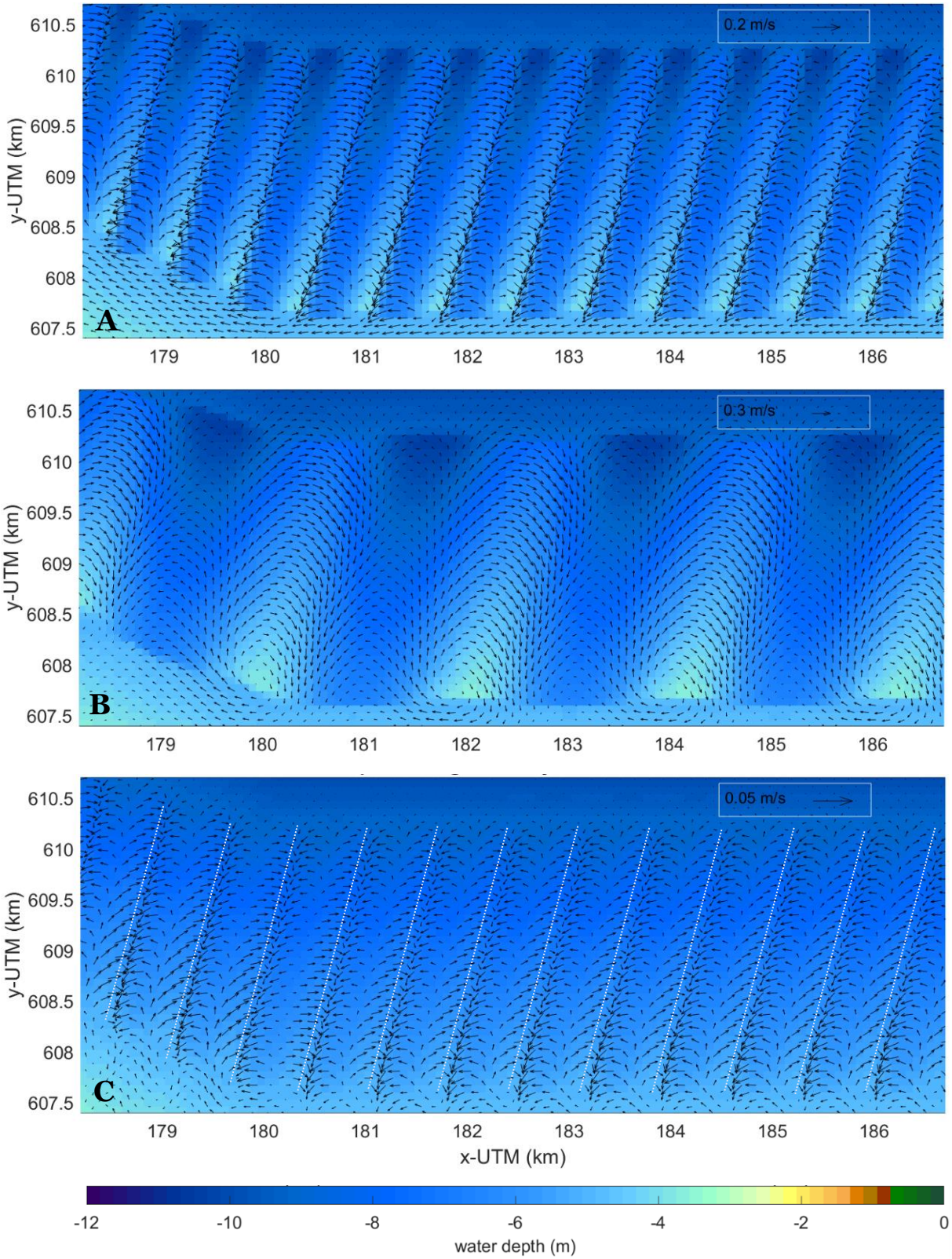

Figure 4.1.1.2. *Difference between the tidally mean depth average velocity of a model run with sawtooth bars and a model run without sawtooth bars forced by the default parameters. For* ***A)*** *sawtooth bars with the default bar characteristics. For* ***B)*** *sawtooth bar with an amplitude of 1.5m, a wavelength of 2100m and an orientation of 14° with respect to the north. For* ***C)*** *sawtooth bars with an amplitude of 0.25m, a wavelength of 700m and an orientation of 14° with respect to the north.*

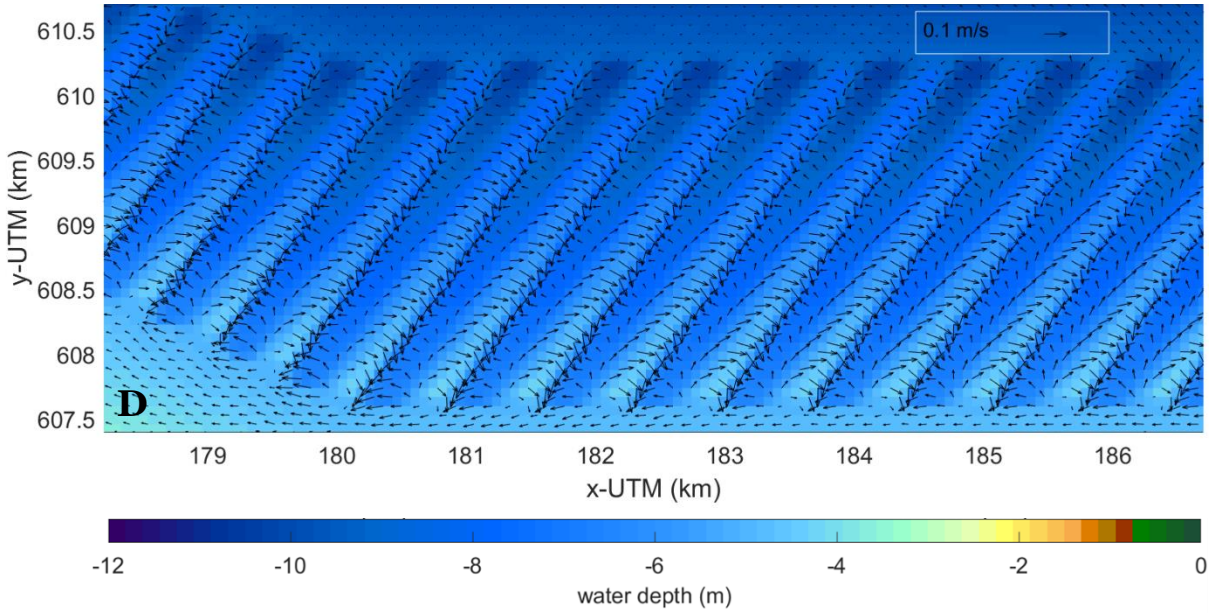

Figure 4.1.1.2. *Difference between the tidally mean depth average velocity of a model run with sawtooth bars and a model run without sawtooth bars forced by the default parameters. For* ***D)*** *sawtooth bars with an amplitude of 1.5m, a wavelength of 700m and an orientation of 35° with respect to the north.*

With varying tidal amplitude, wave height or wind speed, the pattern remains almost the same, only the magnitude differs. When the amplitude, wave height or wind speed is increasing, the magnitude of the flow increases. Enhancement of the tidal amplitude results in a lower low water, which strengthens the flow by waves and wind during low tide. However, for the wave height and wind speed the pattern depends on the relative magnitude of the two forces. When the default forcing parameters were taken of which only the wave height was lowered, the pattern resembles more and more the pattern of only wind (Figure 4.1.1.1.c). Visa versa for the wind speed.

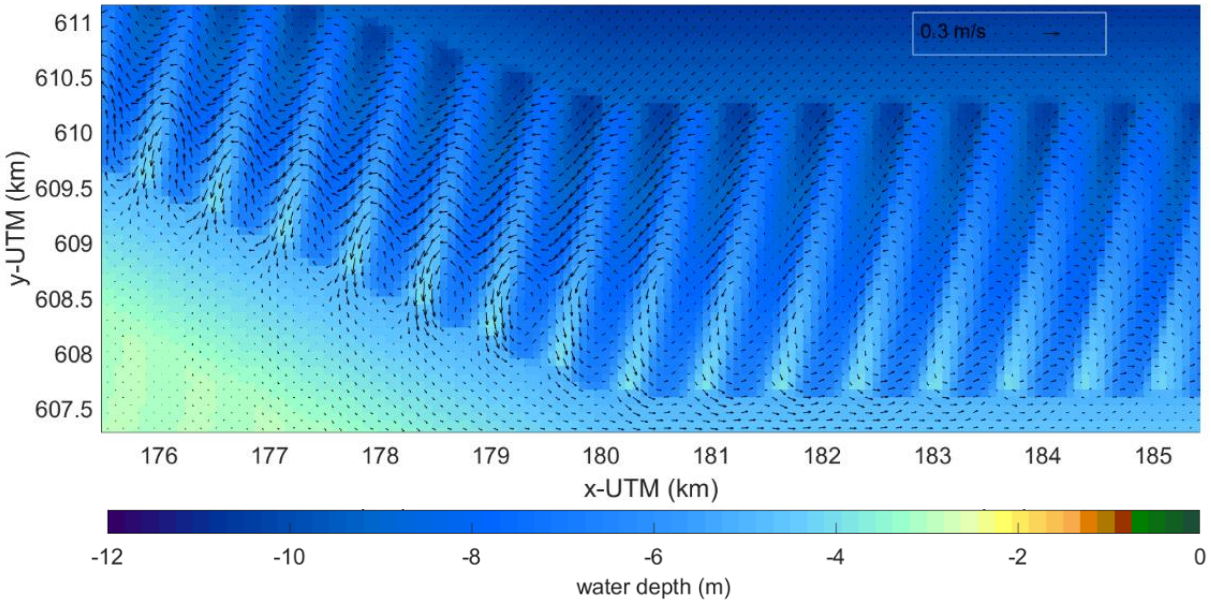

Figure 4.1.1.3. *Difference between the tidally mean depth average velocity of a model run with sawtooth bars and a model run without sawtooth bars forced by the following forcing parameters: 1) Waves: H_s = 5.67m (45°); 2) Wind: 15m/s (-90°), 3); Tide: S2, 1m amplitude. The sawtooth bars that were used had the default bar characteristics.*

4.1.2 Physical interpretation of the flow patterns

With the forcing of tides, waves, and winds (default forcing parameters), the resulting flow is an alongshore flow towards the east. When sawtooth bars are present, this alongshore flow is altered in its direction and magnitude. Towards the crest the flow increases and towards the trough the flow decreases, due to the fluctuating water depth. This is visible as the converging and diverging flow patterns in Figure 4.1.1.2. The flow increases in velocity as the water depth becomes shallower and decreases as the water depth becomes larger, due to the conservation of mass (Equation 3.1.1.2). The alongshore flow path is altered in its direction due to the downdrift orientation of the bars. When the alongshore flow increases in velocity on the bar crest, the shore parallel flow seawards of this position is not yet increasing in flow velocity (Figure 4.1.4.1, cross-section 1). Due to this velocity difference between the locations, the resulting alongshore streamline is bending in the offshore direction. The same phenomenon results in the onshore bending when the alongshore parallel flow is past the centre of the bar crest. Then the velocity is faster at the more offshore location, resulting in an onshore bending of the flow (Figure 4.1.2.1, cross-section 2). Overall, this results in a flow path that attempts to follow the depth contours.

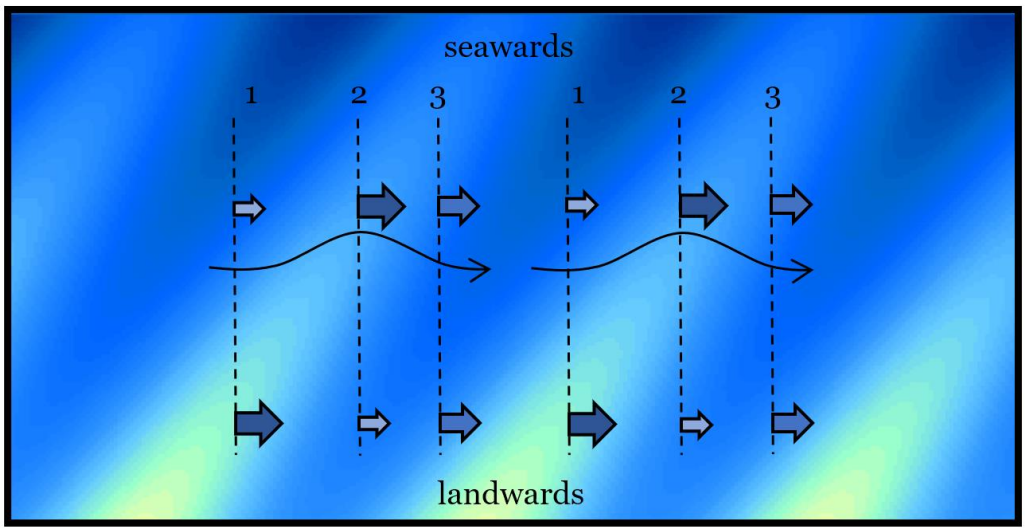

Figure 4.1.2.1. *The bending flow phenomenon over the sawtooth bars. At location 1 the flow velocity is faster at the most landward side which results in the offshore bending of the flow. At location 2 the velocity is faster at the more offshore location, resulting in an onshore bending of the flow. At location 3, the flow is uniform which results in a parallel flow alongshore. The resulting flow path is visualised as the solid black line.*

When hydrodynamics are only forced by tides, the flow pattern due to the presence of sawtooth bars shows no diverging and converging pattern in the downstream area, which is not as expected (Figure 4.1.1.1.a (right)). A flow towards the east is visible in the troughs, so the flow in the troughs is stronger with bars compared to the flows at that location without bars. This could be caused by the bottom stresses. In the bar trough the bottom stresses are smaller compared to the bottom stresses at the same location without bars. Therefore, the flow could become larger in the troughs compared to the flow at the same location without bars.

When the hydrodynamics are only forced by waves (H_s =5.67m), the bending flow path over the bar crests decreases in strength towards the coast (Figure 4.1.1.1.b). This is due to wave dissipation which is mainly caused by bed friction and a small amount is caused by wave breaking (Figure 4.1.2.2). Wave breaking only occurs when the water depth is shallow enough for the waves to reach their maximum wave height, which was possible with a rather high prescribed significant wave height of 5.67m. Wave dissipation is also the cause of the updrift directed current on the onshore side of the crests in Figure 4.1.1.1.b. The waves result in a larger alongshore flow close to the coast when bars are

not present (less wave dissipation) then in the situation where the bars are present. Therefore, when the flow pattern without bars is subtracted from the run with bars, the resulting flow is updrift directed close to the coast as seen in Figure 4.1.1.1.b.

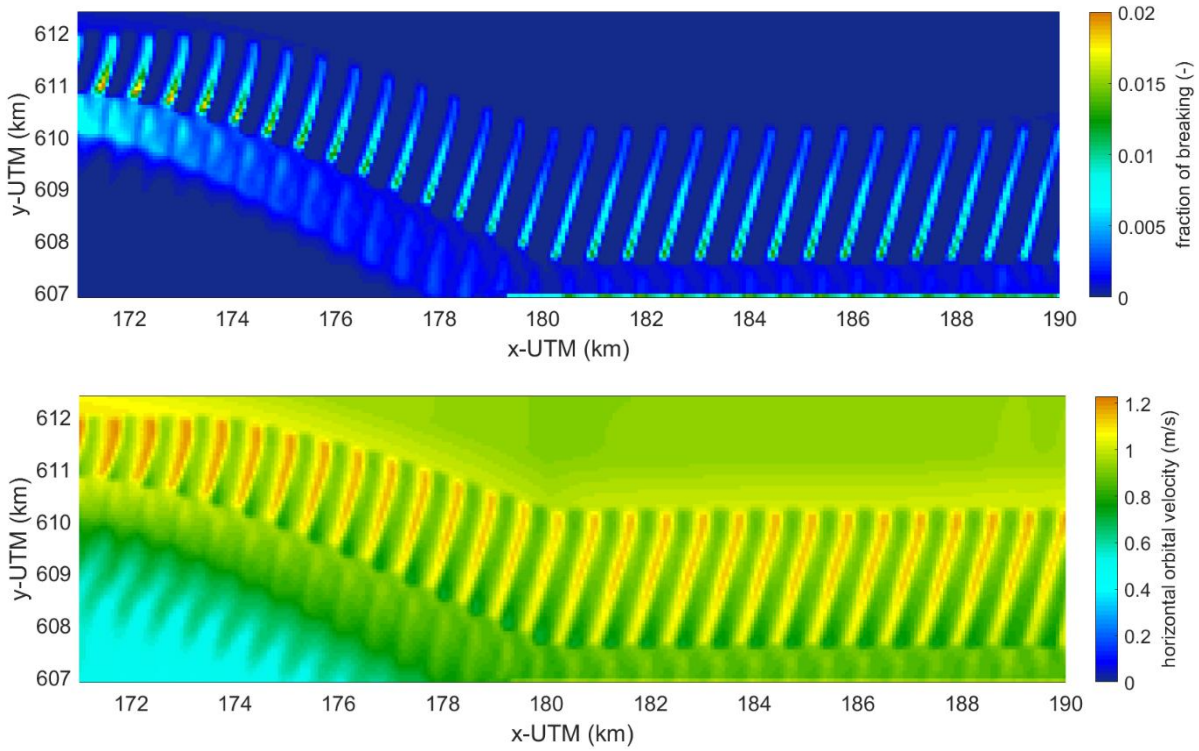

Figure 4.1.2.2. *The fraction of breaking waves (upper figure) and the energy dissipation by waves due to bed friction and wave breaking (lower figure). The model run was forced by a significant wave height of 5.67m coming from -38°. The default bar characteristics were used as bathymetry.*

The dissipation pattern depends on the initiated significant wave height. For a simulation forced by tides, wind, and waves with a significant wave height of 1m, the horizontal orbital velocities are largest at the landward side of the bar crests and the fraction of breaking waves is neglectable (Figure 4.1.2.3.b). For lower waves the orbital velocities increase in shallower waters compared to higher waves, due to their wave height. However, this not visible in the flow pattern since the pattern by wind is still dominating (Figure 4.1.2.3.a), but this becomes of great importance for the sediment transport as discussed in the next section.

When the hydrodynamics are only forced by wind, the flow only due to the presence of sawtooth bars (Figure 4.1.1.1.c), shows a converging flow path at the downstream side of the sawtooth bar crests which is almost equal in magnitude over the whole bar crest. This is because the wind is acting uniformly on the whole area of sawtooth bars. However, the flow magnitudes are a bit smaller on the seaward part of the bars compared to the landward part due to the relative water depth. Wind stress that acts on a larger depth results in a smaller depth average flow than wind stress that acts on a shallower area.

For different bar characteristics, the overall flow pattern remains the same, only the magnitude can differ. For higher bars the flow magnitude is overall higher. With higher bars the water depth becomes shallower above the crests, resulting in larger flow velocities on the crests compared to lower sawtooth bars. The troughs are deeper for higher bars, resulting in lower flow velocities in the troughs compared to lower sawtooth bars. For bars with a larger wavelength the bending flow path becomes

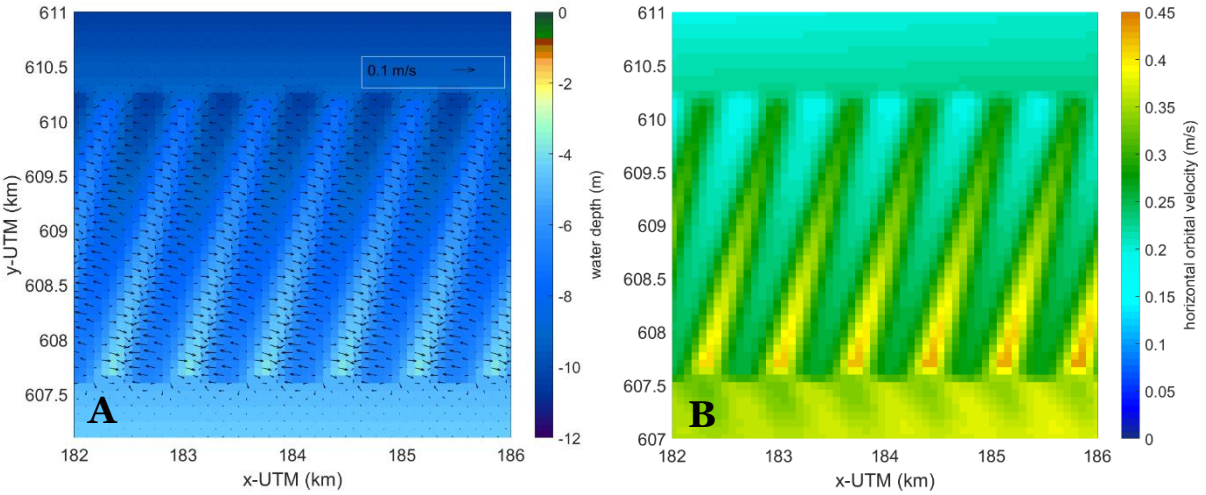

Figure 4.1.2.3. ***A)*** *The tidally averaged flow pattern only due to the presence of sawtooth bars for a simulation with tides (S2; 1m amplitude), wind (15m/s; -90°) and waves (H_s = 1m; -38°).* ***B)*** *The corresponding horizontal orbital velocity. The default bar characteristics were used in the simulation.*

broader but also the flow magnitude becomes larger. This is caused by the larger amount of dissipation on crests of sawtooth bars due to the larger surface area. This results in a larger wave driven alongshore current on the crests. Additionally, with a larger bar wavelength the incoming waves refract more towards the bar crests (Figure 4.1.2.4.). With a wavelength of 700m the mean wave direction on the bars is ±-80° and with a wavelength of 2100m the mean wave direction on the bars is ±-90° (the initial mean wave direction was -38°).

The wave direction defines partly the direction of the alongshore flow and so the flow pattern on the sawtooth bars. For example, when waves enter the area from the east and the wind from the west, the magnitude of both forces, together with the tide, determine the net alongshore flow direction. For eastern waves of 5.67m and western winds of 15m/s with a tide of 1m in amplitude, the alongshore flow was dominated in the downstream area by the wave direction, resulting in a flow pattern complementary to what is explained in Figure 4.1.2.1. However, no eastern waves higher then ±2.4m were observed along the Schiermonnikoog and only a small percentage of the waves enter from this direction (Figure 3.2.1). Therefore, a westward alongshore flow is not representative for real world situation and is therefore not further discussed.

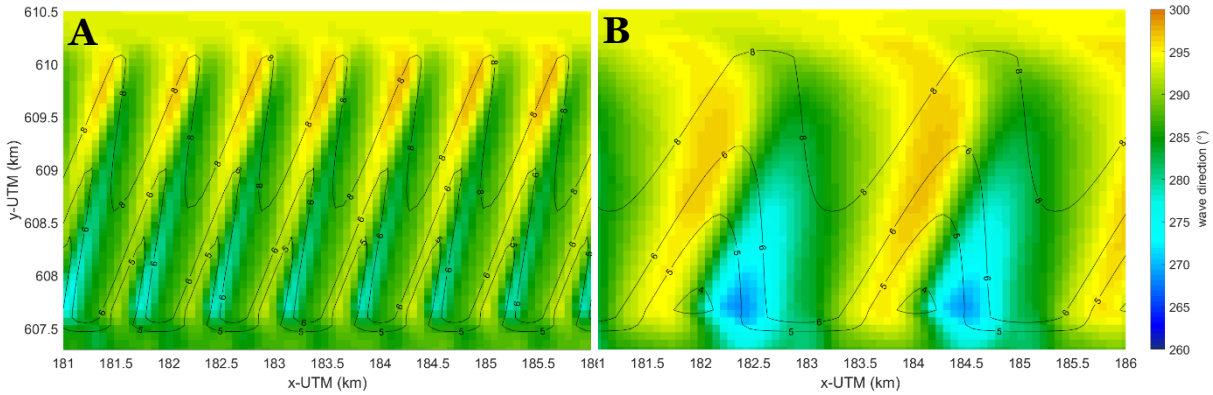

Figure 4.1.2.4. *The mean wave direction for* ***A)*** *the default simulation and* ***B)*** *a simulation with the default forcing parameters and bars with a wavelength of 2100m, a bar hight of 3m and an orientation of 14° with respect to the north.*

4.2 The influence of the sawtooth bars on the sediment transport

This section describes the influence of the sawtooth bars on the sediment transport, taking the forcing mechanisms and bar characteristics into account. The sediment transport patterns shown in this section are the tidally mean sediment transport patterns only due to the presence of sawtooth bars which includes bed load and suspended load (Figure 4.2.1.1). This was achieved by subtracting the tidally mean sediment transport of a run without bars from the tidally mean sediment transport of a run with bars, both with the same initial forcing. These specific sediment transport patterns are called 'bedform induced sediment transport patterns' from here on. Since sediment transport is only representative when forced by all three forcing mechanisms, the sediment transport patterns resulting from each individual forcing are not described.

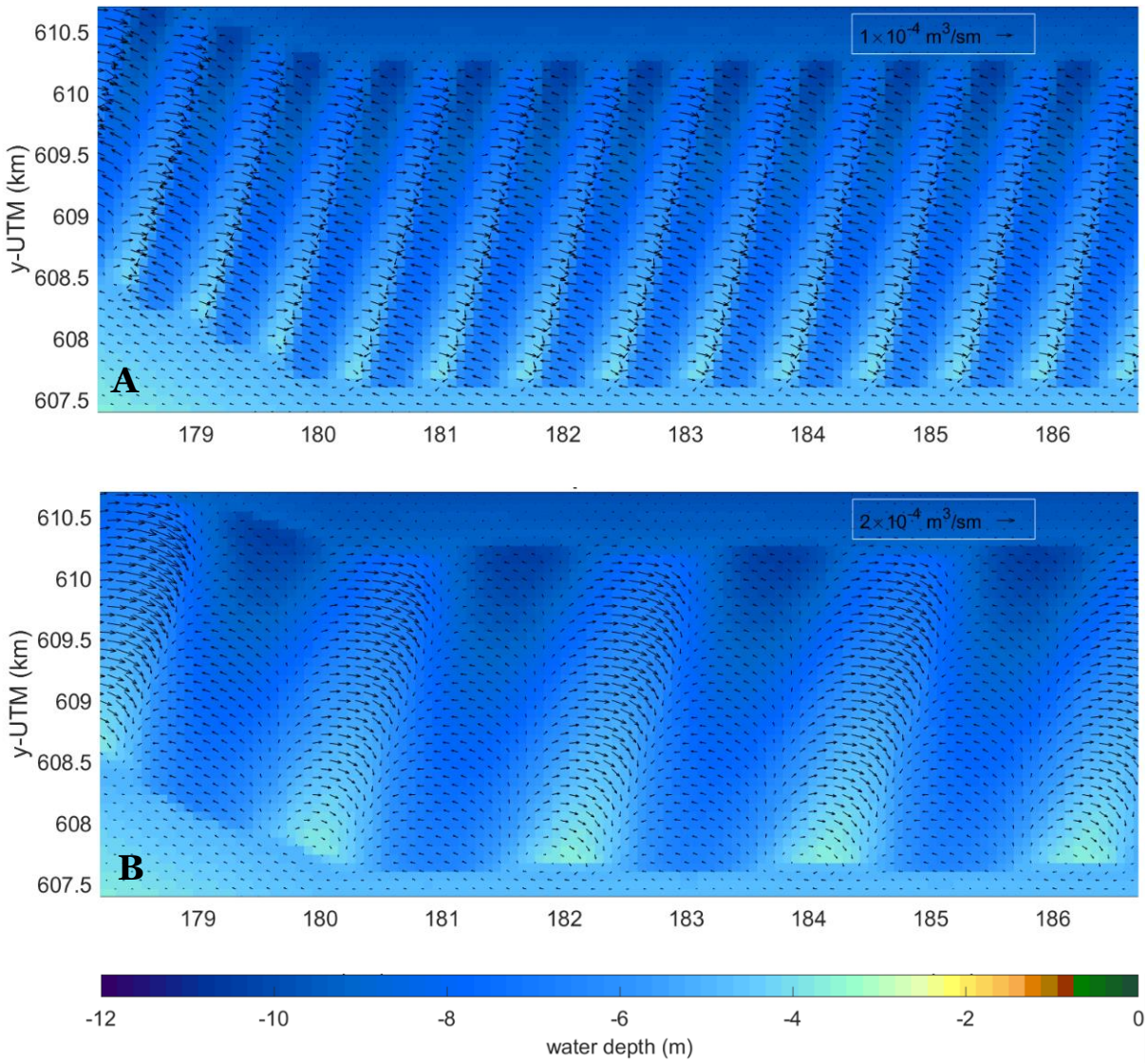

Figure 4.2.1.1. *The bedform induced sediment transport, for **A)** sawtooth bars with the default bar characteristics and **B)** sawtooth bars with an amplitude of 1.5m, a wavelength of 2100m and an orientation of 14° with respect to the north. The hydrodynamics were forced by the default forcing parameters.*

4.2.1 The sediment transport patterns due to the presence of sawtooth bars

Forced by tides, waves, and wind (default settings), the generated bed form induced sediment transport patterns are similar to the bed form induced flow patterns. The sediment transport shows a converging pattern on the downstream side of the crest and a diverging pattern on the updrift side of the crest (Figure 4.2.1.1). The magnitude of the transport is largest on the bar crests in combination with the most offshore location, which is deepest. This is caused by wave forcing, since waves of 5.67m generate a stronger alongshore flow at the seaward part of the bars compared to the landward part.

For different sawtooth bar characteristics (height, wavelength, and orientation), the sediment transport pattern remains roughly the same (Figure 4.2.1.1). The patterns are similar to the depth average velocity patterns as in Figure 4.1.1.2. Therefore, the sediment transport patterns of only two types of bars are shown in figure 4.2.1.1, which are discussed further on.

When the hydrodynamics are forced by default forcing parameters, and only the tidal amplitude, wave height or wind speed is varied, the bed form induced sediment transport patterns remain almost the same, only the magnitude differs. When the amplitude, wave height or wind speed is increasing,

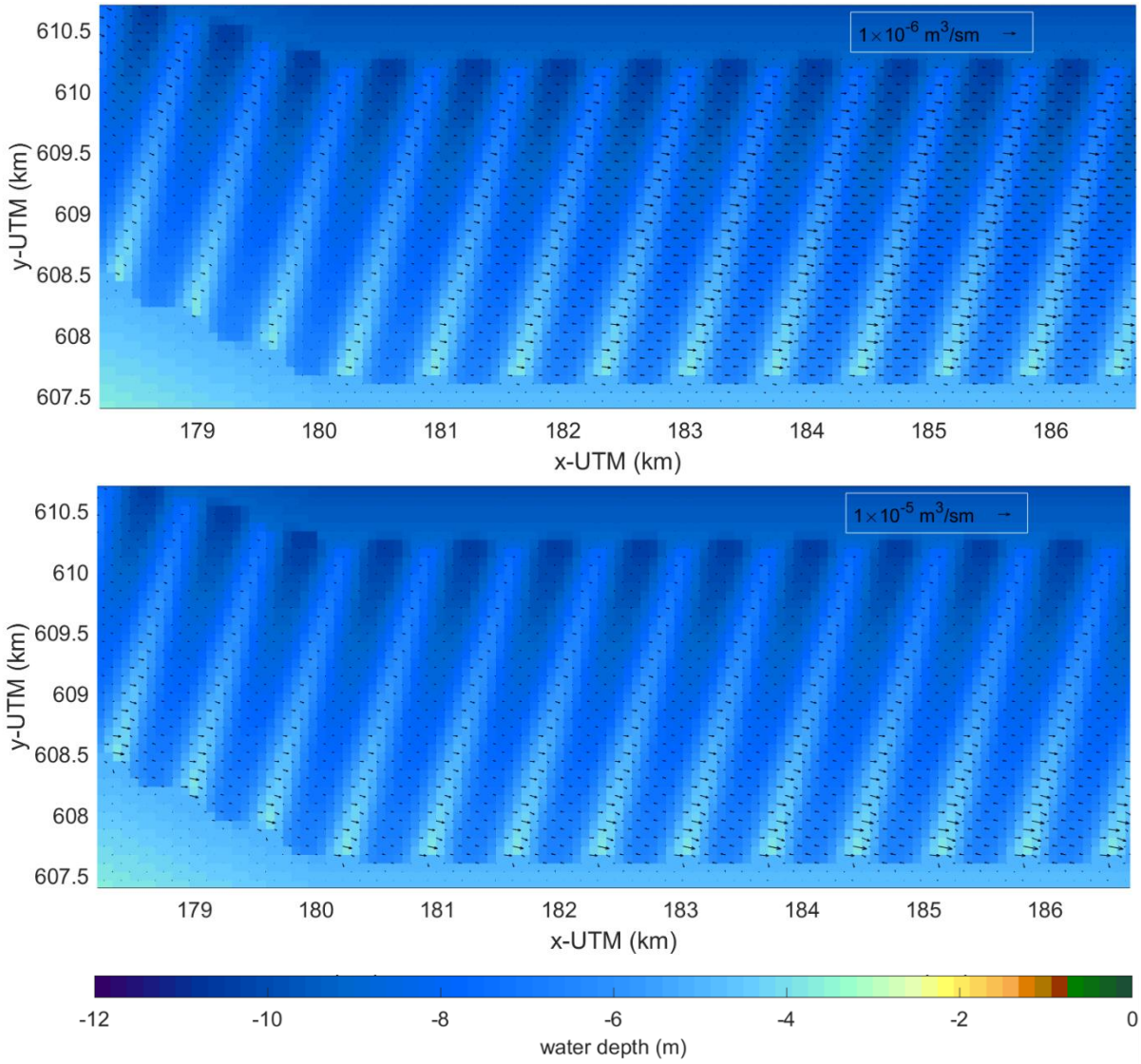

Figure 4.2.1.2. *The difference between the tidally averaged sediment transport of a model run with sawtooth bars and a model run without sawtooth bars forced by* ***A)*** *tides (S2, 1m amplitude) and wind (15m/s; -90°) and* ***B)*** *tides (S2, 1m amplitude), wind (15m/s; -90°) and waves (H_s = 1m; -38°). Sawtooth bars with the default bar characteristics were used in the simulations.*

the magnitude of the sediment transport increases, as is seen for the depth average velocity. However, when waves are absent (only wind and tidal forcing), the magnitude of the sediment transport becomes ±10 times lower compared to a simulation with tidal, wind and wave forcing in which the waves have a significant wave height of only 1m (Figure 4.2.1.2). This suggests that wave forcing is the dominant force resulting in sediment transport.

4.2.2 Physical interpretation of the sediment transport patterns

The bed form induced sediment transport patterns are similar to the flow patterns when forced by tides, waves and wind. This is logic since flow results in shear stresses that initiate sediment motion when they are higher than the critical shear stress.

The sediment transport patterns seem to be dominated by wave forcing, as can be seen in Figure 4.2.1.2. Waves forcing causes shear stress due to the orbital motion and due to the wave driven current. The higher the waves the larger the shear stresses and so the amount of sediment that can be transported. Wind forcing results only in shear stresses due to the wind speed. Therefore, waves are more likely to dominate the sediment transport patterns. This is shown in Figure 4.2.1.2 in which the bed form induced sediment transport is way larger with only a H_s of 1m compared to the simulation in

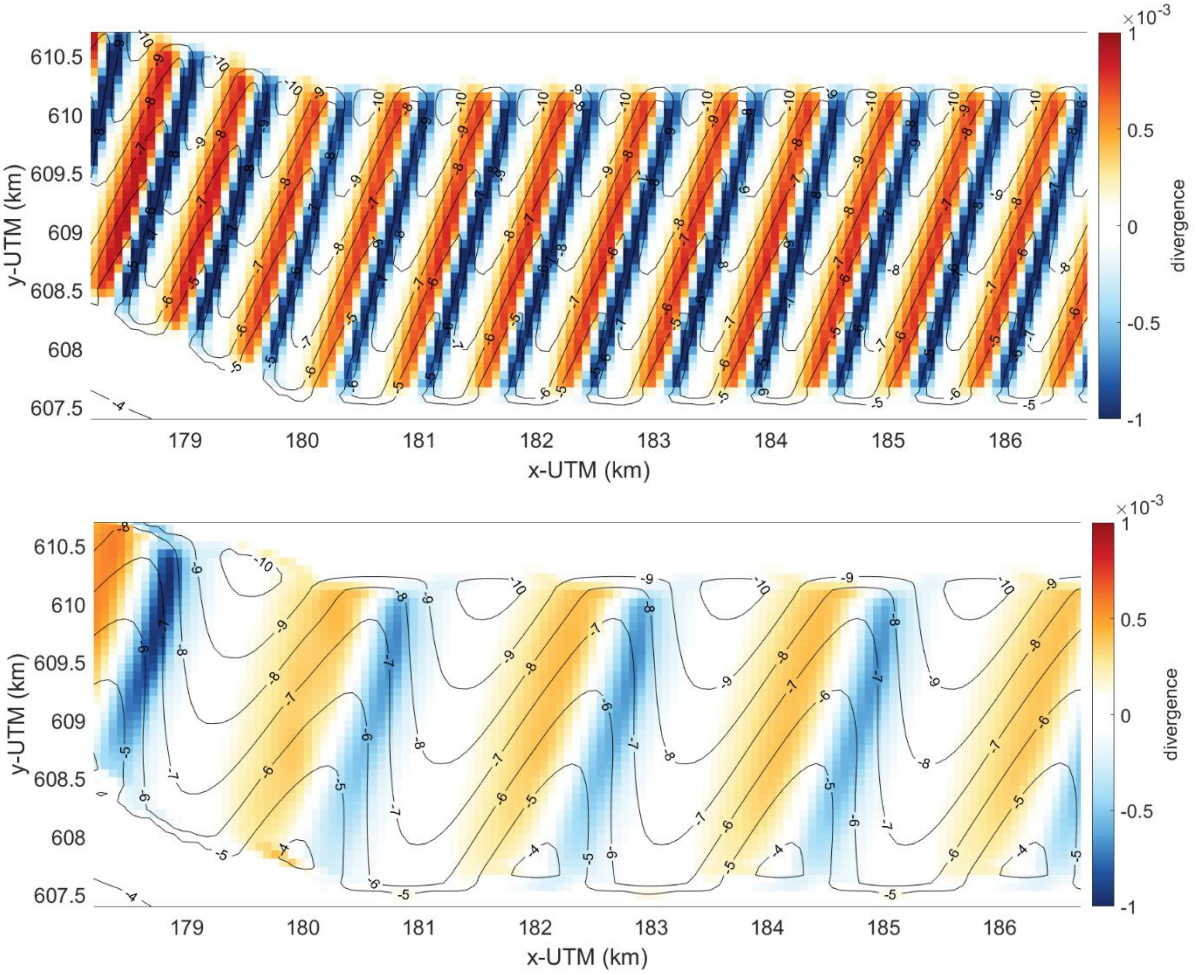

Figure 4.2.2.1. *Divergence of the bed form induced sediment transport of two model simulation with the default forcing parameters but with* ***A)*** *the default bar characteristics and* ***B)*** *a bar height of 3m, a wavelength of 2100m and an orientation of 14° with respect to the north. The solid lines are the depth contour lines. Positive divergence represents a divergent transport pattern and negative divergence represents a convergent transport pattern.*

which the waves are absent. The sediment transport increases mostly on the landward part of the bar crests, which is the same location as where the wave dissipation is largest (Figure 4.1.2.3). Wave dissipation of obliquely incident waves result in a wave driven alongshore current. This causes shear stresses that can initiate sediment transport. For high significant wave heights (5.67m) the dissipation is most abundant on the seaward part of the bars. Therefore, the bedform induced sediment transport is largest at the seaward side of the bars and smallest at the most landward side of the bars (Figure 4.2.1.1.).

Forced by tides, waves, and wind (default settings), the bed form induced sediment transport is converging on the downstream side of the crest and diverging on the updrift side of the crest. Figure 4.2.2.1.a/b shows the divergence of the sediment transport patterns shown in Figure 4.2.1.1.a/b. The reason behind this pattern is related to the change in flow magnitudes. The increase in flow velocity from the trough towards the crest results in an increase in shear stresses and therefore an increase in sediment pick-up in this area. The decrease in flow velocity from the crest towards the trough results in a decrease in shear stresses and therefore the sediment can settle in this area. The magnitude of the diverging and converging sediment transport is larger for bars with a smaller wavelength. Whether these patterns result in bar growth is presented in the next section.

4.3 The relative importance of the forcing mechanisms and bar characteristics for the generation and morphological change of the sawtooth bars

In this Section, the phase difference between the sawtooth bar pattern and the erosion/deposition pattern (ε) and the mean bar growth/decay rate ($\bar{\varphi}$) are presented for varying parameters. Seven parameters were examined to study the effect on $\bar{\varphi}$ and ε: 1) the wind speed, 2) tidal amplitude, 3) wave direction, 4) the wave height, 5) bar wavelength, 6) bar wave height and 7) bar orientation.

4.3.1 Phase difference between the bar pattern and the erosion deposition pattern

The phase difference between the bar pattern and the erosion deposition pattern (ε) was calculated to determine if the bars would grow (phase difference < 90°) or decay (phase difference > 90°) and what their relative migration speed would be. With a phase difference of 90°, the migration speed is optimal and with a phase difference of 0° or 180° degrees no migration occurs, only bar growth or decay. So, the phase difference ε shows the relation between the migration speed and the grow/decay rate. The larger the migration speed, the slower the growth/decay rate and vice versa.

1) Wind speed

With an increasing wind speed the phase difference ε increases, but only with a small amount (Figure 4.3.1.1.a). For all the different wind speeds the phase difference was above 90°, which indicates bar decay. This suggests that with an increasing wind speed the bars decay faster and the migration speed becomes slower.

2) Tidal amplitude

With an increasing tidal amplitude, the phase difference ε is increasing, but only with a few degrees (Figure 4.3.1.1.b). The phase difference was higher than 90° for all tidal amplitudes, which suggests bar decay. This indicates that with an increasing tidal amplitude, the bars decay faster and the migration speed becomes slower. The increasing phase difference is mainly visible for the upstream area. In the downstream area the phase difference remains almost equal for different tidal amplitudes.

3) Wave direction

There is no direct relation visible between the phase difference ε and the wave direction (Figure 4.3.1.1.c). The erosion deposition pattern was for all cases shifted downdrift except for waves from the east (25° and 45°). The phase difference seems larger for waves from the east suggesting larger decay rates and relatively smaller migration speeds.

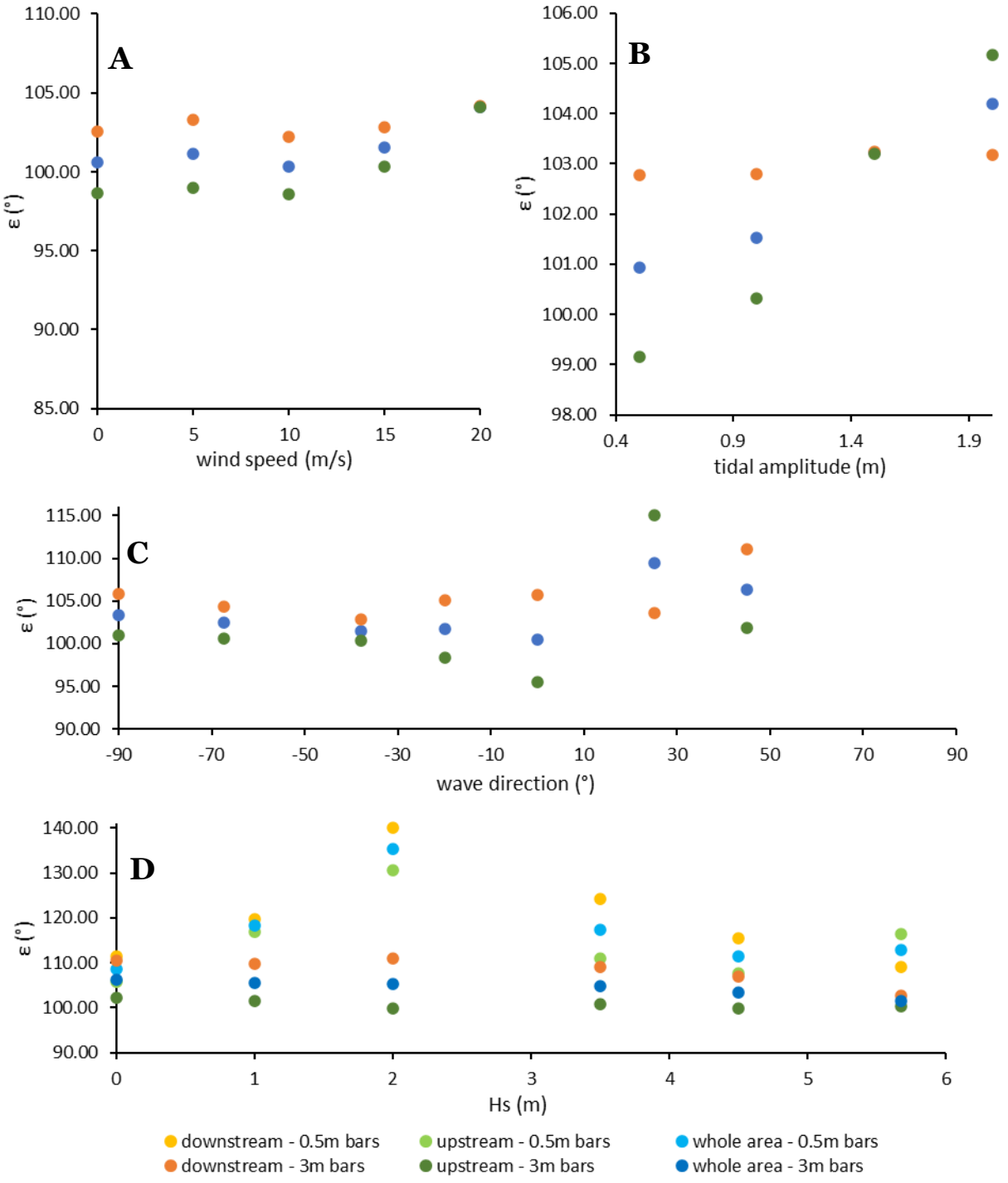

Figure 4.3.1.1. *The phase difference ε measured for the downstream, upstream, and whole sawtooth bar area as function of the* ***A)*** *wind speed* ***B)*** *tidal amplitude* ***C)*** *wave direction* ***D)*** *significant height. The model simulations were forced by tides, waves, and wind (run series 2-5) and the bars had a wavelength of 700m and an orientation of 14° with respect to the north. The bar height is specified in the legend.*

4) Wave height

The wave height does not seem correlated with the phase difference ε (Figure 4.3.1.1.d). All the phase differences are above 90 degrees, so they all would result in sawtooth bar decay. It is visible that for the sawtooth bars of 0.5m high, the phase difference is overall larger compared to the sawtooth bars with a height of 3 meters. Therefore, the bars of 3m high are expected to migrate faster and decay slower compared to the bars of 0.5m high. The peak in ε for 0.5m high bars forced by a significant wave height of 2m is rather odd and the causes is not known. This suggests that 0.5m high bars decay faster with a wave height of 2m.

5) Bar wavelength

With an increasing bar wavelength, the phase difference ε is decreasing (Figure 4.3.1.2.a). For the bars with a wavelength of 1400m and 2100m, the phase difference was below 90° (78° and 63° on average over the whole area), which implies bar growth.

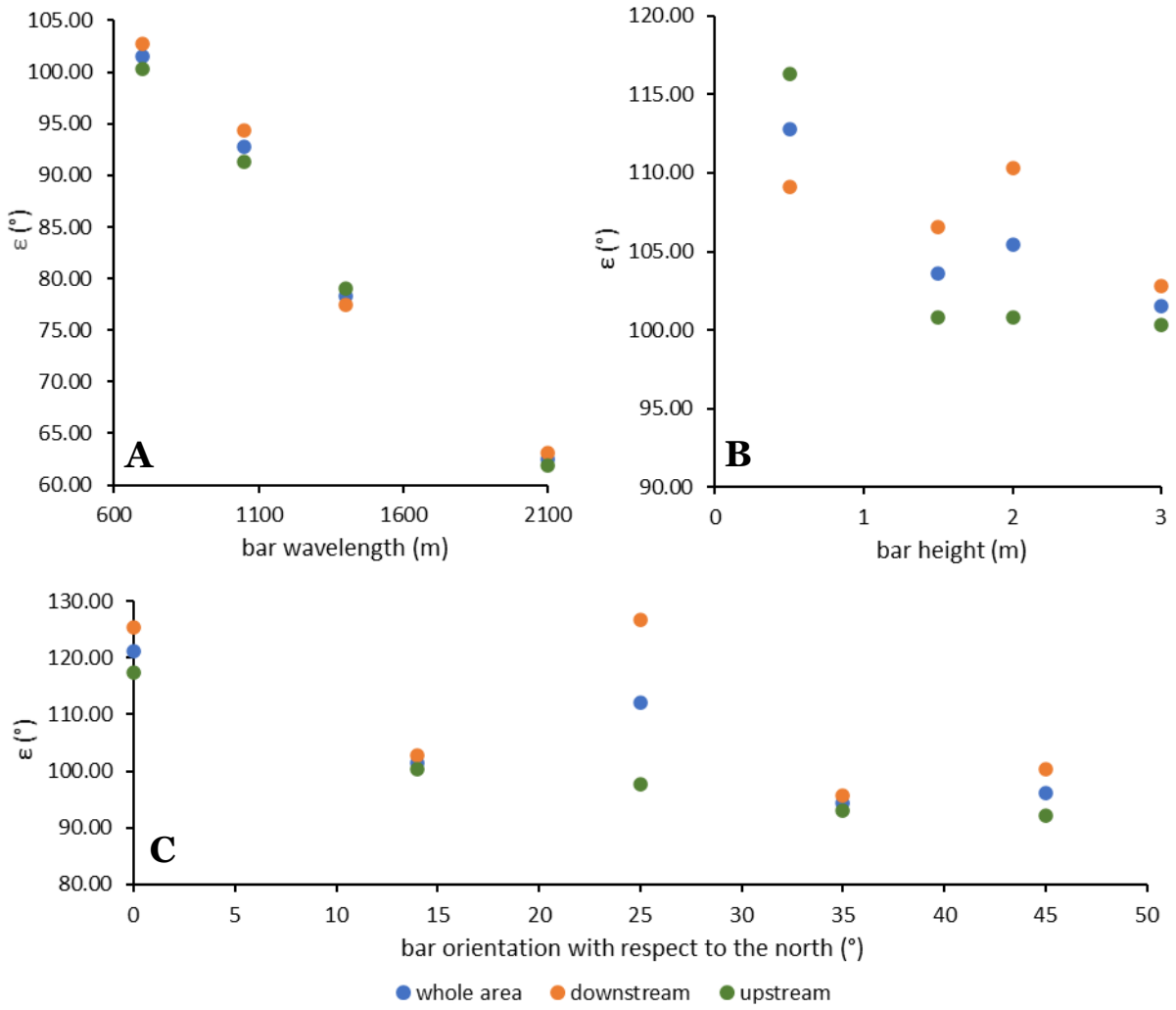

Figure 4.3.1.2. *The phase difference ε measured for the downstream, upstream, and whole sawtooth bar area as function of the* ***A)*** *bar wavelength* ***B)*** *bar height and* ***C)*** *bar orientation with respect to the north. In each plot 1 bar characteristic was varied and the other bar characteristics were kept as default (run series 6-8). The simulations were forced by the default forcing parameters.*

6) Bar height

With an increasing bar height, the phase difference ε is decreasing (Figure 4.3.1.2.b). The phase difference was above 90° for all the bar heights, suggesting bar decay. Additionally, this implies that the larger the bar height the larger the migration speed and the slower the decay.

7) Bar orientation

With an increasing bar orientation, the phase difference ε is decreasing (Figure 4.3.1.2.c). For a bar orientation of 35°, the lowest phase difference ε is seen. However, all phase differences are above 90°, suggesting bar decay. So, this implies that the larger the bar orientation, the larger the migration speed and the slower the decay.

4.3.2 The growth/decay rate of the sawtooth bars

The bar growth/decay rate is expressed as the quantity $\bar{\varphi}$. When $\bar{\varphi}$ is positive, bar growth is observed, and when $\bar{\varphi}$ is negative decay is observed.

1) Wind speed

For an increasing wind speed the quantity $\bar{\varphi}$ becomes more negative which is in line with the phase difference ε. So, the larger the wind speed the faster the bars decay (Figure 4.3.2.1.a).

2) Tidal amplitude

For an increasing tidal amplitude $\bar{\varphi}$ becomes more negative which is in line with the phase difference ε. However, this relation is rather weak because $\bar{\varphi}$ becomes only a bit more negative with a 1.5m increase in tidal amplitude (Figure 4.3.2.1.b). The quantity $\bar{\varphi}$ was negative in all cases. Additionally, a trendline through the data results in a negative y-intersect, which means that for every tidal amplitude the bars decay, when the default settings are taken as other parameters.

3) Wave direction

The sawtooth bars decay less when waves enter the area from the west compared to waves from the east, when $\bar{\varphi}$ is averaged over the whole sawtooth bar area (Figure 4.3.2.1.c). For all wave directions, $\bar{\varphi}$ was negative, so decay in each case. This was also suggested by the phase difference ε. For waves from the east, the decay is larger in downstream area compared to the upstream area. When eastern waves enter the sawtooth bar area, they do not dissipate on the ebb-tidal delta and therefore enter the downstream area with more energy than western waves, resulting in a larger decay rate.

4) Wave height

For an increasing wave height $\bar{\varphi}$ becomes more negative (Figure 4.3.2.1.d). However, there is a difference in the gradient of the trend for $\bar{\varphi}$ with sawtooth bars of 3m high compared to bars of 0.5m high. The higher the sawtooth bars and wave height, the faster the decay. This was not visible in the relation between the wave height and phase difference ε. This is caused by the amount of energy put into the system. A larger wave height results in a larger amount of sediment transport and so larger decay rates.

5) Bar wavelength

With an increasing wavelength $\bar{\varphi}$ becomes more positive. The quantity φ is positive with a bar wavelength of 1400m and 2100m and negative for the other wavelengths (Figure 4.3.2.2.a). This is in line with the phase difference ε. A trendline suggests that bars grow when their wavelength is larger then ±1300m.

6) Bar height

The higher the sawtooth bars, the faster the bars decay (Figure 4.3.2.2.b). This is not visible in the phase difference ε which is a result of the wave dissipation. The higher the bars the larger the amount of wave dissipation and the faster the bars decay.

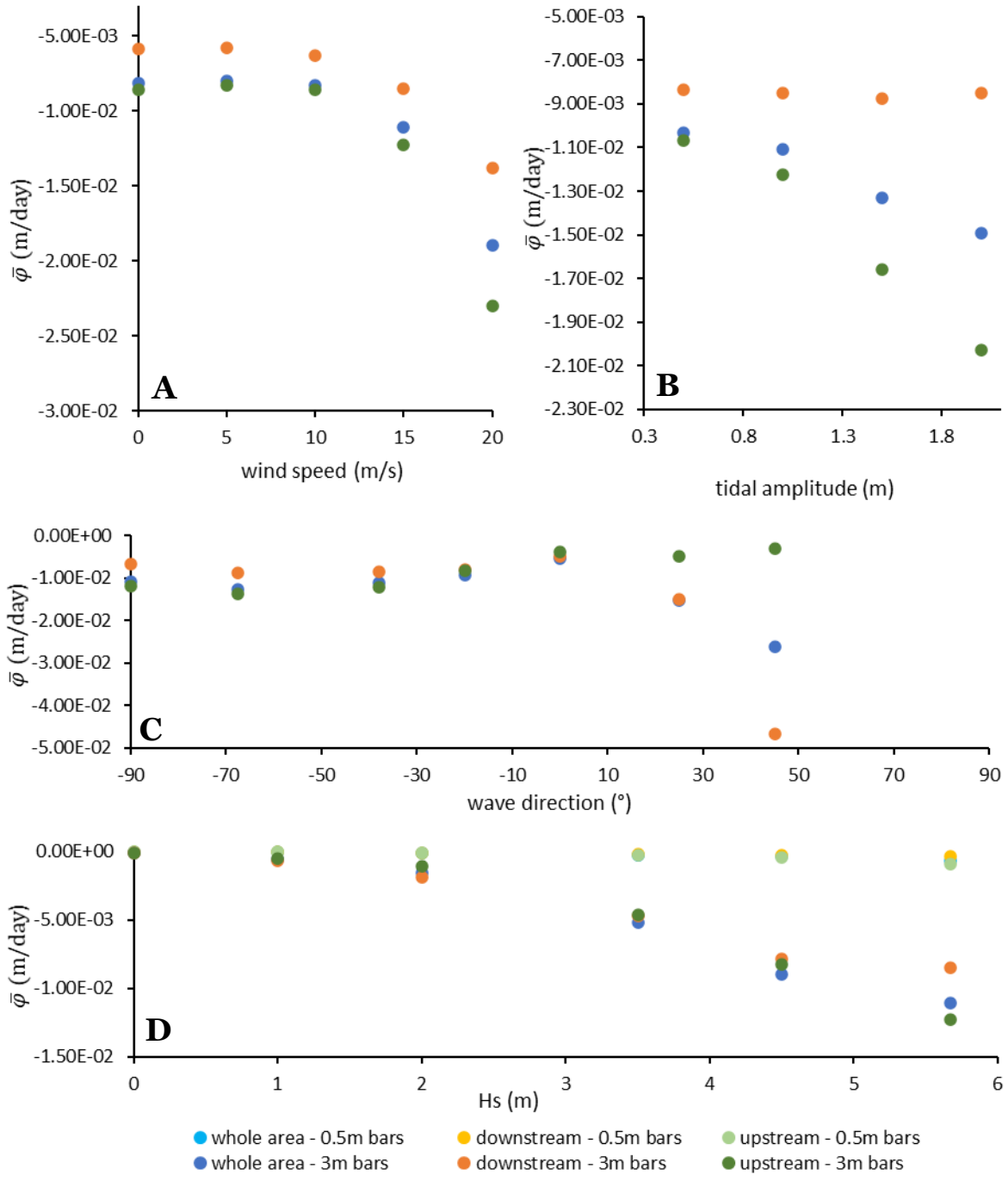

Figure 4.3.2.1. *The quantity $\bar{\varphi}$ measured for the downstream, upstream, and whole sawtooth bar area as function of the **A)** wind speed **B)** tidal amplitude **C)** wave direction **D)** significant height. The model simulations were forced by tides, waves, and wind (run series 2-5) and the bars had a wavelength of 700m and an orientation of 14° with respect to the north. The bar height is specified in the legend.*

7) Bar orientation

The larger the bar orientation with respect to the north, the slower the bars decay (Figure 4.3.2.2.c). So, for all bar orientations, the sawtooth bars would decay, using the default settings as other parameters. This is in line with the outcomes of the phase difference ε.

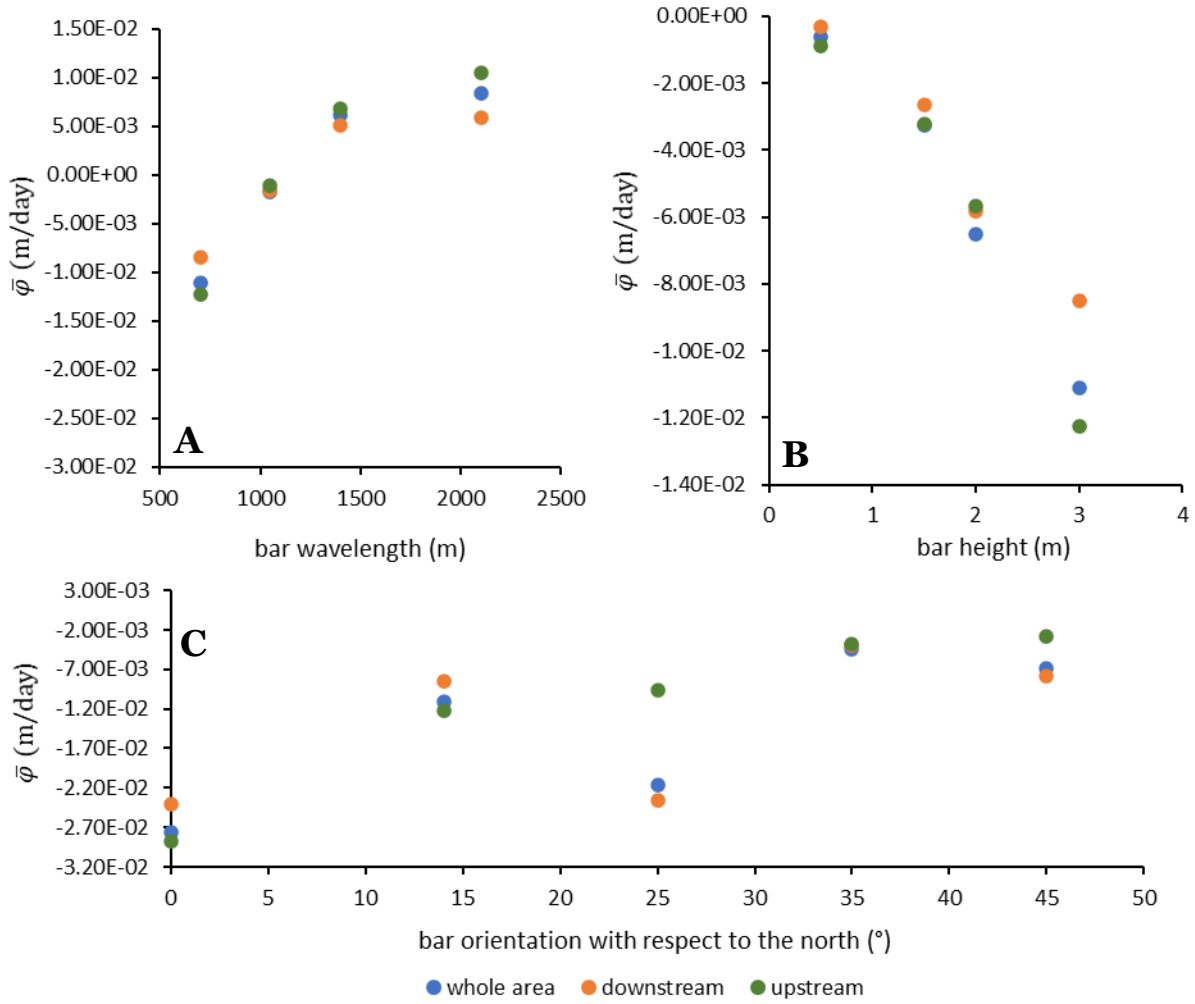

Figure 4.3.2.2. *The quantity $\bar{\varphi}$ measured for the downstream, upstream, and whole sawtooth bar area as function of the* ***A)*** *bar wavelength* ***B)*** *bar height and* ***C)*** *bar orientation with respect to the north. In each plot 1 bar characteristic was varied and the other bar characteristics were kept as default (run series 6-8). The simulations were forced by the default forcing parameters.*

4.4 The relative influence of the forcing mechanisms and bar characteristics on the migration speed of the sawtooth bars

The migration speed of the sawtooth bars was calculated to examine which parameters would cause the sawtooth bars to accelerate and which parameters would cause the bars to decelerate. Seven parameters were examined to study the effect on the migration speed: 1) the wind speed, 2) tidal amplitude, 3) wave direction, 4) the wave height, 5) bar wavelength, 6) bar wave height and 7) bar orientation.

1) Wind speed

With an increasing wind speed the migration speed is increasing (Figure 4.4.1.a). This is not in line with the outcomes of the phase difference ε which is a result of the amount of energy put into the system. The larger the wind speed the larger the amount of energy and so the amount of sediment transport that causes migration.

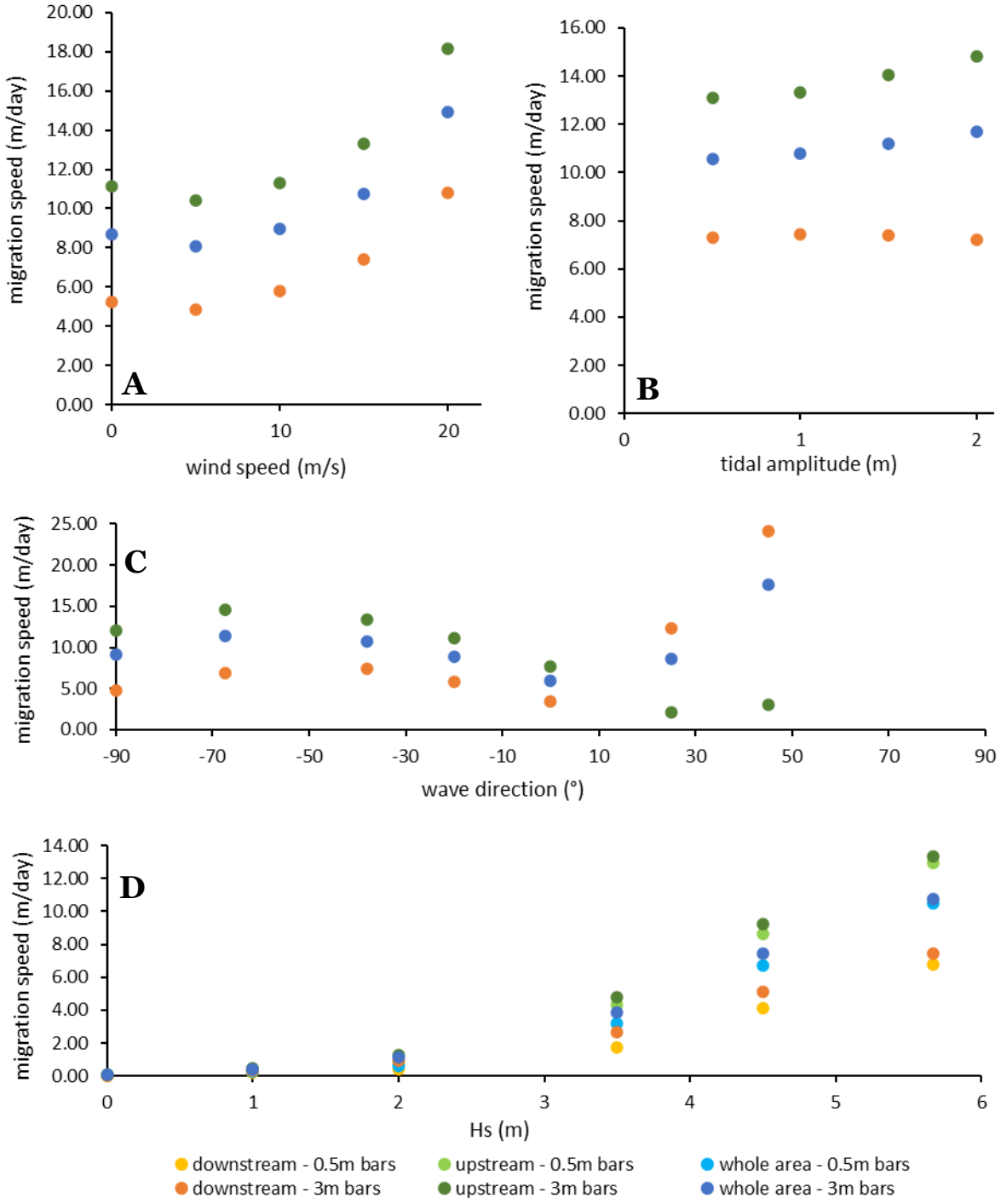

Figure 4.4.1. *The migration speed measured for the downstream, upstream, and whole sawtooth bar area as function of the* ***A)*** *tidal amplitude* ***B)*** *wind speed* ***C)*** *wave direction* ***D)*** *significant height. The model simulations were forced by tides, waves, and wind (run series 2-5) and the bars had a wavelength of 700m and an orientation of 14° with respect to the north. The bar height is specified in the legend.*

2) Tidal amplitude

With an increasing tidal amplitude, the migration speed increases in the upstream area, but only with a small amount (Figure 4.4.1.b). This is not in line with the outcomes of the phase difference ε which is a result of the amount of energy put into the system. The larger the tidal amplitude the larger the amount of energy and so the amount of sediment transport that causes migration. In contrast the migration speed in the downstream area remains almost equal for different tidal amplitudes which is in line with the phase difference ε.

3) Wave direction

The bar migration speed is ±10m/day when forced by western waves between -90° and 0° with a significant wave height of 5.67m (Figure 4.4.1.c). For waves that enter from the east, small migration speeds are visible in the upstream area. This is caused by the downdrift tidal and wind driven alongshore current that opposes the updrift wave driven alongshore current in the upstream area. In contrast, large migration speeds are observed in the downstream area for waves that enter the area from the east. This is due to the fact the eastern waves are not dissipating as much as western waves due to the presence of the shallow ebb-tidal delta.

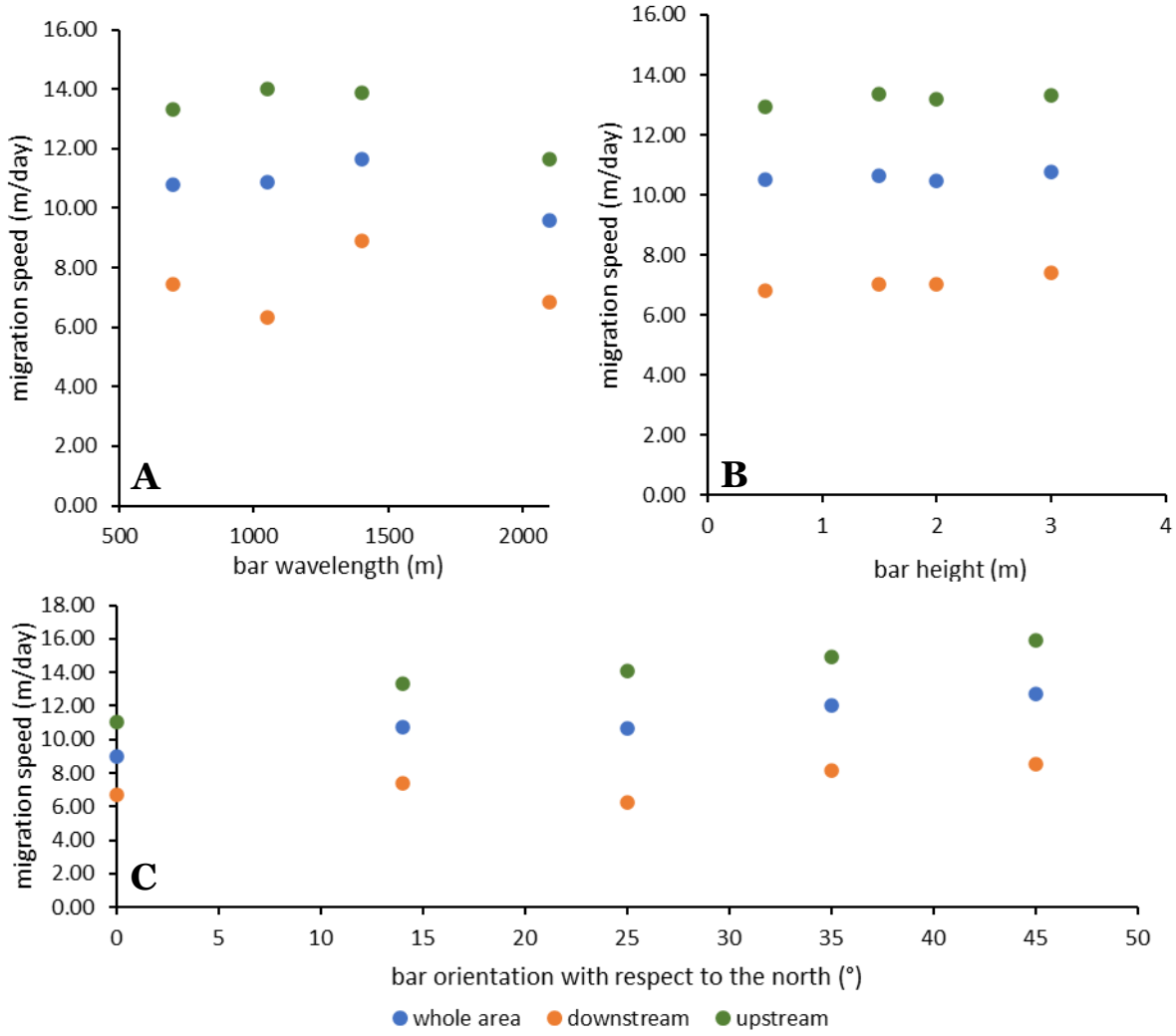

Figure 4.4.2. *The migration speed measured for the downstream, upstream, and whole sawtooth bar area as function of the* ***A)*** *bar wavelength* ***B)*** *bar height and* ***C)*** *bar orientation with respect to the north. In each plot 1 bar characteristic was varied and the other bar characteristics were kept as default (run series 6-8). The simulations were forced by the default forcing parameters.*

4) Wave height

With increasing wave height, the migration speed is increasing (Figure 4.4.1.d). Additionally, the migration speed is overall larger for sawtooth bars with a height of 3m compared to bars with a height of 0.5m. When the significant wave height is zero meters, the migration is almost zero (6-8 cm/day). This suggests that the significant wave height is the most important parameter for bar migration.

5) Bar wavelength

The migration speed is lower for bars with a wavelength of 2100m compared to bars with a wavelength of 1400m or smaller (Figure 4.4.2.a). This is not line with the phase difference ε in which bars with a wavelength of 1050m and 1400m were closest to the phase difference of 90° suggesting the largest migration speed. This is a result of the bar volume. Bars with a larger wavelength have a larger bar volume which takes a longer time to migrate a number of meters with the same forcing, compared to bars with a smaller bar volume.

6) Bar height

The migration speed increases with an increasing bar height, but only with a small amount (Figure 4.4.2.b). This is in line with the phase difference ε and also seen in Figure 4.4.1.d.

7) Bar orientation

With increasing bar orientation with respect to the north, the migration speed is increasing (Figure 4.4.2.c). This is in line with the trend that is visible in the phase difference ε.

4.5 Natural bar growth by random small amplitude perturbation

Long-term simulations with small amplitude perturbations were performed to study which forcing mechanisms would result in natural sawtooth bars development. Three long-term runs were accomplished, forced by tides, waves, and wind, with varying significant wave heights (2m, 3.5m and 5.67m). In the simulation with a significant wave height of 2 meters, bars developed with an upstream orientation, a wavelength of ±1500m and a crest length of ±3.5km (Figure 4.5.1). Because these bars do not resemble sawtooth bars, they are not further discussed in terms of their characteristics. Bars that resembled sawtooth bars appeared in the model simulations with a significant wave height of 3.5m and 5.67m. These bars are analysed in Subsection 4.5.1 and 4.5.2. The possible mechanisms resulting in bar growth or decay are presented in Subsection 4.5.3.

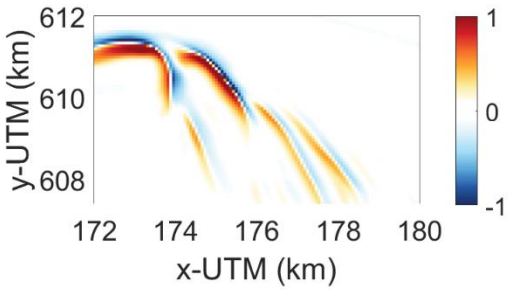

Figure 4.5.1. *The developed bar pattern (H') from a small amplitude perturbation after 400 hydrodynamic days. The model simulation had an initialized significant wave height of 2m (-38°), a tidal amplitude of 1m (S2) and wind of 15m/s coming from the west (-90°).*

4.5.1 Natural bar development forced by a significant wave height of 3.5m

After 54 days, bars developed on the ebb-tidal delta with bar height of ±0.4m and a bar wavelength of ±700m (Figure 4.5.1.1 and 4.5.1.2). The bar height increased to 0.9m between day 54 and day 200. The crest length remained approximately the same over time with an average length of 1.2km. The migration speed on the other hand decreased from ±18m/day to 10m/day between day 54

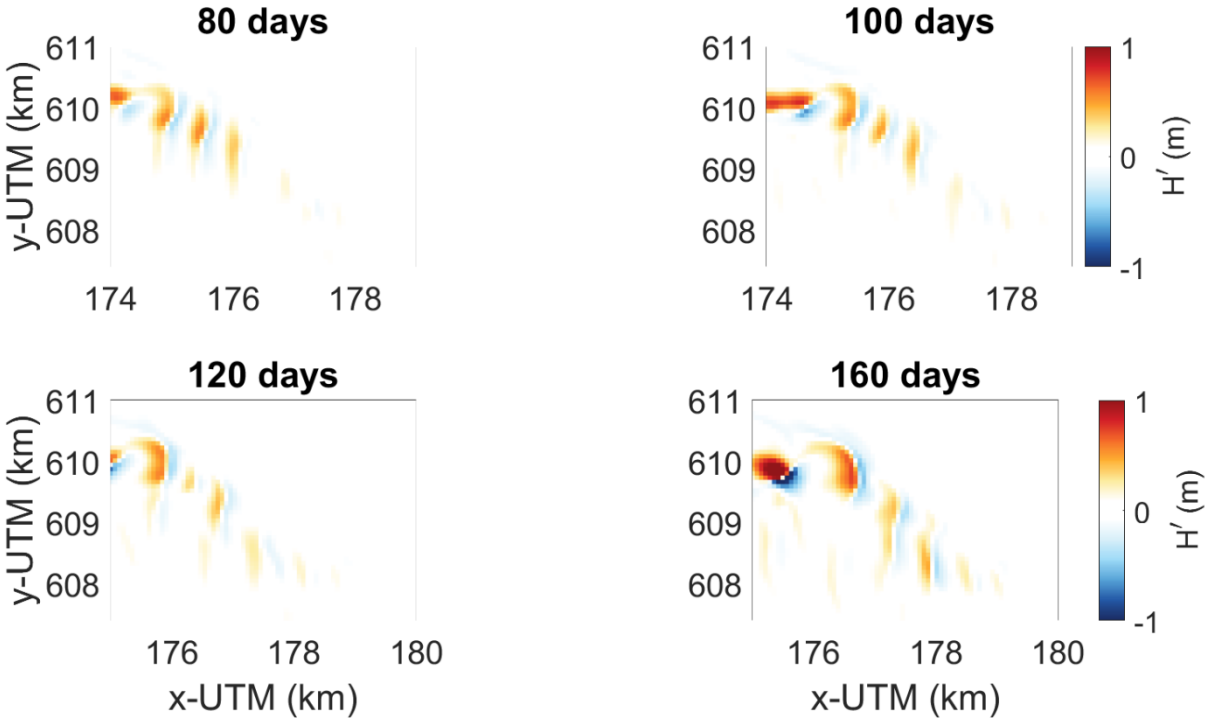

Figure 4.5.1.1. *The developed bar pattern (H') on the ebb-tidal delta after 80, 100, 120 and 160 days. The model simulation was forced by a significant wave height of 3.5m (-38°), a tidal amplitude of 1m (S2) and wind of 15m/s coming from the west (-90°).*

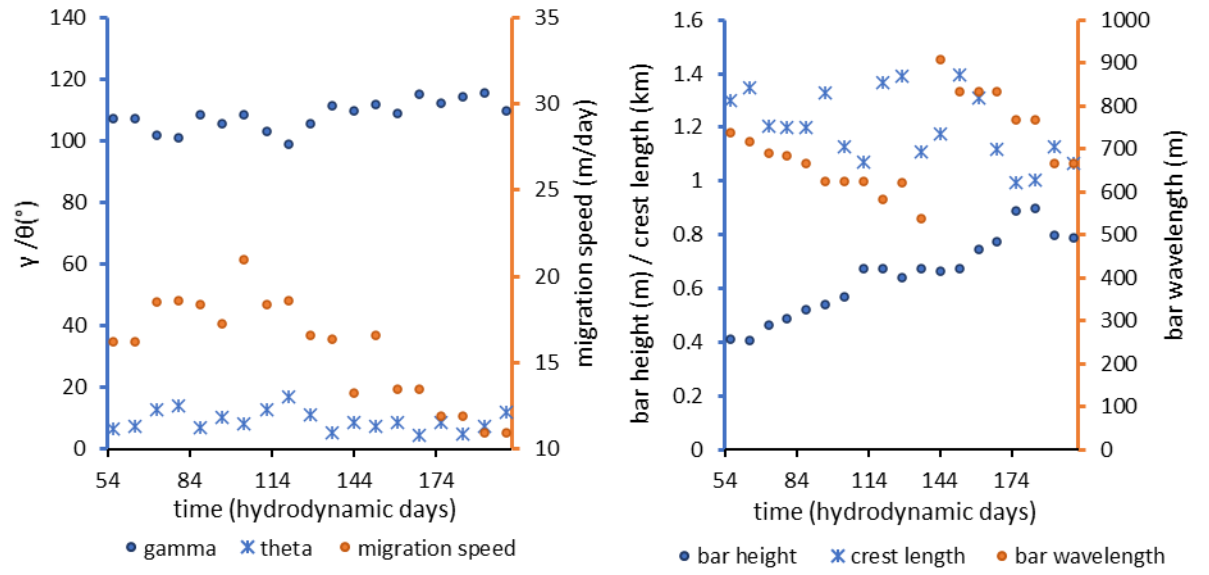

Figure 4.5.1.2. *The bar properties of the bars that evolved on the ebb-tidal delta between day 56 and 200. The model simulation was forced by a significant wave height of 3.5m (-38°), a tidal amplitude of 1m (S2) and wind of 15m/s coming from the west (-90°).*

and day 200. Lastly, the orientation of the bars with respect to the depth contours (γ) is ranging between 107° and 116°. After day 200 the bars disappeared, and shoals start to form in the area.

4.5.2 Natural bar development forced by a significant wave height of 5.67m

Bars developed on the ebb-tidal delta after 30 hydrodynamic days, of which the bar height and wavelength increased over time (Figure 4.5.2.1). The bar height increased from 0.5m to 2m and the wavelength increased from 625m to 1000m between day 30 and day 200 (Figure 4.5.2.2). Additionally, the crest length increased in this time span from 1.40km to 2.26km and the orientation between the bars crests and the depth contours decreased from 109° at day 30 to 58° at day 200 (Figure 4.5.2.2). These characteristics resemble sawtooth bars well. However, the migration speed is extremely high (±23m/day), which is not in line with sawtooth bars. The shape of the bars becomes curved and shoal like from day 200. Therefore, the bar characteristics were quantified until day 200.

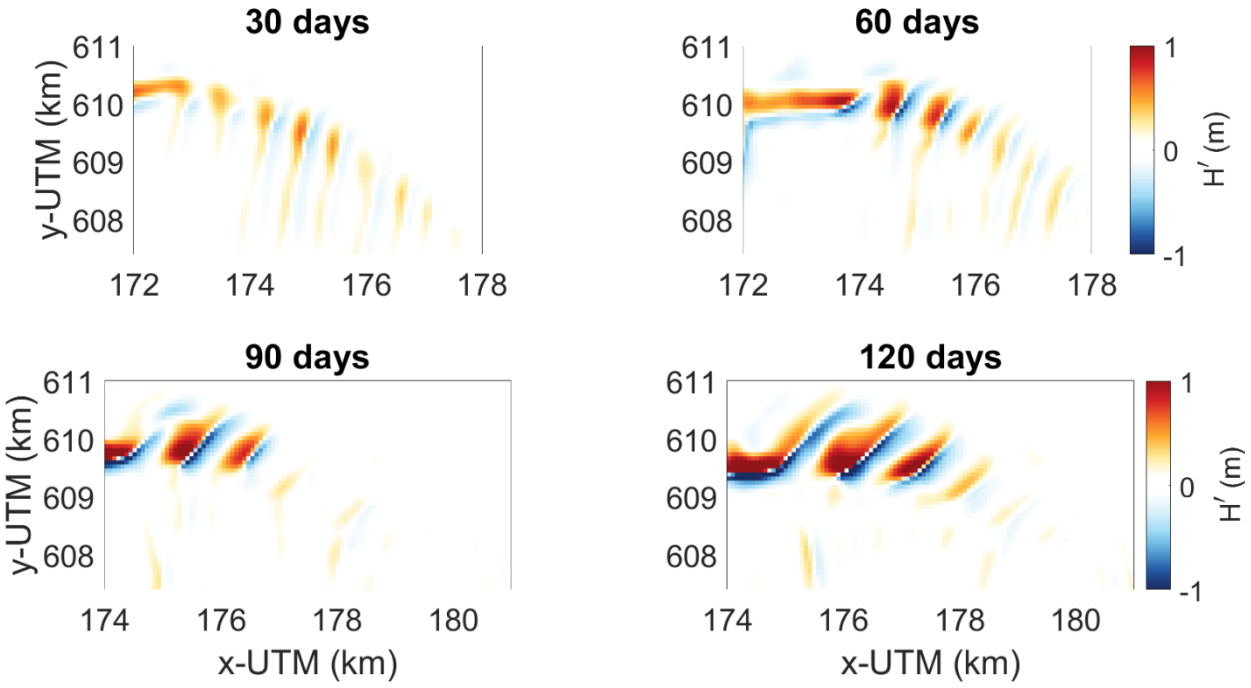

Figure 4.5.2.1. *The developed bar pattern (H') on the ebb-tidal delta after 30, 60, 90 and 120 days. The model simulation was forced by the default forcing parameters*

After 250 days, bars developed in the downstream area (Figure 4.5.2.3). These bars increased in bar height from 0.4m to 1.2m between day 250 and 400. After day 400, the bar height decreased a bit. The wavelength remained almost the same over this time span, ±1500m, as well as the crest length (±2km) (Figure 4.5.2.4). The mean migration speed of these bars is 9.6m/day and the mean orientation between the bar crest and the depth contours is 60°. The bar characteristics were quantified until day 400 due to the development of shoals in the downstream area.

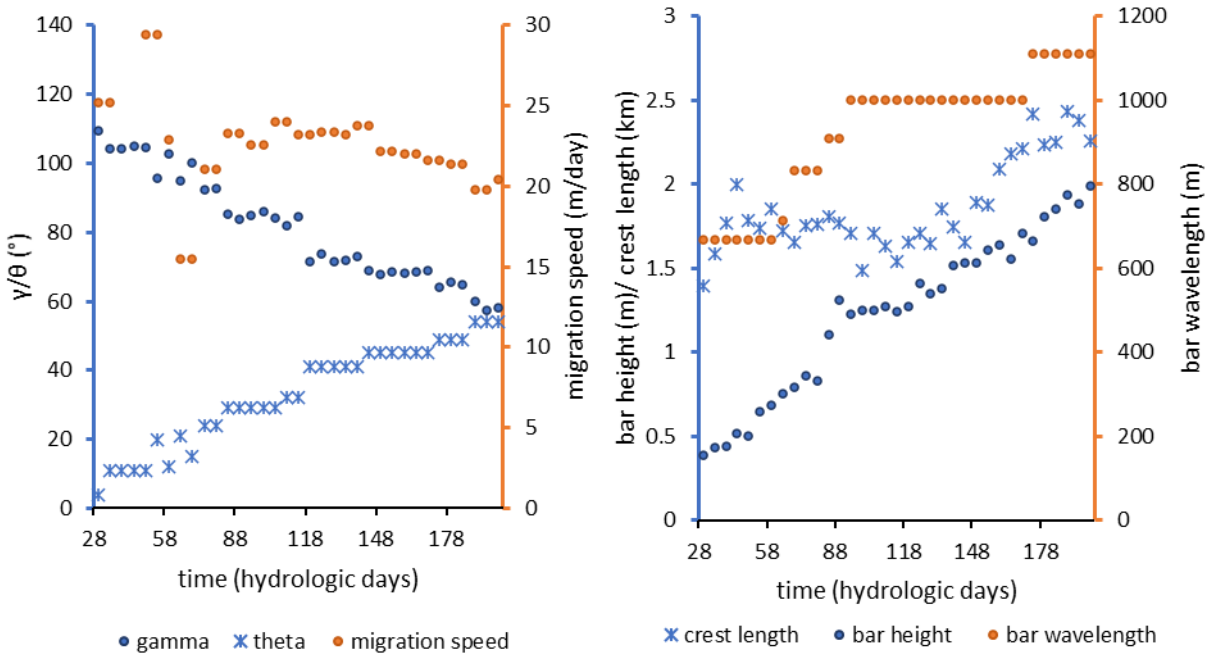

Figure 4.5.2.2. *The bar properties of the bars that evolved on the ebb-tidal delta between day 30 and 200. The model simulation was forced by the default forcing parameters*

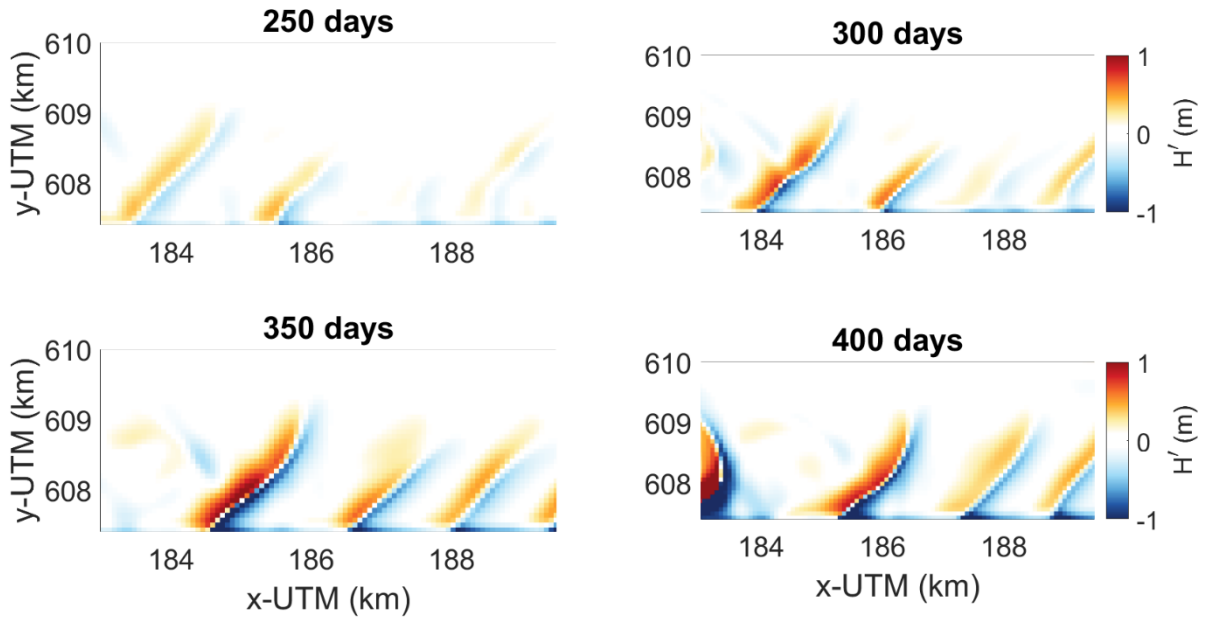

Figure 4.5.2.3. *The developed bar pattern (H') in the downstream area after 250, 300, 350 and 400 days. The model simulation was forced by the default forcing parameters.*

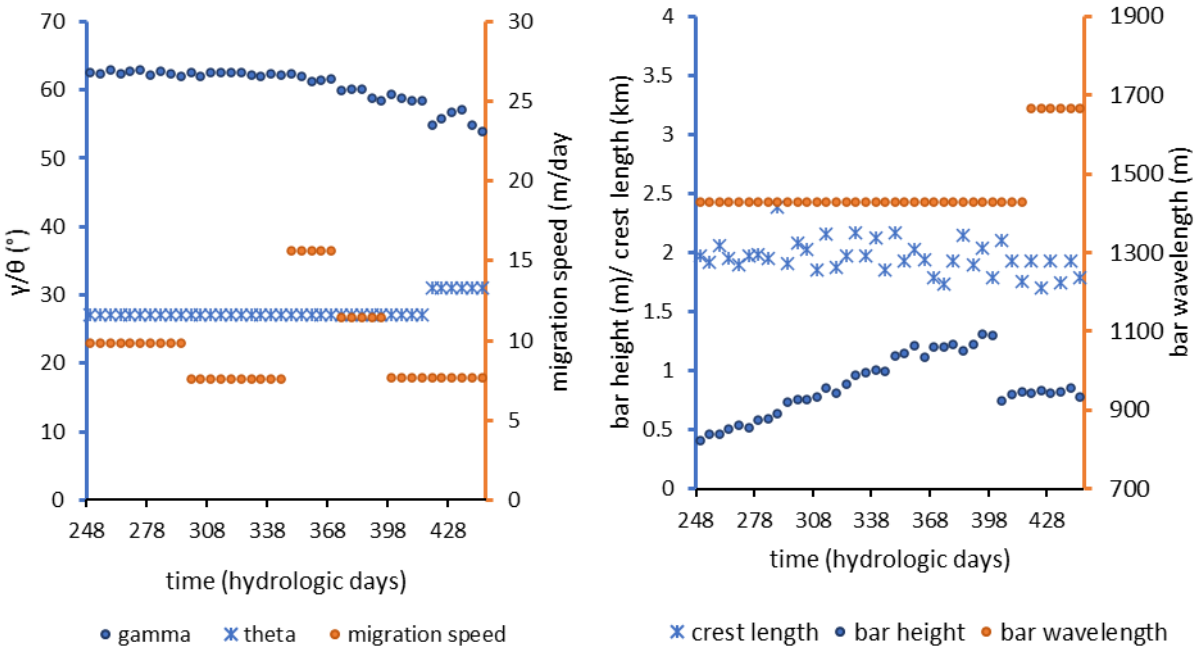

Figure 4.5.2.4. *The bar properties of the bars that evolved in the downstream area between day 250 and 445. The model simulation was forced by the default forcing parameters.*

4.5.3 Possible feedback mechanisms resulting in bar growth/decay

The bars that resembled sawtooth bars the most developed in the long-term simulation in which the hydrodynamics were forced by a significant wave height of 5.67m (default forcing parameters). The bathymetry after 50 days of morphological change was used in two additional simulations to analyse the possible feedback mechanisms (Figure 4.5.3). This bathymetry was forced by 1) a H_s of 2m and 2) a H_s of 5.67m, of which the other forcing parameters were kept as default (Table 3.3.2.2).

The quantity $\bar{\varphi}$ was positive for the simulation forced by a significant wave height of 5.67m and negative for the simulation forced by a significant wave height of 2m. Additionally, the phase difference ε was <90° for the simulation forced by a significant wave height of 5.67m and 90°> for the simulation forced by a significant wave height of 2m. For both simulations, the flow, sediment transport and wave conditions were analysed to study the cause of the observed bar growth/decay.

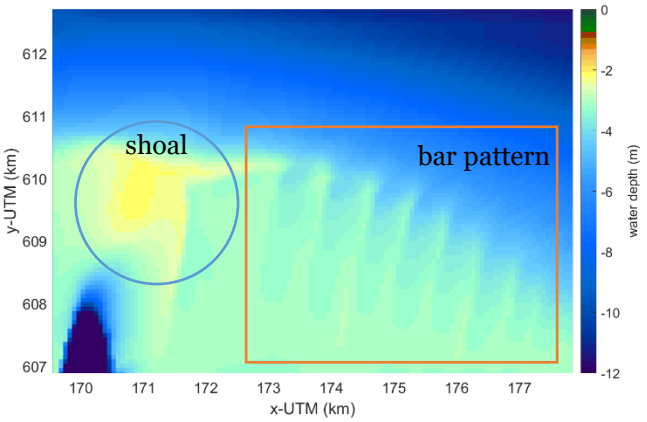

Figure 4.5.3.1. *The bathymetry of the natural developed bars at day 50 of which the hydrodynamics were forced by the default forcing parameters (output long-term run).*

The tidally averaged flow and sediment transport patterns only due to the presence of the bars are similar to the patterns on the prescribed bars as described in Section 4.1 and 4.2. The

sediment transport and flow are converging on the downdrift side of each bar crest and a diverging on the updrift side (Figure 4.5.3.2). No significant differences in the patterns, other than the magnitude, are found between the simulation forced by a significant wave height of 5.67m and the one forced by a significant wave height of 2m.

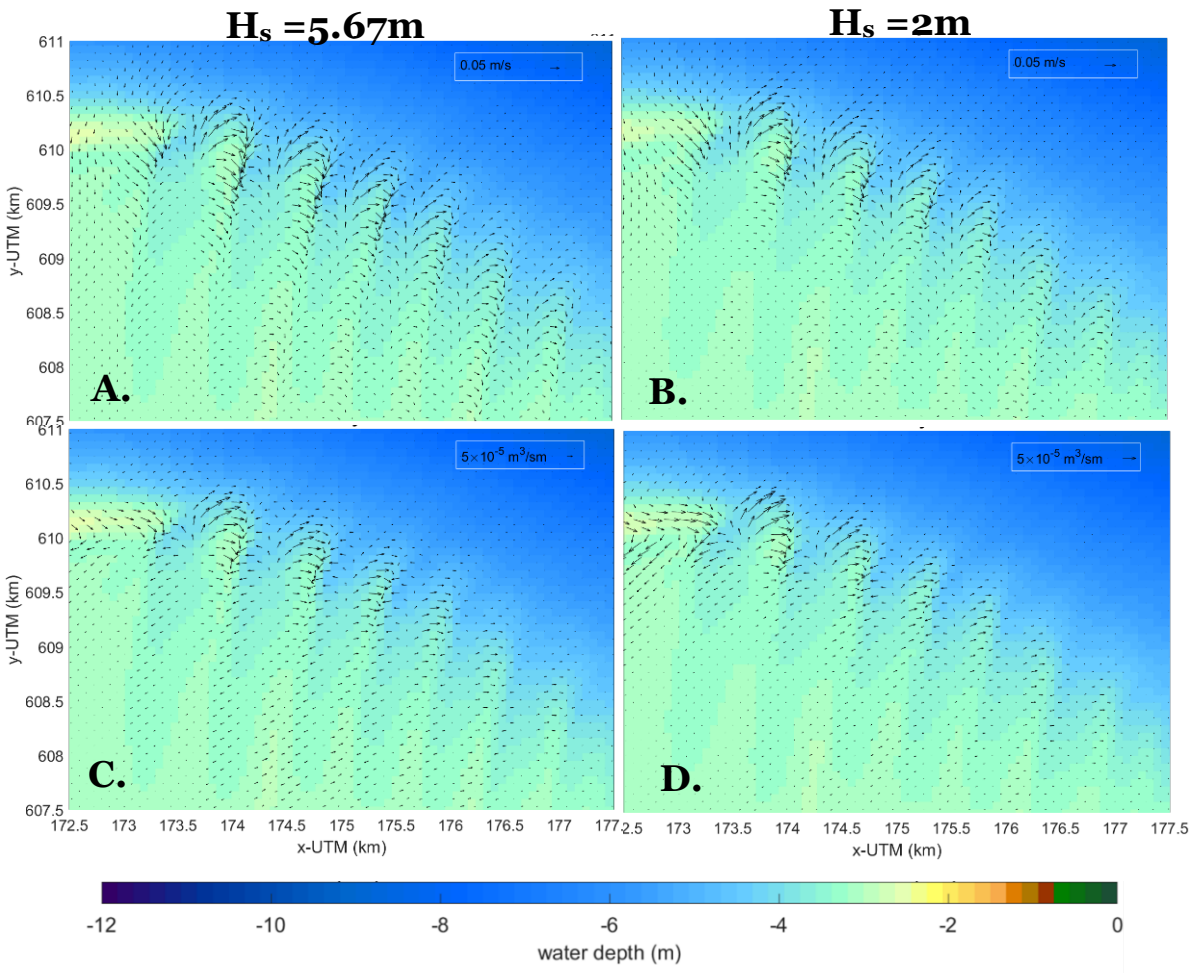

Figure 4.5.3.2. *The bar induced flow velocity for **A)** an initialized H_s of 5.67m and **B)** an initialized H_s of 2m. The bar induced sediment transport for **C)** an initialized H_s of 5.67m and **D)** an initialized H_s of 2m. The waves entered with -38°, the tidal amplitude was 1m (S2) and the wind speed was 15m/s (-90°).*

The mean wave direction on the bars is different for the simulations. With a significant wave height of 5.67m the waves enter the bar area with a ±-90° angle. In contrast, for the simulation with a significant wave height of 2m the waves enter the bar area with a ±-70° angle (Figure 4.5.3.3.c/d). The higher the waves the larger the refraction since the waves 'feel' the bottom depth further seawards. The waves refract to -90 due to the presence of the ebb-tidal delta and the bar crests. However, the orbital velocities and the local significant wave height, are approximately similar on the bars for both simulations (Figure 4.5.3.3.a/b/e/f). This is caused by wave dissipation on the edge of the ebb-tidal delta. Waves that enter the edge of the ebb-tidal delta with a large wave height dissipate more then lower waves.

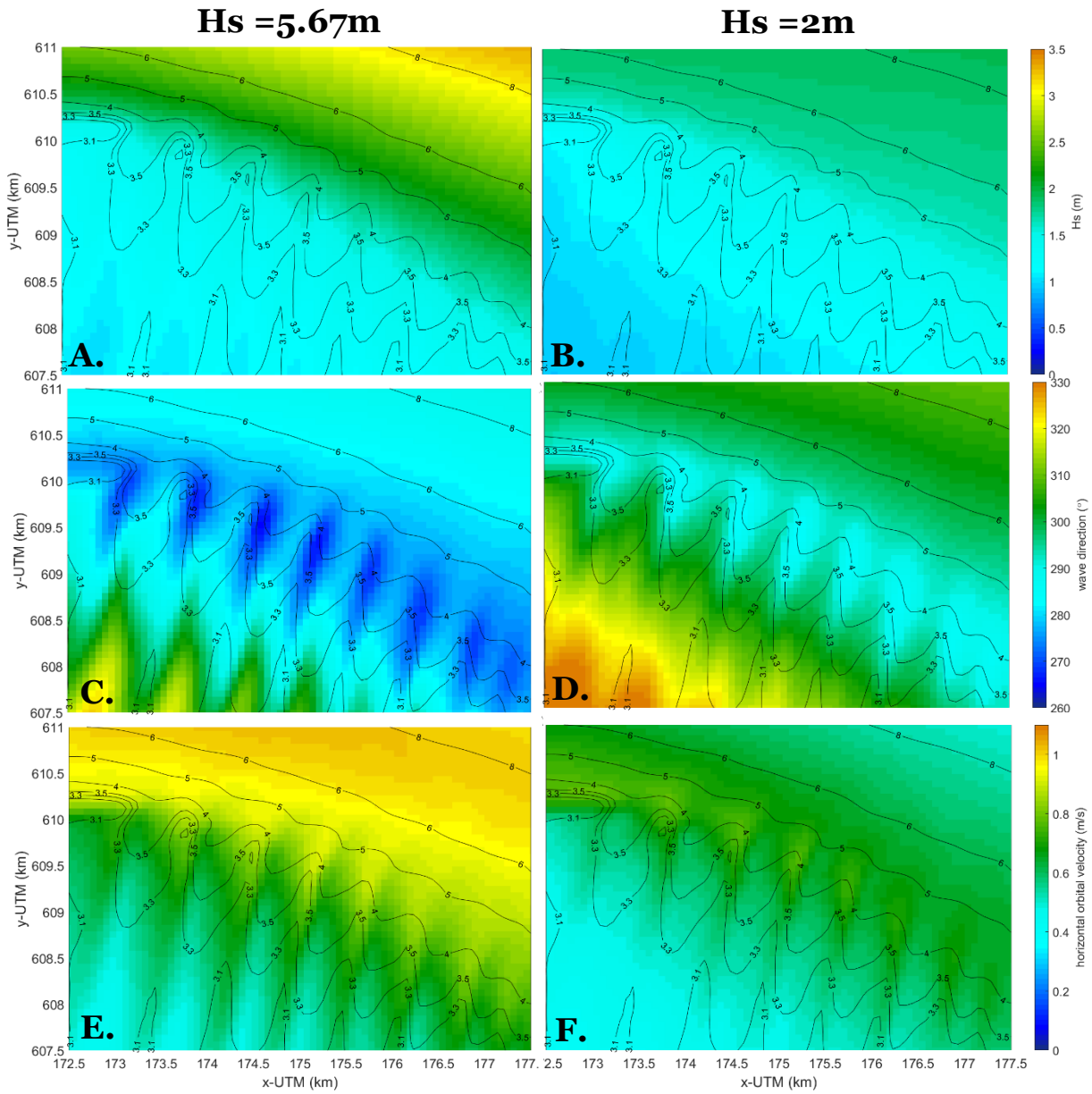

Figure 4.5.3.3. *The tidally mean significant wave height for* ***A)*** *an initialized H_s of 5.67m and* ***B)*** *an initialized H_s of 2m. The tidally averaged mean wave direction for* ***C)*** *an initialized H_s of 5.67m and* ***D)*** *an initialized H_s of 2m. The tidally mean horizontal orbital velocity for* ***E)*** *an initialized H_s of 5.67m and* ***F)*** *an initialized H_s of 2m. The waves entered with -38°, the tidal amplitude was 1m (S2) and the wind speed was 15m/s (-90°).*

Chapter 5. Discussion

5.1 Discussion on the causes for bar growth and decay

For this research two types of runs were accomplished, simulations with prescribed sawtooth bars and simulations with a random small amplitude perturbation in which bars could freely develop. All the simulations with prescribed sawtooth bars with a bar wavelength of 700m or 1050m resulted in bar decay. Only the bars with a wavelength of 1400m and 2100m grew over time. Since sawtooth bar like features developed in the simulations with random small amplitude perturbation, the causes for bar growth/decay, as observed in simulations with prescribed bars, are discussed in terms of 1) location of the bars, 2) the bar characteristics and 3) wave forcing:

1. The observed bar decay for bars of 700m in wavelength could be related to location of the prescribed bars. In the simulations with small amplitude perturbation, forced by a significant wave height of 5.67m and 3.5m, bars developed on the ebb-tidal delta with a similar wavelength. The location where they developed was, lower sloping, shallower and closer to the tidal inlet compared to the location of the prescribed bars.

2. The observed bar decay for bars with a wavelength of 700m and 1050m, with an orientation of 14° with respect to the north, could also be related to unfavourable prescribed bar orientation. The results of the simulation with a random small amplitude perturbation forced by the default forcing parameters (H_s = 5.67m) show that bars can develop with this wavelength. However, the average bar orientation for these bars with respect to the north is 33°. That this orientation is more ideal for bar growth is also seen in Section 4.3 in which the least bar decay is seen for bars with an orientation of 35° with respect to the north, compared to bars with an orientation of 0°, 14°, 25° or 45°.
   In the simulation with a random small amplitude perturbation forced by the default forcing parameters (H_s = 5.67m), bars developed in the downstream area after a large amount of time. These bars had a wavelength of ± 1500m. The mechanism that results in the development of these bars could be the cause for bar growth in the simulations with prescribed bars with a wavelength of 1400m and 2100m. However, sawtooth bars with a wavelength larger than 900m have not been observed in real life (Brakenhoff et al., 2019). The reason why the bars developed in the simulation and not in real life could be related to the wave climate. The bars in the downstream area developed after 200 days with a Hs of 5.67m. Since waves of this height only occur for less than a day per year in the study area (Lenstra et al., 2019), bars with these characteristics can probably not develop in nature. Therefore, these bars not further considered in the discussion.

3. Sawtooth bars developed in the simulations with small amplitude perturbation under storm conditions (H_s =5.67m and H_s =3.5m) and no sawtooth bar like bars developed under fair weather conditions (H_s =2m). That a H_s of 2m is less favourable for bar growth is also seen in the simulations with prescribed bars, in the phase difference ε. This shows that sawtooth bars can be generated by stormy weather with high significant wave heights and that bar decay could be caused by fair weather conditions. Additionally, the local mean wave direction on the bars seems to play a role in the growth/decay of the bars. This is further addressed below.

The unfavourable bar characteristics and the bar location could both result in flow and sediment transport patterns that are not ideal for bar growth. In all the simulations the bar induced sediment transport shows a diverging pattern on the updrift side of the bar crest and a converging pattern on the downdrift side of the bar crest. This is a result of the increase in flow over the bar crests and the decrease in flow in the bar troughs. The diverging pattern indicates an erosional area and the converging pattern a depositional area (Figure 5.1.1). The exact location of the erosion/deposition is of great importance because this determines whether the bars would grow or decay. Figure 5.1.2 visualises the areas of bar growth (red), bar decay (blue), erosion (green square) and deposition (orange square) for sawtooth bars with a wavelength of 700m and 2100m. Averaged over the whole

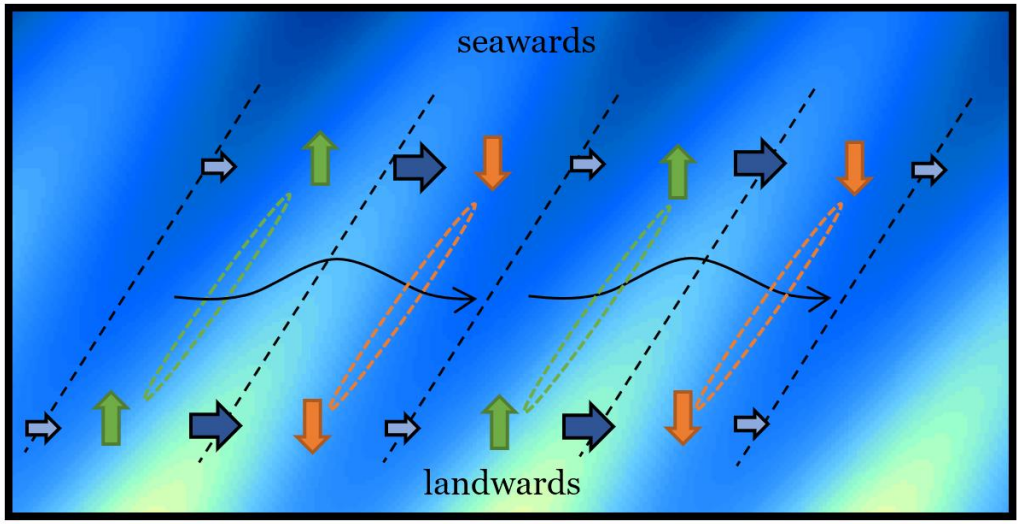

Figure 5.1.1. *The effect of the increasing and decreasing flow velocity for an eastward alongshore flow (blue arrows) on the sediment transport. The orange arrows represent deposition and the orange dotted oval the depositional area. The green arrows represent erosion and the green dotted oval the erosional area.*

area, growth is observed for the sawtooth bars with a wavelength of 2100m and decay is observed for bars with a wavelength of 700m. The figure shows that for bars with a wavelength of 2100m, erosion takes place in the in the trough and on the updrift side of the crest and that deposition takes mainly place on the downdrift side of the crest. This results in bar growth. For bars with a wavelength of 700m erosion takes mainly place on the updrift side of the bar crest and deposition takes mainly place on the downdrift side of the bar crest. Only very small amounts of erosion/deposition are visible in the troughs, but overall, this pattern results in bar decay.

The difference between the bar induced sediment transport patterns for bars with a wavelength of 700m and 2100m is the magnitude, although the same forcing parameters are used. For bars with a wavelength of 2100m the difference in magnitude between the bar crest and trough is larger than for bars with a wavelength of 700m. This is caused by the fact that more wave dissipation takes place on crests of sawtooth bars with a larger wavelength due to the larger surface area, which results in a larger wave driven alongshore current on the crests and so a larger magnitude of the sediment transport. Additionally, with a larger bar wavelength the incoming waves refract more towards the bar crests as is seen in Figure 4.1.2.4. With a wavelength of 700m the mean wave direction on the bars is ±-80° and with a wavelength of 2100m the mean wave direction on the bars is ±-90° (the initial mean wave direction was -38°). This suggests that the change in sediment transport magnitude over the bar crests and troughs and the mean wave direction could be important elements for the bar growth. However, the physical cause for bar growth in the case of bars with a wavelength of 2100m and decay in the case of bars with a wavelength of 700m still remains unknown.

5.2 On the hypotheses regarding sawtooth bar formation

It was hypothesized by Brakenhoff et al. (2019) that sawtooth bars are a type of sand waves forced by tidal and wave-driven currents. Sand waves grow due to the instability between the oscillatory tidal current and the flat bed. The bottom friction and the oscillatory tidal current together generate vertical recirculating cells. Therefore, sand waves cannot be modelled with a depth average model as is used for this study. However, growth is observed for the prescribed sawtooth bars with a wavelength of 1400m and 2100m, and sawtooth bars developed in the runs with a small amplitude perturbation forced by a significant wave height of 3.5m and 5.67m. Therefore, it is not expected that sawtooth bars are a type of sand waves.

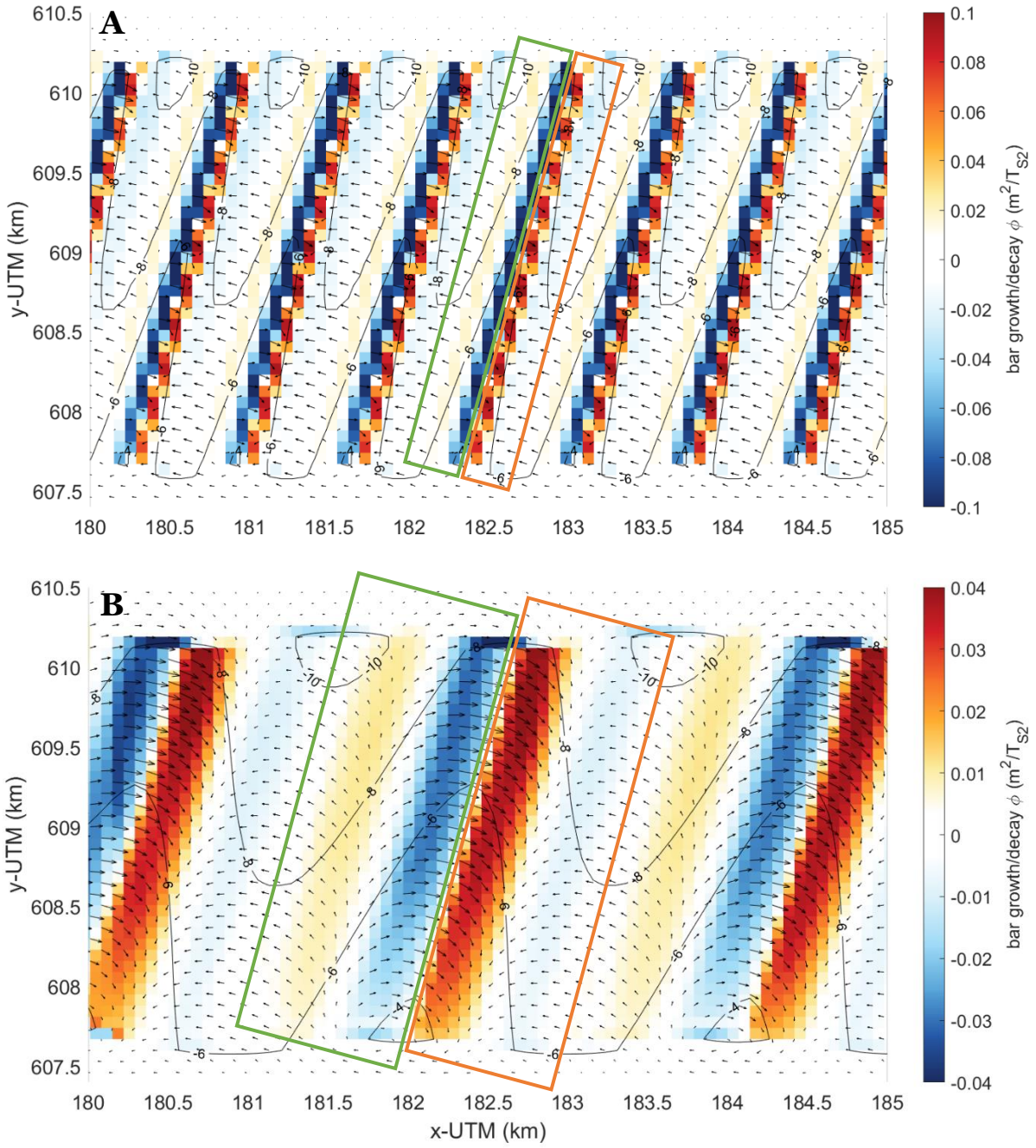

Figure 5.1.2. *The bar growth/decay rate φ for a run with sawtooth bars of* ***A)*** *700m and* ***B)*** *2100m in wavelength. The bars are 3m high and have an orientation of 14° with respect to the north. The simulations were forced by the default forcing parameters. The vectors represent the tidally averaged bed form induced sediment transport, and the solid black lines are the lines of equal depth. The green squares are the areas of erosion and the orange squares the areas of deposition.*

Brakenhoff et al., (2019) hypothesized that the instability mechanism resulting in the generation of the sawtooth bars could be caused by high angle waves. High angle waves, as seen in the models of Ashton and Murray (2006), could result in an instability due to the generation of a so-called shadow zone in the downdrift part of emerging shoals on the ebb-tidal delta. Bars developed, that resembled sawtooth bars, in the long-term run with a prescribed random small amplitude perturbation and forced by a significant wave height of 5.67m. The results show that the bars appeared in the shadow zone of a shoal and that the incoming waves are high angle waves (±-90°). Additionally, when these

developed bars were forced by waves with a significant wave height of 2m the local mean wave angle became less high ±-65° and the bars decayed. This was also observed for the simulations with prescribed bars with a wavelength of 2100m (growth) compared to bars with a wavelength of 700m (decay). This suggests that sawtooth bars could be generated by high angle wave instability when the angle and the energy of the incoming waves is large enough.

The flow patterns seen on Shoreface Connected sand Ridges (SCR) are a bit like the patterns observed over the sawtooth bars. Sawtooth bars and SCR differ in bar wavelength, crest length and orientation which is updrift for SCR. The updrift orientation with a relatively small angle between the bar crest and the coast (20° - 25°) together with the approximately 5 km wavelength results in an offshore deflection of the alongshore current over the bar as explained in Figure 2.3.1.2 (Trowbridge, 1995). For sawtooth bars an offshore deflection is also seen but the cause is different since the orientation is downdrift and bars are smaller. On SCR the offshore deflection of the alongshore current is caused by the fact that the flow is stronger in the shallow area at the inner flank of the ridge compared to the deep outer flank (Figure 2.3.1.2.a). In contrast, on sawtooth bars the deflection is caused by the flow that increases in magnitude on the crests and decreases in the troughs (Figure 4.1.2.1). So, the mechanism that generates sawtooth bars seems not similar to the generation mechanism of SCR. However, the weather conditions needed for the generation of SCR, are similar to the weather conditions used in this study for sawtooth bars where growth is seen. Stormy weather, which includes a relatively large significant wave height and wind speed, is necessary for the generation of SCR, which also seems the key to sawtooth bar growth.

5.3 Modelled outcomes compared to observations

The significant wave height seems to be the key parameter for migration. When waves were absent, almost no migration was observed. Field observations show that sawtooth bars migrate between 2 and 112m/year. The migration speeds as found in this study from the simulations with prescribed bars could be compared to the observed yearly migration speeds with the use of the wave data collected by Rijkswaterstaat between 1994 and 2014 from the station of Schiermonnikoog (Lenstra et al., 2019) (Appendix A). The data contained the occurrence (% per year) per observed significant wave height. The migration speeds were determined per observed significant wave height with the use of the polynomial functions shown in Figure 5.3.1. One polynomial corresponds to the migration speeds for bars with a height of 3m and the other for bars with a height of 0.5m (averaged over the whole sawtooth bar area). This results in a migration speed of 161m/year for 0.5m high bars and 227m/year for 3m high bars, when 90.6% of the yearly waves is accounted for. That higher bars tend to migrate faster is also seen for the sawtooth bars in the North Sea (Brakenhoff et al., 2019). Hence, these results overestimate the yearly migration speed compared to observations. Additionally, the migration speeds for the freely developed bars on the ebb-tidal delta, as found in the simulations

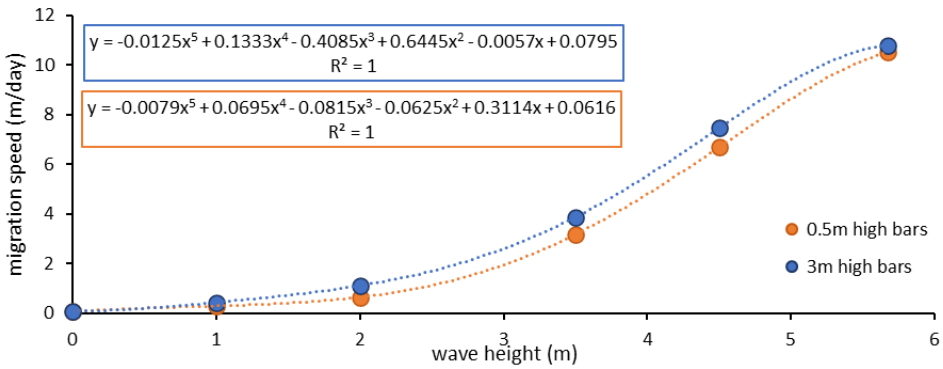

Figure 5.3.1. *The migration speed as function of the initialized significant wave height for bars of 0.5 m high and 3m high with a wavelength of 700m and an orientation of 14° with respect to the north (run series 3).*

with small amplitude perturbation, are even larger compared to the migration speeds in the simulations with prescribed bars with the same forcing. This can be a result of the location. Since the bars developed in a shallower area and closer to the tidal inlet compared to the prescribed bars, wave and tidal forces are more pronounced, which might be the cause for the larger migration speeds.

Observation show that sawtooth bars have on average an angle of 66° between the bar crests and the depth contour lines. In the long-term run with small amplitude perturbation and an initialized significant wave height of 5.67m, sawtooth bars appeared on the ebb-tidal delta with an average orientation of 81° with respect to the depth contours lines. This orientation is similar to the observed orientation. However, in the long-term run with small amplitude perturbation forced by a significant wave height of 3.5m, bars developed with an average orientation of 108°. Why these bars have a larger orientation is not known.

The observations show that sawtooth bars with a larger wavelength tend to have longer crest lengths. This is in line with the bars that developed in the simulations with small amplitude perturbation. For example, the bars that developed on the ebb-tidal delta forced by a significant wave hight of 5.67m, increased in wavelength from 700m to 1100m and increased in crest length from 1.4km to 2.26km in the same time span.

It was observed that the sawtooth bars disappear in eastern direction along each ebb-tidal delta. This might be due to the depth of occurrence and the transverse sloping bottom in combination with the mean wave direction. This study shows that sawtooth bars can form on the shallow low sloping ebb-tidal delta. Since the slope of cross-shore bottom becomes larger towards the east, this could cause the disappearance of the sawtooth bars in easterly direction.

5.3 Future research

Future research should mainly focus on the generation mechanism of the sawtooth bars, to find the physical key for bar growth and decay. The results show that sawtooth bars can be generated by stormy weather with high significant wave heights and that bar decay could be caused by fair weather conditions. Additionally, 'high-angle wave instability' could be the mechanism that triggers the generation of the bars under these stormy weather conditions. More research is necessary to test whether this is the case. This should include the shoal and channel cycle, since the formation of shoals on the ebb-tidal delta could have a large influence on the orientation of the area and therefore the angle of the incoming waves. Additionally, since this study was limited to a depth-average model, the hypothesis that sawtooth bars could be a type of sand waves should be tested with the use of a 3D model or a 2DV model. Although this study suggests that sawtooth bars are not a type of sand waves, the generation mechanism could still be related to processes in the vertical water column.

The observations of the sawtooth bars in the North Sea show that there is a decrease in bar height and wavelength in eastern direction when comparing different tidal inlets (Brakenhoff et al., 2019). Two hypotheses were opposed that still need future research: 1) that the bar height is related to the size of the ebb-tidal deltas and 2) that the bar height is related to the tide since the tidal amplitude is increasing in easterly direction. The first hypothesis was not studied in this thesis. However, it is shown that high-angle waves could be the instability mechanism resulting in the generation of the bars. A smaller ebb-tidal delta results in a smaller shadow zone in which sawtooth bars can develop. More research is necessary to proof this. The second hypothesis could also not be verified by this study. The results show that when the hydrodynamics are forced by wind waves and tides, of which only the tidal amplitude is increased, the magnitude of the flow resulting from waves and wind are increasing as well. Enhancement of the tidal amplitude results in a lower low water, which strengthens the flow by waves and wind during low tide. However, it is not clear how the increase in tidal amplitude results in a decrease of the bar height and wavelength.

Chapter 6. Conclusions

The main objective of this study was to clarify the generation mechanism and the morphological drivers of sawtooth bars. This included research on the sawtooth bar dynamics and the interaction with the hydrodynamics and sediment transport. To accomplish this a Delft3D model was set-up and two types of runs were done 1) simulations with prescribed sawtooth bars and 2) simulations with a random small amplitude perturbation in which bars could freely develop.

In the North Sea, the forcing of tides, waves and wind mainly results in an eastward alongshore flow. The flow is altered in its direction and velocity due to the presence of sawtooth bars, physically caused by the continuity equation. Due to the acceleration of the alongshore flow on the bar crests and deceleration on the bar troughs in combination with the downdrift orientation of the bars, the resulting tidally averaged flow pattern attempts to follow the depth contours. This is also seen for the sediment transport pattern which results in migration and bar growth or decay. Sediment transport is predominantly caused by the forcing of waves, which is suspended load dominated.

Whether sawtooth bars grow, or decay depends primarily on the bar characteristics, the location of the bars and the forcing by waves. Therefore, bar decay was often observed in the simulations with prescribed bars. This could be concluded with the results of the runs with a small amplitude perturbation in which bars developed that resembled sawtooth bars. In two runs, forced by a significant wave height of 5.67m and 3.5m entering from the northeast, bars developed with wavelengths of 700 to 1100m, bar heights of 0.5 to 2m, crest lengths of 1 to 2.4km and an orientation between 58° and 115° with respect to the depth contour lines. These bars developed in a shallower area on the ebb-tidal delta, compared to the location of the prescribed bars in the other runs, and had slightly different bar characteristics. Also, the forcing by waves seems important since no sawtooth bar type of bars developed in a run with small amplitude perturbation forced by a significant wave height of 2m. A different type of bars developed with an updrift orientation and a wavelength of ±1500m. That a significant wave height of 2m is less favourable for sawtooth bar growth was also visible in the simulations with prescribed bars. Additionally, the local mean wave direction on the bars seems to have an influence on the bar growth/decay. Waves that enter the bar area with a large angle (±90°) ('high-angle waves') between the wave crest and the shoreline trend resulted in bar growth. So, sawtooth bars can be generated by stormy weather with high significant wave heights in combination with high-angle waves, and bar decay can be a result of fair-weather conditions.

The migration speed of the sawtooth bars increases with an increasing significant wave height, wind speed and tidal amplitude, of which the wave height is the most important factor. Without waves, almost no migration is observed. With increasing wave height, the migration speed is increasing. The modelled migration speed scaled to a normal wave climate ranges between 161 and 227m/year. This depends on the bar height since higher bars tend to migrate faster. However, the migration speed of the freely developed bars as observed in the runs with small amplitude perturbation are even higher with the same forcing, which is possibly related to the location of the bars. Hence, the outcomes of this study overestimate the yearly migration speed compared to observations.

Appendix A. Wave data (1994-2014) from the station of Schiermonnikoog

Wave data was collected by Rijkswaterstaat between 1994 and 2014 from the station of Schiermonnikoog. 20 years of hourly wave measurements were sorted on the wave direction (west, northwest, north and northeast). For each wave direction the significant wave height data was binned in steps. For each binned increment, the average significant wave height, average T_{m01} and average wave direction was calculated. Only waves that enter the area between -90 and +50° were taken into an account, which represents 90.6% of the incoming waves (Lenstra et al., 2019).

Table A.1. *Wave data collected by Rijkswaterstaat between 1994 and 2014 from the station of Schiermonnikoog (Lenstra et al., 2019).*

Wave direction group	Bin	T_{m02} (s)	H_s (m)	Mean wave direction (°)	Occurence (%)
WEST (-112.5° to -67.5°)	0 - 0.5 m	3.43	0.4	-84.52	2.19
	0.5 - 1 m	3.7	0.76	-88.23	7.87
	1 - 2 m	4.37	1.39	-86.45	10.07
	2 - 3 m	5.38	2.36	-81.04	1.77
	3 - 6 m	6.15	3.42	-75.84	0.31
NORTHWEST (-67.5° to - 22.5°)	0 - 0.5 m	4.1	0.35	-42.16	5
	0.5 - 1 m	4.51	0.75	-43.58	8.75
	1 - 2 m	5.04	1.45	-43.86	12.92
	2 - 3 m	5.76	2.41	-43.18	4.58
	3 - 4 m	6.63	3.43	-42.70	1.65
	4 - 5 m	7.37	4.4	-40.44	0.55
	5 - 8 m	8.35	5.67	-37.67	0.19
NORTH (-22.5° to 22.5°)	0 - 0.5 m	4	0.35	-2.75	4.87
	0.5 - 1 m	4.52	0.74	-3.88	7.77
	1 - 2 m	5.02	1.4	-6.49	7.63
	2 - 3 m	5.66	2.39	-8.75	1.71
	3 - 6 m	6.69	3.6	-10.31	0.41
NORTHEAST (22.5° to 67.5°)	0 - 0.5 m	3.35	0.38	42.66	2.72
	0.5 - 1 m	3.73	0.74	46.45	5.18
	1 - 2 m	4.38	1.37	47.17	3.92
	2 - 4 m	5.34	2.37	39.16	0.54

References

Ashton, A. D., & Murray, A. B. (2006). High-angle wave instability and emergent shoreline shapes: 1. Modeling of sand waves, flying spits, and capes. *Journal of Geophysical Research: Earth Surface*, *111*(F4).

Balke, T., Stock, M., Jensen, K., Bouma, T. J., & Kleyer, M. (2016). A global analysis of the seaward salt marsh extent: The importance of tidal range. *Water Resources Research*, *52*(5), 3775-3786.

Battjes, J. A., & Janssen, J. P. F. M. (1978). Energy loss and set-up due to breaking of random waves. In *Coastal Engineering 1978* (pp. 569-587).

Besio, G., Blondeaux, P., Brocchini, M., Hulscher, S. J., Idier, D., Knaapen, M. A. F., ... & Vittori, G. (2008). The morphodynamics of tidal sand waves: A model overview. *Coastal engineering*, *55*(7-8), 657-670.

Besio G, Blondeaux P, Vittori G (2006) On the formation of sand waves and sand banks. J Fluid Mech 557:1–17. https://doi.org/10.1017/ S002211200600925

Blondeaux P, Vittori G (2011) The formation of tidal sand waves: fully three-dimensional versusshallowwater approaches. Cont Shelf Res 31(9):990–996.

Brakenhoff, L., Ruessink, G., & van der Vegt, M. (2019). Characteristics of saw-tooth bars on the ebb-tidal deltas of the Wadden Islands. *Ocean Dynamics*, *69*(11-12), 1273-1285.

Calvete, D., Falqués, A., De Swart, H. E., & Walgreen, M. (2001). Modelling the formation of shoreface-connected sand ridges on storm-dominated inner shelves. *Journal of Fluid Mechanics*, *441*, 169-193.

Calvete, D., & De Swart, H. E. (2003). A nonlinear model study on the long-term behavior of shore face–connected sand ridges. *Journal of Geophysical Research: Oceans*, *108*(C5).

Davis Jr, R. A., & Hayes, M. O. (1984). What is a wave-dominated coast?. *Marine geology*, *60*(1-4), 313-329.

De Swart, H. E., & Zimmerman, J. T. F. (2009). Morphodynamics of tidal inlet systems. Annual review of fluid mechanics, 41, 203-229.

Coelingh, J. P., Van Wijk, A. J. M., & Holtslag, A. A. M. (1996). Analysis of wind speed observations over the North Sea. *Journal of Wind Engineering and Industrial Aerodynamics*, *61*(1), 51-69.

Deltares (2014). Simulation of multi-dimensional hydrodynamic flows and transport phenomena, including sediments. User Manual Delft3D-FLOW, the Netherlands 690.

Dodd, N., Blondeaux, P., Calvete, D., De Swart, H. E., Falqués, A., Hulscher, S. J., ... & Vittori, G. (2003). Understanding coastal morphodynamics using stability methods. *Journal of coastal research*, 849-865.

Duffy, G. P., & Hughes-Clarke, J. E. (2005). Application of spatial cross correlation to detection of migration of submarine sand dunes. *Journal of Geophysical Research: Earth Surface*, *110*(F4).

Elias, E. P. L., Van der Spek, A. J. F., Wang, Z. B., & De Ronde, J. (2012). Morphodynamic development and sediment budget of the Dutch Wadden Sea over the last century. *Netherlands Journal of Geosciences*, *91*(3), 293-310.

Escoffier, F. F. (1940). "The stability of tidal inlets," Shore and Beach, 8, 111-114.

Falques, A., Calvete, D., De Swart, H. E., & Dodd, N. (1999). Morphodynamics of shoreface-connected ridges. In *Coastal Engineering 1998* (pp. 2851-2864).

FitzGerald, D. M. (1988). Shoreline erosional-depositional processes associated with tidal inlets. In: Hydrodynamics and sediment dynamics of tidal inlets. Springer,pp.186–225

Hasselmann, K., Barnett, T. P., Bouws, E., Carlson, H., Cartwright, D. E., Enke, K., ... & Meerburg, A. (1973). Measurements of wind-wave growth and swell decay during the Joint North Sea Wave Project (JONSWAP). *Ergänzungsheft 8-12*.

Knaapen, M. A. F., & Hulscher, S. J. (2002). Regeneration of sand waves after dredging. *Coastal Engineering*, *46*(4), 277-289.

KNW Atlas. The KNMI North Sea Wind (KNW) Atlas. Wind rose for wind speed at different heights for location FINO-1 | Image library | KNMI Projects

Kvale, E. P. (2006). The origin of neap–spring tidal cycles. *Marine geology*, *235*(1-4), 5-18.

Lenstra, K. J., Pluis, S. R., Ridderinkhof, W., Ruessink, G., & van der Vegt, M. (2019). Cyclic channel-shoal dynamics at the Ameland inlet: the impact on waves, tides, and sediment transport. *Ocean Dynamics*, *69*(4), 409-425.

Miles, J. W. (1957). On the generation of surface waves by shear flows. *Journal of Fluid Mechanics*, *3*(2), 185-204.

Németh, A. A., Hulscher, S. J., & de Vriend, H. J. (2002). Modelling sand wave migration in shallow shelf seas. Continental Shelf Research, 22(18-19), 2795-2806.

Ridderinkhof, W., Hoekstra, P., Van der Vegt, M., & De Swart, H. E. (2016). Cyclic behavior of sandy shoals on the ebb-tidal deltas of the Wadden Sea. *Continental Shelf Research*, *115*, 14-26.

Sha, L. P. (1989). Variation in ebb-delta morphologies along the West and East Frisian Islands, The Netherlands and Germany. *Marine Geology*, *89*(1-2), 11-28.

Sha, L. P., & Van den Berg, J. H. (1993). Variation in ebb-tidal delta geometry along the coast of the Netherlands and the German Bight. *Journal of Coastal Research*, 730-746.Smith, S. (2013). Statistics, Probability and Noise. In S. Smith (Ed.), *Digital signal processing: a practical guide for engineers and scientists* (pp. 11-17). Burlington: Elsevier Science.

Son, C. S., Flemming, B. W., & Bartholomä, A. (2011). Evidence for sediment recirculation on an ebb-tidal delta of the East Frisian barrier-island system, southern North Sea. Geo-Marine Letters, 31(2), 87-100.

Soulsby, R. L., A. G. Davies, J Fredsøe, D. Huntley, I. G. Jonsson, D Myrhaug, R. R. Simons, A Temperville, and T Zitman (1993). Bed shear-stresses due to combined waves and currents. Book of Abstracts, MAST-2, G8M Coastal Morphodynamics. In: Overall Workshop, Grenoble, pp. 2–1.

Trowbridge, J. H. 1995 A mechanism for the formation and maintenance of shore-oblique sand ridges on storm-dominated shelves. J. Geophys. Res. 100 (C8), 16071–16086.

Valerius J, Feldmann J, van Zoest M, Milbradt P, Zeiler M (2013) Documentation of morphological products from the AufMod project Functional Seabed Model, data format: Text files (CSV, XYZ). Bundesamt für Seeschiffart und Hydrographie. 11pp

Van der Westhuysen, A. J., Zijlema, M., & Battjes, J. A. (2007). Nonlinear saturation-based whitecapping dissipation in SWAN for deep and shallow water. *Coastal Engineering*, *54*(2), 151-170.

Van Rijn, L. C. (2007a). Unified view of sediment transport by currents and waves. I: Initiation of motion, bed roughness, and bed-load transport. *Journal of Hydraulic engineering*, *133*(6), 649-667.

Van Rijn, L. C. (2007b). Unified view of sediment transport by currents and waves. II: Suspended transport. *Journal of Hydraulic Engineering*, *133*(6), 668-689.

Van Rijn, L. C., Walstra, D. J. R., & Ormondt, M. V. (2004). Description of TRANSPOR2004 and Implementation in Delft3D-ONLINE. *Z3748*.

Van Santen, R. B., De Swart, H. E., & van Dijk, T. A. G. P. (2011). Sensitivity of tidal sand wavelength to environmental parameters: A combined data analysis and modelling approach. *Continental Shelf Research*, *31*(9), 966-978.

Wang, Z. B., Hoekstra, P., Burchard, H., Ridderinkhof, H., De Swart, H. E., & Stive, M. J. F. (2012). Morphodynamics of the Wadden Sea and its barrier island system. *Ocean & coastal management*, *68*, 39-57.

Zijlema, M., Van Vledder, G. P., & Holthuijsen, L. H. (2012). Bottom friction and wind drag for wave models. *Coastal Engineering*, *65*, 19-26.